Spectroscopic Investigations of Fluid Flow in Soap Bubbles

&

Au-Nanoparticles and Its Polyaniline Composite Synthesis

A dissertation submitted to
Indian Institute of Technology Guwahati
for the degree of Doctorate of Philosophy
in Chemistry

By

Tridib Kumar Sarma

Department of Chemistry
Indian Institute of Technology Guwahati
Guwahati 781039, INDIA
January, 2004

Dedicated to my beloved Ma and Deuta

(Parents)

------ Tridib

INDIAN INSTITUTE OF TECHNOLOGY GUWAHATI

Department of Chemistry

STATEMENT

I hereby declare that the matter embodied in this thesis is the result of investigations carried out by me in the Department of Chemistry, Indian Institute of Technology Guwahati, India under the supervision of Dr. Arun Chattopadhyay, Associate Professor in Chemistry.

In keeping with the general practice of reporting observations, due acknowledgements have been made wherever the work described is based on the findings of other investigations.

Tridib Kumar Sarma

Tridib Kumar Sarma

I. I. T. Guwahati

January, 2004

Dr. Arun Chattopadhyay
Associate Professor
INDIAN INSTITUTE OF TECHNOLOGY GUWAHATI
Department of Chemistry
E-mail: arun@iitg.ernet.in
Tel. 91 361 26902304
Fax. 91 361 2690762

CERTIFICATE

This is to certify that Mr. Tridib Kumar Sarma has been working under my supervision since August 1999. I am forwarding his thesis, entitled, " Spectroscopic Investigations of Fluid Flow in Soap Bubbles & Au- Nanoparticles and Its Polyaniline Composite Synthesis" being submitted for the degree of Doctorate of Philosophy of this Institute. I certify that he has fulfilled all the requirements according to the rules of this Institute, and that the investigations embodied in this thesis have not been submitted elsewhere for a degree.

I. I. T. Guwahati
January, 2004

Dr. Arun Chattopadhyay
Supervisor

INDIAN INSTITUTE OF TECHNOLOGY GUWAHATI

Department of Chemistry

COURSE CERTIFICATE

This is to certify that Mr. Tridib Kumar Sarma has satisfactorily completed all the courses required for the Ph. D. degree programme. These courses include:

CH 611	Bioinorganic Chemistry
CH 620	Art in Organic Synthesis
CH 630	A Fundamental Approach to Physical Chemistry
CH 631	Experimental Spectroscopy

Mr. Tridib Kumar Sarma has successfully completed his Ph. D. qualifying examination in February, 2001.

Dr. Jubaraj B. Baruah
Head
Department of Chemistry
I. I. T. Guwahati

Dr. Anil Kumar Saikia
Secretary
Departmental Post Graduate Committee
Department of Chemistry
I. I. T. Guwahati

INDIAN INSTITUTE OF TECHNOLOGY GUWAHATI

Department of Chemistry

Ph. D. Grade Card

Name: Tridib Kumar Sarma

Roll No.: 994504

Department: Chemistry

Semester: July-November, 1999

Course	Course Name	Credit	Grade
CH 611	Bioinorganic Chemistry	6	AA
CH 620	Art in Organic Synthesis	6	BC
CH 630	A Fundamental Approach to Physical Chemistry	6	BB
CH 631	Experimental Spectroscopy	6	BB

Semester Performance Index (S.P.I.). 8.25

Cumulative Performance Index (C.P.I.). 8.25

I. I. T. Guwahati

January, 2004

Assistant Registrar

Academic Section

Preface

When I joined the chemistry department at IIT Guwahati to start my research work, I had absolutely no idea from where to start, the kinds of problems needed to be solved in a PhD research work. It is a new institute, still at its growing stage. Being the first student in our group, I was fortunate enough to have active participation in setting up a new laboratory, in a beautiful institute. We started our research work with limited existing facilities. Indeed I had access to only one UV-visible spectrophotometer to start my work. However facilities are growing day by day, with growing number of students in the permanent campus.

The results of four and half years of work, presented here are noble in their own small way meant to inspire thought and provide enlightenment. Good science is a work of art, where the results, whether concepts, equations, or images, bring out the underlying structure of nature and are artistically pleasing by themselves. I hope that, the reader will find the works reported in this thesis to be interesting and informative.

Many people have contributed to this research work. First and foremost is Dr. Arun Chattopadhyay who has been an excellent supervisor, and taught me how one can start understanding a problem in the simplest possible way. He gave me freedom to pursue my own interests. His scientific thinking, valuable suggestions, discussions and constant support helped me immensely during the entire course of study.

I would like to acknowledge my sincere gratitude to Dr. Anumita Paul for her constant inspiration, help and valuable suggestions during my Ph. D. tenure. Prof. Mihir K. Chaudhuri, being the Chairman of my doctoral committee, has been a source of inspiration for me. Through the scientific discussions he has provided valuable suggestions throughout the entire period. I also acknowledge the help and inspiration from Dr. Manabendra Ray, whom I used to disturb every now and then, whenever I faced any kind of puzzle with my research works. I am grateful to Dr. J. B. Barua for his support and encouragement. My sincere thanks are due to all other faculty members in the department and Dr. Nikhil Gucchait for their help and inspiration.

Dr. Deepa Dey, staying far in Japan also, has been helping and encouraging me continuously during the whole tenure. I am always inspired by her dedication and enthusiasm for chemistry. She used to provide research publications in journals related to my works, saying "this may be important for you" many a time before we actually came to know about the publication. I enjoyed frequent scientific discussions with my group members and the research scholars of the department, both present and past members and my thanks are due to all of them, especially Devasish with whom I was involved in a large number of the projects carried out, and Alam who never allowed us to be in desperation. The technical staffs of the department deserve recognition due to their contribution in maintaining the laboratory infrastructure.

The financial support from Council of Scientific and Industrial Research (CSIR), New Delhi is duly acknowledged. I thank Indian Institute of Technology, Guwahati for all the facilities that were made available to me and for the initial financial support.

I also acknowledge my gratitude to Material Research Center, Indian Institute of Science, Bangalore and RSIC, North Eastern Hills University, Shillong for all the instrumentation facilities provided to me. Help from Mr. Sidananda Sarma as well as Mr. Lokesh Chakraborty of physics department has been invaluable.

Several groups of people were not directly related to my research, but it would not have happened without them. My parents instilled in me the worth of hard work and have provided enough motivation to see the world beautiful. My brothers and family members are constantly behind me at every moment. My teachers in schools, B. Barooah College and Gauhati University introduced me to the natural world and gave me the tools to pursue those interests. While studying at different stages, many friends have made the years especially enjoyable with whom I have gotten to explore nearly the whole land of blue hills and green valley.

Abstract

My Ph.D. thesis consists of experimental investigations in the following two areas.

(i) Stabilization of single soap bubbles and their spectroscopic investigation.
Observation of Marangoni effect driven upwardly mobile fluid layer in a soap bubble film.
Control of the fluid movement by controlling surfactant concentration gradient.

(ii) Synthesis of Au-nanoparticles (NPs) from reduction of $HAuCl_4$ by H_2O_2.
Generation of shape-selected Au-NPs.
Preparation of Au NP-conducting polyaniline (PANI) composite.
Solubilization of the composite in aqueous starch solution.
Colloidal polyaniline and Au-NPs-PANI composite nanoparticle synthesis.

The thesis consists of five chapters.

Chapter 1

Introduction

This chapter contains an overview of studies related to soap films and bubbles, microfluidics on a soap bubble film, soap films as a biological membrane and control of directional fluidic movement on a soap bubble film. It also contains a brief review of importance of nanotechnology and conducting polymers from technological perspectives. In this section a brief summary of the works performed in this thesis have been presented and the scopes for future development have also been discussed.

Chapter 2

In this chapter we describe observation and control of Marangoni convection driven upward fluid flow in a soap bubble. This chapter has been divided into two sub-chapters, with each sub-chapter containing introduction, experimental section, results and discussion and conclusion.

Chapter 2.1

Simultaneous measurement of flowing fluid layer and film thickness in a soap bubble using a UV-visible spectrophotometer

Here we report the observation of Marangoni convection driven fluid flow in various soap bubble films using a UV-visible spectrophotometer. Our observation of simultaneous time-dependent measurement of the thickness of fluid layer and thickness of the bubble film, is based on the fact that partial reflection of a beam of light from the surfaces of a thin, semitransparent film causes interference in the light beam when the film thickness is of the order of a wavelength of light. When the wavelength of light is scanned with a soap bubble film being in a UV- visible spectrophotometer, a set of maxima and minima of absorbance occurring at different wavelengths is observed. The number of such maxima and minima and the separation between two maxima or minima depend on the thickness of the bubble film and thus can be used to monitor the film thickness.

Marangoni effect driven fluid flow also resulted in the appearance of absorption maxima and minima similar to those due to film thickness. However the wavelength separation between two maxima or minima due to Marangoni effect driven flowing fluid layer was much smaller than to those due to film thickness and the intensity of absorbance due to Marangoni effect was also much smaller than that due to film thickness interference. Thus we could simultaneously measure film thickness and the thickness of the fluid layer driven by Marangoni effect. It was observed that the fluid layer thickness remained nearly constant for both vertical and horizontal bubbles (i.e. bubbles with alignment geometry different with respect to the support on which they rest) even though the film thickness had changed with time. The observed values of fluid layer thickness were about 6.94 ± 0.15 mm for a vertical bubble and about 4.75 ± 0.09 mm for a horizontal bubble. However no interference maxima or minima due to Marangoni driven fluid flow was observed for a single vertical soap film. Our observations suggest that Marangoni effect driven upward fluid movement helps restore the thickness of the film at the beginning after the formation of the bubble. Simultaneous gravitational drainage of water and surfactants occur from the film that reduces the film thickness with time. After a certain period in the lifetime of the bubble film no upwardly mobile fluid could be observed while the film thickness gradually decreased to its final equilibrium value reported to be of the order of 5-10 nm.

Chapter 2.2

Visible Spectroscopic Observation of Controlled Fluid Flow up along a Soap Bubble Film from a Pool of Solution

We have also achieved control over the fluid movement against gravity from a solution below, up along a bubble film, guided by Marangoni effect. Our method is based on controlling the surfactant concentration gradient between the bubble film and the surfactant solution on to which the bubble floats. The fluid flow was monitored by time dependent changes in the visible absorption spectrum of Rhodamine B, a laser dye, as it moved up along the bubble film from the solution below. We observed that when the concentration of surfactants in the solution below was higher than that in the film, fluid flow up along the bubble film could be observed. However, when the concentration of surfactant in the solution was equal to or lower than in the film, fluid movement could not be observed.

A small difference in initial surfactant concentration with a value as low as 2%, between the bubble and the pool of solution on which the bubble floats, is enough to initiate upward fluid movement. We could observe the controlled upward fluid movement until the surfactant concentration gradient was 5%. Further increase in the surfactant concentration gradient lead to dramatic increase in the flow rate that could not be followed using the present setup. Based upon our experimental evidences we concluded that Marangoni effect driven fluid movement up along a bubble film can be influenced by controlling the concentration gradient between the parent solutions, one from which the bubble is made and the other one on which the bubble floats.

Chapter 3

In this chapter we discuss the development of novel methods for the generation of Au nanoparticles (Au NPs), Au NP-conducting polyaniline composite (Au NP-PANI) and colloidal PANI and Au NP-PANI composite particles. The chapter consists of three sub-chapters with each describing introduction, experimental section, results and discussion and conclusions.

Chapter 3.1

A Simple Method of Electroless Deposition of Au NPs on Two and Three - Dimensional Surfaces of Various Materials

In this chapter we have reported a new method for the generation of Au nanoparticles in aqueous medium using H_2O_2 as the reducing agent. It is well known that in alkaline medium H_2O_2 reduces $HAuCl_4$ to Au-bulk precipitate. However, we have found that Au NPs are formed when $HAuCl_4$ in aqueous solution (acidic pH) is treated with H_2O_2. Addition of H_2O_2 to $HAuCl_4$ solution with controlled concentration produces colloidal Au NPs with characteristic plasmon absorption band at 530 nm. Au NPs could also be prepared using the same method in presence of microwave radiation. Transmission electron microscopic measurements confirmed the formation of NPs with average particle size of 20 nm in diameter when synthesized in presence of sodium dodecyl sulfate (SDS) micelles as stabilizer.

We have also observed that the Au NPs synthesized using the present method could be deposited on unfunctionalized surfaces of various materials. Previously treated glass and quartz plates as well as polymer surfaces in form of over-head projector paper (OHP) were kept in contact with Au NPs that were prepared from $HAuCl_4$ using H_2O_2 in presence of microwave radiation. The deposited NPs were characterized using UV-visible spectroscopy, scanning electron microscopy and X-ray diffraction method. The time-dependent gradual depositions of NPs on surfaces were also monitored by UV-visible spectroscopy, X-ray diffraction and optical microscopy.

Chapter 3.2

Synthesis of Au nanoparticle-Conductive polyaniline composite using H_2O_2 as both reducing and oxidizing agent

The reduction of $HAuCl_4$ by H_2O_2 with the formation of the Au NPs lead us to develop a method for the formation of Au nanoparticle-conducting polyaniline composite in aqueous medium using H_2O_2 both for reduction of $HAuCl_4$ and oxidation of aniline (polymerization). The incorporation of Au-NPs inside the polymer moiety increased the electrical conductivity by two orders of magnitude than the polymer itself (typical values being 0.3 Scm^{-1} for the Au NP-conducting PANI composite and 2.4 X 10^{-3} Scm^{-1} for the

conducting polyaniline only). The incorporation of Au-NPs inside the polymer matrix was confirmed by X-ray diffraction study. The method is important as it reduces the number of steps typically required in a set of sequential reactions leading to formation of a composite.

Chapter 3.3

Synthesis of nanometer size aqueous colloidal conducting polyaniline and Au-nanoparticle-polyaniline composite particles in aqueous medium

In this sub-chapter we have discussed the controlled polymerization leading to the formation of colloidal conducting PANI and Au NP-PANI composite particles in aqueous micellar media (SDS, 1.2 x 10^{-2}M) in the presence of H_2O_2. The control was achieved by the introduction of the monomer, aniline from the vapor phase. The formation of the PANI and the composite was confirmed by UV-visible, FTIR and XRD measurements. TEM studies revealed that PANI particles of nanometer diameters were formed. On the other hand, in case of Au NP-PANI composite, self-assembled aggregated particles were formed in the nanometer domain. Core shell structure with a layer of PANI on the Au NP surface was also observed from the TEM studies.

Chapter 4

In this chapter we describe the use of starch for shape selective synthesis of Au NPs and for reversible encapsulation of PANI as well as Au NP-PANI composite. This chapter is divided into two sub-chapters.

Chapter 4.1

Reversible encapsulation of conducting polyaniline and Au nanoparticle-conducting polyaniline composite in starch

The insolubility of conductive polyaniline (PANI) in water and most of the common organic solvents has limited its application potential. Several strategies, primarily involving modification of the PANI backbone, have been devised for making the conducting polymer water soluble and thus biocompatible. In this aspect, we have solubilized the conducting PANI as well as Au NP-PANI composite in aqueous medium by incorporating them inside starch, which is known to attain helical conformation in presence of small molecules like I_2,

n-butanol and carbon nanotubes. Encapsulation inside starch moiety here has been achieved by dissolving PANI as well as Au-NPs-PANI composite in aqueous solutions of starch with the help of an ultrasonicator bath. The encapsulation has been found to be completely reversible and both PANI and the composite could be recovered by introducing molecular iodine in the aqueous starch solution of either of them. In addition, we have shown that PANI could liberate I_2 from starch–iodine complex while the polymer itself gets encapsulated inside starch. Further, hydrolyzing starch by an enzyme could also liberate PANI from starch-PANI composite. Transmission electron microscopic observations suggest that PANI and the composite were dispersed in starch solution in the form of particles of average diameters on the order of 10-20 nm.

Chapter 4.2

Starch Mediated Shape-Selective Synthesis of Au-NPs with Tunable Longitudinal Plasmon Resonance

A large number of chemical and photochemical methods have been developed for the shape selective synthesis of the metal NPs where the optical, electronic and magnetic properties of these NPs can be tuned by varying the one, two and three-dimensional shapes of the NPs. Although a large number of synthetic methods exist for the shape-selective synthesis of Ag NPs, the same is not true for Au NPs. We have used starch as the template for the synthesis of Au-NPs of various shapes using H_2O_2 as the reducing agent in aqueous medium in the presence of ultrasonic wave. We have observed that, while keeping the concentration of the starch and H_2O_2 constant, the increase in the concentration of the parent metal salt $HAuCl_4$ led to the formation of NPs, the shape of which changed from spherical to triangular to hexagonal. This shape changes resulted in the appearance followed by red shift of the longitudinal plasmon resonance band while the transverse plasmon band remained nearly the same at 530 nm. The shape of the NPs formed was confirmed by TEM. Further, introduction of a starch digestive enzyme diastage (fungal) with enzyme activity 1:2000, in the starch-Au NP solution resulted in the precipitation of enzyme coated Au NPs, which may find use in targeted delivery at a desired site.

Chapter 5

In this chapter we describe a novel method for the deposition of polyaniline in a filter paper and use them for sensor applications.

Chapter 5.1

A polyaniline containing filter paper that can be used as a sensor, acid, base and end-point indicator and also filters acids and bases

Conducting form of PANI is a conjugated polymer with a number of unique properties. When cast into membranes, PANI shows unprecedented selectivity towards molecules essential for the development of sensors and actuators, membranes for gas separation as well as discrimination of chiral compounds in the presence of a chiral dopant. In this work, we have synthesized conducting form of PANI in a filter paper and then use the filter paper as (a) an acid, base and end-point indicator (b) as a sensor for the ammonia solution and vapor and (c) as a filter for acid and base. The use of the PANI containing filter paper as an acid-base sensor stems from the fact that emeraldine salt (green) and its base (blue) form can be reversibly converted in presence of a base and an acid respectively.

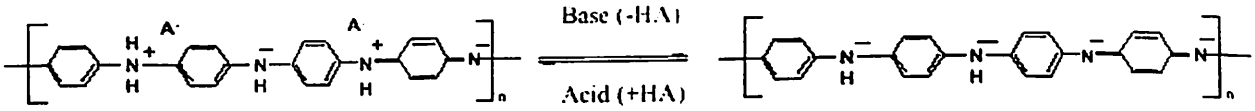

We have found that the PANI containing filter paper could detect the presence of ammonia in a solution with concentration as low as 14 ppm with the conversion of green filter paper into blue form. The ammonia vapor has also been detected in the same way by keeping the green paper above a solution with ammonia concentration as low as 45 ppm. Finally, the green filter paper could be used to decrease the pH of a basic solution and the blue paper could also be used to increase the pH of an acid solution by passing the appropriate solution through the relevant filter paper.

Contents

A.	Statement	I
B.	Certificate	II
C.	Course Certificate	III
D.	Ph. D. Grade Card	IV
E.	Preface	V
F.	Abstract	VII
G.	Contents	XIV
H.	**Chapter 1 – Introduction**	
	1.1 Soap films and Bubbles	1
	1.2 Microfluidics on a soap film or bubble membrane	2
	1.3 Nano science and technology	5
	1.4 Conducting Polymers	6
	1.5 Our direction	8
	1.6 Relevance and scope of the work reported in the thesis	9
	1.7 References	12
I.	**Chapter 2**	
	2.1 Simultaneous measurement of flowing fluid layer and film thickness of a soap bubble using a UV-visible spectrophotometer	
	2.1.1 Introduction	18
	2.1.2 Experimental Section	22
	2.1.3 Results and Discussion	23
	2.1.4 Conclusions	26
	2.1.5 Appendix	32
	2.1.6 References	34
	2.2 Visible Spectroscopic observation of controlled fluid flow up along a soap bubble film from a pool of solution	
	2.2.1 Introduction	36
	2.2.2 Experimental section	37

2.2.3 Results and discussion 39

2.2.4 Conclusions 46

2.2.5 References 46

J. Chapter 3

3.1 A simple method of electroless deposition of Au-nanoparticles on two and three-dimensional surfaces of various materials

3.1.1 Introduction 49

3.1.2 Experimental Section 52

3.1.3 Results and discussion 53

3.1.4 Conclusion 59

3.1.5 References 60

3.2 Synthesis of Au nanoparticles-conducting polyaniline composite using H_2O_2 as both reducing and oxidizing agent

3.2.1 Introduction 63

3.2.2 Experimental section 65

3.2.3 Results and discussion 66

3.2.4 Conclusion 72

3.2.5 References 72

3.3 Synthesis of nanometer size colloidal conducting polyaniline and Au nanoparticles-polyaniline composite particles in aqueous medium

3.3.1 Introduction 75

3.3.2 Experimental section 77

3.3.3 Results and discussion 78

3.3.4 Conclusion 84

3.3.5 References 84

K. Chapter 4

4.1 Reversible encapsulation of nanometer size polyaniline and Au nanoparticle-polyaniline composite in starch

4.1.1 Introduction 87

4.1.2 Experimental section 89

4.1.3 Results and discussion 91

4.1.4 Conclusion 99

4.1.5 References 99

4.2 Starch mediated shape-selective synthesis of Au-nanoparticles with tunable longitudinal plasmon resonance

4.2.1 Introduction 103

4.2.2 Experimental Section 104

4.2.3 Results and discussion 106

4.2.4 Conclusion 114

4.2.5 References 114

L. **Chapter 5**

5.1 A polyaniline containing filter paper that acts as a sensor, acid, base and end -point indicator and also filters acids and bases

5.1.1 Introduction 116

5.1.2 Experimental Section 119

5.1.3 Results and discussion 121

5.1.4 Conclusion 127

5.1.5 References 128

M. Colored Plates 131

N. List of publications 137

CHAPTER 1

INTRODUCTION

Introduction

1.1 Soap Films and Bubbles

Foams represent one of the oldest and well-explored unsupported membrane system, with the gas phase dispersed within a liquid phase and stabilized by surfactant adsorbed at the gas-liquid interface. Literature[1], both theoretical and experimental, concerned with the stability of the foam films, rheological properties on the surfaces of the foam films, hydrodynamic forces operating on the foam lamellae, and effect of various factors such as surfactant concentration, addition of salts, viscosity, temperature etc. has been growing for a long time. With the development of instrumental techniques[2], various spectroscopic as well as microscopic measurements have been carried out to study the surface properties and core structure of the foam films. The enormous increase in the scientific exploration of the structure of the foam films have been fueled by tremendous application potential associated with them. Understanding the behavior of foam films[3] has application potential in cosmetic products, fire retardants, food products, oil recovery, isolation of hazardous gases, aerosols, and aggressive liquids (ammonium, isocyanite etc.). Polymer foams have been used as thermo-insulating materials[3]. Moreover, three-dimensionally ordered arrays of air bubbles in a polymer matrix have been generated that may have potential applications in the development of photonic band gap materials, microlens arrays and beam steering devices[4]. Model studies on the foams generated from phospholipids and protein/lipid monolayers at liquid interfaces provide important data about the behavior of lung surfactants[5]. In the case of soap films and bubbles, the stability of the membrane plays an important role in the effective application of the foams.

Another important area of research involving soap films and bubbles is the study of self-assembled behavior of their constituents, transportation and functionalization of molecules and also to study molecular interactions between two contacting phases at small distances at the air-water interface. Soap bubble films have been used traditionally as a model biological membrane. The effectiveness of the conventional membrane mimetic systems such as supported bilayer membranes on solid and liquid surfaces, micelles, vesicles and biopolymers[6] are based on the assembled behavior of the amphiphilic molecules in

water as they occur in natural environment. Soap films constitute one different kind of biomimetic system containing a thin layer of water sandwiched between two monolayers of amphipathic molecules, which have structures completely opposite to the lipid bilayer membrane[7]. Nano soap films, namely common black film (CBF) and Newton black film (NBF) have typical dimension of 20 nm, and are formed at the last stage of drainage of fluids from a foam film, reflect very little light and appear black under a microscope. Thin CBF has the structure of a reverse bilayer membrane, whereas NBF, without the free aqueous core between two layers of surfactant molecules, forms a foam bilayer having molecular orientation opposite to lipid bilayers. This is shown schematically in Figure 1.1

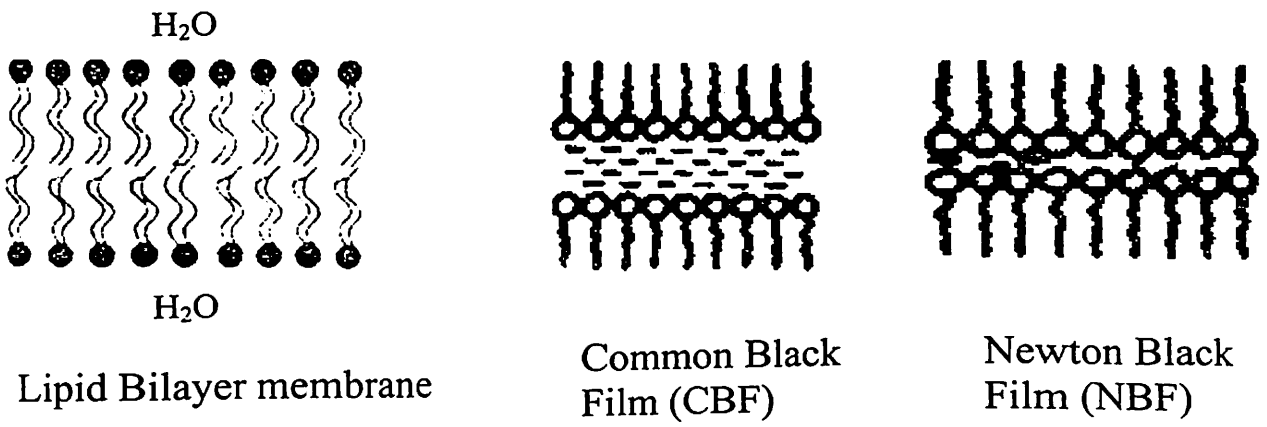

Figure 1.1. The molecular orientation of monolayers of amphipathic molecules in a lipid bilayer membrane, common black film and Newton black film. Spheres represent the polar head groups.

1.2 Microfluidics on a soap film or bubble membrane

Microfluidics, the technology involving manipulation of fluid movements in small channels, is expected to bring revolutionary changes in the technological world ranging from biotechnology, medicinal chemistry to microelectronic systems[8]. As a natural consequence, interest in microfluidics research has grown rapidly—in part because of the broad spectrum of potential engineering applications. A large number of methods[9] have been reported for the fabrication of microfluidic devices and understanding the mechanism of fluid movements in the small channels. Current research has seen significant advances made in chemical analysis systems, microinstrumentation for surgical use, physiological monitoring

systems, DNA chips and drug delivery technology[10, 8b]. The long-range impact that such developments may have on healthcare has yet to be fully defined. Because of the physical properties of fluids at the microscale[11], the design and fabrication of microfluidic devices involve more than miniaturization of "macrofluidic" systems. Many efforts are directed towards the integration of liquid-handling capabilities into a miniatured systems, but in most of the fabricated microfluidic systems mechanical pumping, electro-osmosis, electrowetting and thermocapillary pumping have been used to pump, transport, position and mix liquid samples. Although enormous research has been carried out on the development and understanding of the fluid flow at the solid-liquid interface, very little studies have been made on the transport of fluids along the liquid-air interface.

Studies related to microfluidics on soap bubble films are likely to influence enormously in proper understanding in this direction, as soap bubbles and films have traditionally been used as a model biological membrane to have insight the interfacial transport of fluids on the cell membrane. In soap films the directional fluid flow is driven by the capillary forces, an invincible phenomenon in all biological transport processes, with the liquid flowing in small channels of micrometer dimension. Understanding the fluid movement in bio-mimetic membranes may offer certain advantages over the prevailing techniques, as they work without any mechanical pump, actuator, electro-osmotic force etc.

The movements of liquids resulting from unbalanced surface tension forces constitute an important surface phenomenon, known as the Marangoni effect[12]. Marangoni effect generates considerable impact on the tangential mobility of film interfaces in presence of surfactant[13]. On an interface, as soon as liquid starts draining from a film stabilized by a surfactant, a gradient in surface tension is created at the interface. This gradient causes the surfactant mass transfer through the diffusion flow from the bulk to the film surface and surface flow in the direction of the surfactant adsorption gradient. When regulated properly, these types of flows are of value in several industrial applications, such as the design and operation of microfluidic devices[14], development of lithography techniques[15, 9c], spraying of insecticides, paints and inks[16] and integrated DNA separation techniques[17]. The Marangoni convection driven fluid flow is known to impart an important role in wetting and dewetting[18], interfacial transport of fluids[19], thinning of soap bubbles and films[3]. Troian and

coworker[20, 11a] have demonstrated the unusual fingering pattern formation guided by the instabilities created by the surface tension gradient of liquids on a solid surface. Recently, self-assembled structures of nanoparticles of various materials governed by thermally induced Marangoni convection driven fluid flow have been reported[21]. Both theoretical and experimental investigations studying the role of Marangoni convection driven flow of liquids on various interfacial phenomena are vast and still growing.

We have chosen to investigate fluid movements in single soap bubble films using spectroscopic techniques. Spectroscopic investigations[2a-f] in soap films have resulted in the understanding of time-dependent changes in film thickness, drainage of various components, microenvironments of the aqueous core of a black soap film, and the structure of thin films. We have been able to stabilize a single soap bubble and investigate the fluid movement up along the film spectroscopically. We observed Marangoni convection driven fluid flow up along the film against the gravitational drainage. We also report the time-dependent simultaneous measurements of thickness of fluid layer and thickness of the bubble film. The measurement is based on the time-dependent monitoring of film thickness in a soap bubble, by observing the interference maxima and minima occurring in the UV-visible region of wavelength. It was also observed that interference maxima and minima occurred due to the upward fluid flow along the soap bubble film, superimposed on those due to film thickness. We have measured the thickness of the fluid layer flowing upward along the soap bubble using UV-visible spectroscopic method, both for vertical and horizontal bubbles. Our observations suggest that the thickness in each case remained nearly constant throughout the observation period although the thickness of the bubble film changed considerably during that time. Our observations also indicate that liquid from the reservoir flows upward along the bubble film due to the surface tension gradient created by stretching of a film to form the soap bubble. The intensity of the interference maxima of absorbance due to the moving liquid layer diminished gradually with the thinning of the bubble film. The flow was not observed after some time, although the film thickness at that time was considerably higher than the final low thickness. In addition, the thickness of the fluid flowing upward was observed to be much larger than the film thickness and was independent of the film thickness.

Controlling the fluid movement inside the small channels has been considered a major challenge for the construction of the microfluidic devices as well as in basic understanding of the phenomena occurring in the biological systems. Directional fluid flow along the cell membranes, instrumental in the directional sensing as well as for many important factors such as bioassays, takes place when there is a concentration gradient across the cell wall[22]. Directional fluid flow has also technological importance in tears of wines, micro-electromechanical systems (MEMS), spreading and recoil of fluids on a solid surface, development of commercial "Lab-on-a-chip", processing in food, agriculture, cosmetic and pharmaceutical industries[23].

We have developed a new method for controlling the fluid movement upward along a soap bubble film, by controlling the surfactant concentration gradient between the bubble and the solution on which the bubble floats. The fluid flow was monitored by time-dependent changes in the visible absorption spectra of a laser dye as it moved into the bubble film from a solution below. Our results indicate that the rate of flow of fluid from a solution up along the bubble film is governed by small differences in initial surfactant concentration between them. In order for the liquid from solution to move up, the bubble film must have lower surfactant concentration than the solution below. We observed a controlled upward movement along the bubble film, which depends entirely on the surfactant concentration difference between the soap bubble film and the solution below, with higher concentration difference leading to faster fluid movement upward. We could observe an upward fluid movement from a solution to the bubble film, with an initial surfactant concentration gradient as low as 2%.

1.3 Nano Science and Technology

Nanotechnology is a multidisciplinary field aimed at fabricating, studying, manipulating and exploiting the properties of structures at least with one dimension at the nanometer length scale. The area of nanotechnology has undergone a remarkable growth in the past few years. These developments have been fueled by the expectation that the unusual properties of material, that become evident as the dimensions of the structural components shrink under 100 nm, may be exploited in materials applications. There has been continuous

growth in the development of methodologies for the generation of metal particles of various sizes and shapes, metal oxides, semiconductors, nonmetals such as carbon, polymers, biominerals, proteins and peptides[24] and literature is vast.

Among others, metal nanoparticles have attracted wide attention due to their potential applications in microelectronics, catalyses, magnetic devices, chemisorption, aerosols, powder metallurgy etc[25]. As efficacy in these applications is dependent strongly on the size, shape and composition (e.g. bimetallic, alloys, composites) of the metal nanoparticles, colloid chemistry is challenged to control not only the metal nanoparticle sizes, but the shapes and morphologies as well. The technological potential involving nanoparticle based material fabrication[26] and optimization of the size and shape, spatial orientation and control over the surface morphologies have led to input of tremendous research work in the development of practical strategies. One of the recent trends in nanoparticle research is directed towards the biosynthesis of nanoparticles by microbes and studies regarding the growth and fate of nanoparticles on the biological membranes[27]. In addition, the utilization of nucleic acids, proteins and enzymes as building blocks in the self-assembly of nanoscale functional devices[28] is of great interest.

1.4 Conducting polymers

Conducting polymers, termed as the "fourth generation of polymers", have revolutionized the application potential of polymeric materials[29]. Electrically conducting polymers are important in modern technology as they have application potentials in optical and microelectronic devices, chemical sensors, catalyses, drug delivery and energy storage systems[30]. Extensive studies have been carried out to understand the mechanism and applications for the unusual chemical, electrical and optical properties associated with the polymer in both insulating and conducting forms. Among the conducting polymers, polyaniline has been studied in great detail due to its redox properties, varied optical properties in different environments, tunable electrical conductivity both in doped and undoped forms, comparatively lower density than metal, good environmental stability and ease of preparation from commonly available chemicals.

Doped Polyaniline with metal salts, semiconductors or other materials have led to the development of composite materials with multi dimensional functionality. A recent trend has been to incorporate metal nanoparticles[31] inside the conducting polymer matrix leading to the development of a new class of hybrid materials, incorporating the application potentials both of the nanoparticles as well as the conducting polymer. Several groups have reported the formation of nanoparticle-polymer composite as well as core shell particles with the metal nanoparticles as the core and conducting polymer as shell or visa versa[32]. Methodologies have been developed for the formation of hollow polymer capsules or metal capsules after dissolving the core that finds immense importance in drug delivery systems[33]. Periodic inverse opal structures of conducting polyaniline have also been reported using organized colloidal arrays as the template and subsequent dissolution of the template[34]. The inverse opals are the building blocks for the construction of the photonic band gap materials.

However the application of polyaniline lays below its potential due to its insolubility in aqueous medium or in common organic solvents, hence the biocompatibility of the conducting polyaniline has been considered a major drawback[35]. Several alternative approaches have been made in order to solubilize polyaniline in aqueous medium. One approach deals with the functionalization of the polyaniline backbone that leads to formation of substituted polyaniline matrix e.g. the formation of sulfonated polyaniline[36]. Another method for the synthesis of water-soluble polyaniline involves the polymerization of aniline catalyzed by water-soluble enzymes such as horse reddish peroxidase[37] (HRP). Other strategies involve the incorporation of polyaniline inside water-soluble polymers such as sulfonated polystyrene or cyclodextrins[38], to make them water-soluble. However the most prolific alternative has been the formation of colloidal polyaniline in aqueous medium, with the polyaniline particles having dimension in the nanometer domain. Several techniques have been used to control the size and shape of the nano-dimensional polyaniline particles, keeping in mind the application potential associated with them. Polyaniline nanotubes, nanofibers and large arrays of oriented nanowires of polyaniline[39] have been reported. They are formed via different pathways such as self-assembled mechanism, use of porous membranes as the templates or by electrochemical pathways and are found to have immense importance in biomolecule separation and as sensors.

1.5. Our direction

We have developed a new method of synthesis of Au nanoparticles in aqueous medium by reduction of $HAuCl_4$ with H_2O_2. In addition, we have been able to deposit the Au nanoparticles on two and three-dimensional surfaces of various materials, with a simple dipping technique, without functionalization of either the nanoparticles or the surface on which the nanoparticles are deposited. Further we have generated Au nanoparticle-conducting polyaniline composite in a one-pot synthesis, using H_2O_2 both as oxidizing as well as reducing agent. The incorporation of Au nanoparticles in the polyaniline matrix enhanced the electrical conductivity by hundred fold, which holds promise for the future applications in optoelectronic devices and biomedical applications. The synthesis of colloidal conducting polyaniline and Au nanoparticle-polyaniline composite in aqueous medium was possible by controlling the monomer concentration using vapor phase introduction of aniline for the synthesis in a microemulsion system. This simple approach may help in enhanced applicability and biocompatibility of polyaniline.

Shape control is an alternative tool to size control to adjust optical, electronic or catalytic properties of the materials in the nanometer domain. We have achieved the shape selective synthesis of Au nanoparticles using starch, a commonly available biopolymer, as a template, with geometries of nanoparticles consisting of spherical, triangular and hexagonal shape, which resulted in control over the surface plasmon resonance of the nanoparticles. The nanoparticles synthesized in the presence of starch and ultrasonic waves were produced with a preferential shape by controlling the concentration of $HAuCl_4$. The nanoparticles could be removed from starch by a digesting enzyme. However, they result into a precipitate along with the enzyme upon removal from the starch encapsulation.

In addition, we have developed a method of incorporation of nanometer sized polyaniline as well as Au nanoparticle-polyaniline composite inside starch moiety with the help of ultrasonic waves. The encapsulation is reversible as introduction of a small amount of molecular iodine into the starch-polyaniline composite releases the polymer from the matrix. The additional advantage of using starch is that there exists specific enzyme to digest the polymer, which is useful for targeted delivery and appropriate use of the nanoparticles at

a desired site. This has been demonstrated by recovering the polyaniline from starch encapsulation after digestion with an enzyme. Finally, we report a new method of synthesis of conducting polyaniline in a filter paper (cellulose membrane) have used the paper as ammonia sensor, acid-base indicator and to filter acid and base from a solution.

1.6. Relevance and scope of the work reported in the thesis

Directed self-assembly of nanoparticles is opening newer avenues in technology through the controlled fabrication of nanoscopic materials with unique optical, electronic and magnetic properties. There has been tremendous development in research works towards the generation of hierarchical self-assembled patterns, governed by properties of suitable ligands surrounding the nanoparticle core, where the surface bound ligands define the particle's interaction with the surroundings. In another approach, colloidal particles have been assembled based on the hydrodynamic forces existing at an interface, where the fluidic motion on the interface influences the molecular interactions in the colloids. Colloidal self-assembly guided by the Marangoni convection driven fluid flow on a solid-liquid interface has already been explored that leads to the formation of unique colloidal self-assembled patterns[21]. Interface between two immiscible fluids, has been shown to be ideal for the assembly of micrometer-size colloidal particles[40]. A fluid-fluid interface has been shown as an idyllic platform for the self-assembled pattern formation by providing easy access to the nanoparticles for their chemical modification by the reaction of attached ligands with reagents in both fluids[41]. Semiconductor nanocrystals (Quantum dots) encapsulated in phospholipid block-copolymer micelles have been demonstrated as effective in-vitro fluorescent probes for studying the biological interactions[42], such as hybridization of specific complementary sequences in DNA, lineage-tracing experiments in embryogenesis.

An exciting and hitherto considerably unexplored dynamic biomimetic template to study the self-assembled behavior of the nanoparticles is the soap bubble interface. The soap bubble surface may open new avenues for the crystal growth in nanometer dimension and pattern formation as governed by the hydrodynamic forces present at the interface. Since the thickness of the foam lamellae is governed by the drainage rate, the size and shape of the nanocrystals can be controlled based on the drainage rate. Very little studies have been

performed in this direction. Recently Sastry and coworkers have demonstrated[43] the formation of Au nanoparticles of various morphology, using aqueous foams as the template. They argued that the various morphologies of Au nanoflakes, highly anisotropic and flat nanoplates formed arises from the complex spatial structure of the reaction sites in the foam lamellae. In this thesis, we have explored the controlled Marangoni driven fluid movement along the soap bubble film by controlling the surfactant concentration gradient, which may be useful for studying the growth and self-assembled pattern formation of nanocrystals at the gas-liquid interface.

The hydrodynamics on the soap bubble surface is governed by capillary forces, prevalent in most of the biological membrane systems and instrumental in governing the layer-by-layer deposition of the new crystal layers during the growth in crystals[44]. Thus soap bubble surface may act as a medium for studying the effect of the hydrodynamic forces on the growth of crystal structure. Davey and co-workers[45] have shown that stabilizing surfactants at the air-bubble/solution interface in foams could be used as nucleation centers for the growth of glycine and $CaCO_3$ crystals. They have also experimentally demonstrated how the crystal morphology could vary from pyramidal and plate like morphology to bipyramidal in case of glycine crystals, by controlling the induction time for nucleation on a soap bubble film or by using different surfactant constituents for the formation of the bubble. They could also generate crystals much smaller in dimension in soap foam lamellae, indicating that the thickness of the liquid layer in stable foam can be used to restrict the size of the product crystals. Again, it is well known that the three-dimensional shape of grains in a polycrystal is similar to the shape of individual soap bubbles[46] made by blowing air into a soap solution contained in a transparent box. The soap froth is a very good model for the grain structure of a simple polycrystalline material, and many similar features can be observed in the two systems. The soap bubbles are analogous to the grains, and the surfaces of the bubbles are analogous to the grain boundaries.

The field of nanoscience and technology is still at its infancy, as attractive and promising as these developments sound, the obstacles in fabrication of nanostructured devices are daunting. The trend is to take the inspiration from biology and work towards

fusion of materials with biotechnology[47] for future developments. Nanotechnology shows great promise for providing us in the near future with many breakthroughs that will change the direction of technological advances in a wide range of applications.

In this thesis work, we have been able to stabilize a single soap bubble for spectroscopic observations of phenomena occurring in the bubble film. We have discovered the Marangoni effect driven fluid flow present in single soap bubble and measured the thickness of such layers of fluid in a few cases. We also have been successful in controlling such fluid flow using surfactant concentration gradient as the control parameter. This work not only adds a new dimension to already established vast field of foams but also brings froth an exciting possibility of applications of the knowledge to the field of nanoscience and technology. We have not been able to complete all the required studies in this direction. However, we hope to have been able to create a beginning that may have a lasting influence in the field.

On the other front, we have been able to develop a few experimental methods of generation of environmentally friendly way of synthesis of Au nanoparticles (NPs); Au NP-conducting polyaniline (PANI) composite; solubilization of PANI and Au-NP-PANI composite particles in aqueous starch in the form of nanoparticles followed their recovery from encapsulation; synthesis of shape-selective and tunable plasmon resonance band specific Au NPs and finally a way of growing PANI in an ordinary filter useful in many applications. The guiding principle has been to find newer, simpler and straightforward ways of generating NPs and their composite especially with a polymer like PANI. As small as the results themselves are, through the works carried out in this thesis, we hope to have been able to make a little contribution to find a place for ourselves in the annals of science.

1.7 References

1. (a) Schramm L. L.; Wassmuth F. in *Foams: Fundamentals and Applications in the Petroleum Industry*, Schramm, L. L. Ed. Advances in Chemistry Series 242, American Chemical Society, Washington, DC, **1994** (b) Prud'Homme, R. K., Khan, S. A., Eds. *Foams: Theory, Measurements and Applications*; Surfactant Science Series; Mercel Dekker: New York, **1995**; Vol. 57 (c) Adamson, A. W.; Gast, A. P. *Physical Chemistry of Surfaces*, 6th ed.; John Wiley and Sons: New York, **1997** (d) *Foams: Physics, Chemistry and Structure*; Wilson, A. J., Ed.; Springer-Verlag: Berlin, **1989.**
2. (a) Umemura, J.; Matsumoto, M., Kawai, T.; Takenaka, T. *Can. J. Chem.* **1985**, *63*, 1713 (b) Be'lorgey, O.; Benattar, J. J. *Phys. Rev. Lett.* **1991**, *66*, 313 (c) Du, X.; Liang, Y. *Phys. Chem. Chem. Phys.*, **2000**, 2, 137 (d) Cohen, R.; Exerowa, D.; Kolarov, T.; Yamanaka, T.; Tano, T. *Langmuir* **1997**, *13*, 3172 (e) Huibers, P. D. T.; Shah, D. O. *Langmuir* **1997**, *13*, 5995 (f) Chattopadhyay, A., *Langmuir*, **1999**, 15, 7881 (g) Menger, F. M.; Angelova, M. I. *Acc. Chem. Res.* **1998**, 31, 789 (h) Sonneville-Aubrun, O., Bergeron, V.; Gulik-Krzywicki, T.; Jonsson, B., Wennerstrom, H.; Lindner, P.; Cabane, B. *Langmuir*, **2000**, 16, 1566 (i) Denkov, N. D.; Cooper, P.; Martin, J.-Y *Langmuir*, **1999**, 8514.
3. Exerowa, D. R.; Krugliakov, P. M. *Foams and Foam Films: Theory, Experiment, Application*; Studies in Interface Science; Elsevier: Amsterdam, **1998**; Vol. 5
4. Srinivasarao, M.; Collings, D.; Philips, A.; Patel, S. *Science*, **2001**, 292, 79
5. (a) Exerowa, D.; Lalchev, Z.; Marinov, D.; Ognyanov, K. *Langmuir*, **1986**, 2, 664 (b) Pattle, R. E. *Nature*, **1955**, 175, 1125 (c) Horn, L.; Gershfeld, *Biophys. J.* **1977**, 18, 301.
6. (a) Fuhrhop, J. H.; Koning, J. *Membrane and Molecular Assemblies: The Synkinetic Approach*; The Royal Society of Chemistry: London **1994** (b) *Biomimetic Polymers*; Gebelein, C. G., Ed.; Plenum Press: London, **1990** (c) Sackmann, E. *Science* **1996**, *271*, 43. (d) Heywood, B. R. and Mann, S. *Adv. Mater.* **1994**, 6, 9 (e) Mann, S.; Ozin, G. A. *Nature* **1996**, 382, 313 (f) Walsh, D., and Mann, S. *Nature* **1995**, 377, 320 (f)

Mann, S. *BIOMINERALIZATION: Principles and Concepts in Bioinorganic Materials Chemistry,* Oxford University Press: London, **2001**

7. (a) Cistola, D. P.; Atkinson, D.; Hamilton, J. A.; Small, D. A. *Biochemistry* **1986**, *25*, 2804. (b) Cistola, D. P.; Hamilton, J. A.; Jackson, D.; Small, D. A. *Biochemistry* **1988**, *27*, 1881.
8. (a) Wilbur, J. L.; Whitesides, G. M. in *Nanotechnology*, Timp, G. ed. Springer-Verlag, new York, **1999** (b) Delamarche, E.; Bernard, A.; Schmid, H.; Michel, B.; Biebuyck, H.; *Science*, **1997**, 276, 779 (c) Fu, A. Y.; Spence, C.; Scherer, A.; Arnold, F. H.; Quake, S. R. *Nature Biotechnol.* **1999**, 17, 1109 (d) Unger, M. A.; Chou, H. P.; Thorsen, T.; Scherer, A.; Quake, R. *Science*, **2000**, 288, 113 (e) DeRisi, J. L.; Ilyer, V. R.; Brown, P. O. *Science*, **1997**, 278, 680
9. (a) Gallardo, B. S.; Gupta, V. K.; Eagerton, F. D.; Jong, L. I.; Craig, V. S.; Shah, R. R.; Abbott, N. L. *Science*, **1999**, 283, 57 (b) Xia, Y. and Whitesides, G. M., *Angew. Chem. Int. Ed.* **1998**, 37, 550 (c) Brittain, S.; Paul, K.; Zhao, X. M. and Whitesides, G. M., *Physics World* **1998**,11, 31 (d) Zhao, B.; Moore, J. S.; Beebe, D. J. *Science*, **2001**, 291, 1023 (e) Freemantle, M. *Chem. Eng. News* **1999**, 77, 27 (f) Salimi-Moosavi, H.; Tang, T.; Harrison, D. J. *J. Am. Chem. Soc.* **1997**, 119, 8716 (g) Ichimura, K.; Oh, S. –K.; Nakagawa, M. *Science*, **2000**, 288, 1624 (h) Weigl, B. H.; Yaner, P. *Science*, **1999**, 283, 346 (i) Prins, M. W. J.; Welters, W. J. J.; Weekamp, J. W. *Science*, **2001**, 291, 277 (j) Jackman, R. J.; Brittain, S. T.; Adams, A.; Prentiss, M. G. Whitesides, G. M., *Science* **1998**, 280, 2089.
10. (a) Qin, D.; Xia, Y.; Rogers, J. A.; Jackman, R. J.; Zhao, X.-M.; Whitesides, G. M. In *Microsystem Technology in Chemistry and Life Sciences*, vol.194, Manz, A. and Becker, H., Eds.; Springer-Verlag, Berlin, **1998** (b) Burns, M. A.; Johnson, B. N.; Brahmasandra, S. N.; Handique, K.; Webster, J. R.; Krishnan, M.; Sammarco, T. S.; Man, P. M.; Jones, D.; Heldsinger, D.; Mastrangelo, C. H.; Burke, D. T. *Science*, **1998**, 282, 484 (d) Kakuta, M.; Jayawickrama, D. A.; Wolters, A. M.; Manz, A.; Sweedler, J. V. *Anal. Chem.* **2003**, *75*, 956 (e) Mao, H. B.; Yang, T. L.; Cremer, P. S. *Anal. Chem.* **2002**, *74*, 379
11. (a) Kataoka, D. E.; Troian, S. M. *Nature*, **1999**, 402, 794 (b) Schasfoort, R. B. M.; Schlautmann, S.; Hendrikse, J.; van den Berg, A. *Science*, **1999**, 286, 942 (c) Song,

H.; Ismagilov, R. F. *J. Am. Chem. Soc.* **2003**, 125, 14613 (d) Song, H.; Tice, J. D.; Ismagilov, R. F. *Angew. Chem. Int. Ed.* **2003**, 42, 768

12. Edwards, D.; Brenner, H.; Wasan D., *Interfacial transport processes and Rheology,* Butterworth-Heinemann: Boston, **1991**
13. Bain, C. D. *CHEMPHYSCHEM* **2001**, 2, 580
14. Carre´, A.; Gastel, J. C.; Shanahan, M. E. R. *Nature* **1996**, *379*, 432
15. Jackman, R. J.; Duffy, D. C.; Ostuni, E.; Willmore, N. D. Whitesides, G. M., *Anal. Chem.* **1998**,70, 2280.
16. Golovin, A. A.; Nepomnyashchy, A. A.; Pismen, L. M. *J. Fluid. Mech.* **1997**, *341*, 317.
17. Grunze, M. *Science*, **1999**, 283, 41
18. (a) Kargupta, K.; Konnur, R.; Sharma, A., *Langmuir,* **2000**, *16*, 10243 (b) Decamps, C.; De Coninck, J., *Langmuir,* **2000**, *16*, 10150. (c) Daniel, S.; Chaudhury, M. K.; Chen, J. C., *Science*, **2001**, 291, 633
19. (a) Chaudhury, M. K.; Whitesides, G. M., *Science*, **1992**, 256, 1539 (b) Bain, C. D.; Burnett-Hall, G.; Montgomerie, R., *Nature*, **1994**, 372, 414
20. Troian, S. M.; Wu, X. L.; Safran, S. A. *Phys. Rev. Lett.* **1989**, 62, 1496
21. Maillard, M.; Motte, L.; Ngo, A. T.; Pileni, M. P., *J. Phys. Chem.* **2000**, 104, 11871
22. (a) Dekker: L. V.; Segal, A. W., *Science,* **2000**, *287*, 982 (b) Parent, C. A.; Devreotes, P. N., *Science,* **1999**, *284*, 765 (c) Hadd, A. G.; Raymond, D. E.; Haliwell, J. W.; Jacobson, S. C.; Ramsey, S. C., *Anal. Chem.*, **1997**, 69, 1407 (d) Lagally, E. T.; Medintz, I.; Mathies, R. A., *Anal. Chem.*, **2001**, 72, 2995
23. (a) Jeon, N. L.; Dertinger, S. K. W.; Chiu, D. T.; Choi, I. S.; Stroock, A. D.; Whitesides, G. M. *Langmuir* **2000**, *16*, 8311. (b) Caelen, I.; Bernard, A.; Juncker, D.; Michel, B.; Heinzelmann, H.; Delamarche, E., *Langmuir,* **2000**, *16*, 9125 (c) Wen, L.; Papadopoulos, K. D., *Langmuir,* **2000**, *16*, 7612
24. For representation, (a) Link, S.; El-Sayed, M. A. *J. Phys. Chem. B,* **1999**, 103, 8410 (b) Henglein, A. *J. Phys. Chem.* **1993**, *97*, 8457 (c) Puntes, V. F.; Krishnan, K. M.; Alivisatos, A. P. *Science* **2001**, 291, 2115 (d) Ahmadi, T. S.; Wang, Z. L.; Green, T. C.; Henglein, A.; El-Sayed, M. A. *Science*, **1996**, 272, 1924 (e) Mirkin, C. A. *Inorg. Chem.* **2000**, 39, 2258 (f) Alivisatos, A. P. *Science* **1996**, 271, 933 (g) Trindade, T.;

O'Brien, P.; Pickett, N. L. *Chem. Mater.* **2001**, 13, 3843 (h) Donald A. *Physics World*, **1999**, 27 (i) Xia, Y.; Gates, B.; Yin, Y.; Lu, Y. *Adv. Mater.* **2000**, 12, 693 (j) Iijima, S. *Nature*, **1991**, 354, 56 (k) Terrones, M.; Torrones, H.; Banhart, F.; Charlier, J. –C.; Ajayan, P. M. *Science*, **2000**, 288, 1226 (l) MacDiarmid, A. G. *Angew. Chem. Int. Ed.* **2001**, 40, 2581 (m) Parthasarathy, R.; Martin, C. R., *Nature*, **1994**, 369, 298 (n) Reches, M.; Gazit, E. *Science*, **2003**, 300, 625

25. (a) Service, R. F., *Science*, **1999**, 286, 442 (b) Service, R. F. *Science*, **2000**, 290, 1524 (c) Gittins, D. L.; Bethell, D.; Schiffrin, D. J.; Nichols, R. J. *Nature* **2000**, 408, 67 (d) Craighead, H. G. *Science*, **2000**, 290, 1532 (e) Klein, D. L.; Roth R.; Lim, A. K. L.; Alivisatos, A. P.; McEuen, P. L. *Nature*, **1997**, 389, 699 (f) Jarrold, M. F. *Science*, **1991**, 252, 1085 (g) Ingram, R. S.; Hostetler, M. J.; Murray, R. W.; Schaff, T. G.; Khoury, J.; Whetten, R. L.; Bigioni, T. P.; Guthrie, D. K.; First, P. N., *J. Am. Chem. Soc.*, **1997**, 119, 9279
26. (a) Jager, E. D. H.; Smela, E.; Inganas, O. *Science*, **2000**, 290, 1540 (b) Shipway, A. N.; Katz, E.; Willner, I. *CHEMPHYSCHEM* **2000**, 1, 18 (c) Holtz, J. H.; Asher, S. A. *Nature* **1997**, 389, 829 (d) Velev, O. D.; Kaler, E. W. *Langmuir* **1999**, 15, 3693
27. (a) Mukherjee, P.; Ahmad, A.; Mandal, D.; Senapati, S.; Sainkar, S. R.; Khan, M. I.; Ramani, R.; Parischa, R.; Ajayakumar, P. V.; Alam, M.; Sastry, M.; Kumar, R. *Angew. Chem. Int. Ed.* **2001**, 40, 3585 (b) Li, Z.; Chung, S. W.; Nam, J. M.; Ginger, D. S.; Mirkin, C. A. *Angew. Chem. Int. Ed.* **2003**, 42, 2306 (c) Lee, S. W.; Lee, S. K.; Belcher, A. M. *Adv. Mater.* **2003**, 15, 689
28. (a) Mirkin, C. A.; Letsinger, R. L.; Mucic, R. C.; Storhoff, J. J. *Nature*, **1996**, 382, 607 (b) Xiao, Y.; Patolsky, F.; Katz, E.; Hainfeld, J. F.; Willner, I. *Science*, **2003**, 299, 1877 (c) Nam, J.-M.; Thaxton, C.S.; Mirkin, C.A. *Science* **2003**, *301*, 1884 (d) Park, S. J.; Tanton, T. A.; Mirkin, C. A. *Science*, **2002**, 295, 1503
29. Heeger, A. J. *Angew. Chem. Int. Ed.* **2001**, 40, 2591
30. (a) Holtz J. H.; Asher, S. A., *Nature*, **1997**, 389, 829 (b) He, H.; Zhu, J.; Tao, N. J.; Nagahara, L. A.; Amlani I.; Tsui, R., *J. Am. Chem. Soc.*, **2001**, 123, 7730 (c) Martin, C. R. *Science* **1994**, *266*, 1961 (d) Burroughes, J. H.; Jones, C. A.; friend, R. H. *Nature*, **1988**, 335, 137 (e) Wohlgenannt, M.; Tandon, K.; Mazumdar, S.;

Ramasesha, S.; Vardeny, Z. V. *Nature*, **2001**, 409, 494 (f) Yu, G.; Gao, J.; Hummelen, J. C.; Wudl, F.; Heeger, A. J. *Science*, **1995**, 270, 1789

31. (a) Zhou, Y.; Itoh, H.; Uemura, T.; Naka K.; Chujo, Y., *Chem. Commun.*, **2001**, 613 (b) Corbierre, M. K.; Cameron, N. S.; Sutton, M.; Mochrie, S. G. J.; Lurio, L. B.; Rühm A.; Lennox, R. B., *J. Am. Chem. Soc.*, **2001**, 123, 10411 (c) Manners, I., *Science*, **2001**, 294, 1664 (d) Liu, Y. C.; Chuang, T. C. *J. Phys. Chem. B,* **2003**, 107, 12383
32. (a) Freeman, R. G.; Grabar, K. C.; Allison, K. J.; Bright, R. M.; Davies, J. A.; Guthrie, A. P.; Hommer, M. B.; Jackson, M. A., Smith, P. C.; Walter, D. G.; Natan, M. J. *Science,* **1995**, 267, 1629 (b) Brown, K. R.; Natan, M. J. *Langmuir,* **1998**, 14, 726 (c) Marinakos, S. M.; Anderson, M. F.; Ryan, J. A.; Martin, L. D.; Feldheim, D. L., *J. Phys. Chem. B,* **2001**, 105, 8872
33. Marinakos, S. M.; Anderson, M. F.; Ryan, J. A.; Martin, L. D.; Feldheim, D. L. *J. Phys. Chem. B* **2001**, 105, 8872
34. Wang, D.; Caruso, F., *Adv. Mater.* **2001**, 13, 350
35. (a) Genies, E. M.; Boyle, A.; Lapkowski, M.; Tsintavis, C. *Synth. Met.* **1990**, 36, 139. (b) MacDiarmid, A. G.; Chiang, J. C.; Richter, A. F. *Synth. Met.* **1987**, 18, 285.
36. (a) Yue, J.; Wang, Z. H.; Cromack, K. R.; Epstein, A. J.; MacDiarmid, A. G., *J. Am. Chem. Soc.* **1991**, 113, 2665 (b) Wei, X. L.; Wang, Z. H.; Long, S. M.; Bobeczko, C.; Epstein, A. J., *J. Am. Chem. Soc.* **1996**, 118, 2545 (c) Chan, H. S. O.; Neuendorf, A. J.; Ng, S. C.; Wong, P. M. L.; Young, D. J., *Chem. Commun.* **1998**, 1327 (d) Chen, S-A; Hwang, G-W, *J. Am. Chem. Soc.* **1995**, 117, 10055
37. (a) Liu, W.; Kumar, J.; Tripathy, S.; Senecal, K. J.; Samuelson, L., *J. Am. Chem. Soc.* **1999**, 121, 71 (b) Liu, W.; Cholli, A. L.; Nagarajan, R.; Kumar, J.; Tripathy, S.; Bruno, F. F.; Samuelson, L., *J. Am. Chem. Soc.* **1999**, 121, 11345
38. Yoshida, K.; Shimomura, T.; Ito, K.; Hayakawa, R., *Langmuir*, **1999**, 15, 910
39. (a) Huang, J.; Virji, S.; Weiller, B. H.; Kaner, R. B., *J. Am. Chem. Soc.* **2003**, 125, 314 (b) Wei, Z.; Zhang, Z.; Wan, M., *Langmuir*, **2002**, 18, 917 (c) Liang, L.; Liu, J.; Windisch Jr., C. F.; Exarhos, G. J.; Lin, Y., *Angew. Chem. Int. Ed.* **2002**, 41, 3665
40. Dinsmore, A. D.; Hsu, M. F.; Nikolaides, M. G.; Marquez, M.; Bausch, A. R.; Weitz, D. A. *Science*, **2002**, 298, 1006

41. Lin, Y.; Skaff, H.; Emrick, T.; Dinsmore, A. D.; Russel, T. P. *Science*, **2003**, 299, 226
42. Dubertret, B.; Skourides, P.; Norris, D. J.; Noireaux, V.; Brivanlou, A. H.; Libchaber, A. *Science*, **2002**, 298, 1759
43. Mandal, S.; Arumugam, S. K.; Adyanthaya, S. D.; Pasricha, R.; Sastry, M. *J. Mater. Chem.* **2003**, 13, (DOI: 10.1039/b 308180j)
44. Reviakine, I.; Georgious, D. K.; Velikov, P. G. *J. Am. Chem. Soc.* **2003**, 125, 11684
45. Chen, B. D.; Cilliers, J. J.; Davey, R. J.; Garside, J.; Woodburn, E. T. *J. Am. Chem. Soc.* **1998**, 120, 1625
46. (a) Graner, F.; Jiang, Y.; Janiaud, E.; Flament, C. *Phys. Rev. E* **2001**, 63, 011402 (b) Glazier, J. A.; Weaire, D. *J. Phys.: Condens. Matter*, **1992**, 4, 1867 (c) Jiang, Y.; Swart, P. J.; Saxena, A.; Asipauskas, M.; Glazier, J. A. *Phys. Rev. E*, **1999**, 59, 5819
47. (a) Niemeyer, C. M., *Angew. Chem. Int. Ed.* **2003**, 42, 5796 (b) Niemeyer, C. M., Adler, M. *Angew. Chem. Int. Ed.*, **2002**, 41, 3779 (c) Niemeyer, C. M. *Angew. Chem. Int. Ed.*, **2001**, 40, 5128 (d) Niemeyer, C. M. *Science*, **2002**, 297, 62.

CHAPTER 2

SPECTROSCOPIC OBSERVATION AND CONTROL OF MARANGONI CONVECTION DRIVEN UPWARD FLUID MOVEMENT ALONG A SINGLE SOAP BUBBLE FILM

2.1 Simultaneous Measurement of Flowing Fluid Layer and Film Thickness of a Soap Bubble using a UV-Visible spectrophotometer

2.1.1 Introduction

Marangoni effect (ME), known for more than a century, is the flow of a liquid driven by surface tension gradient that can be created by gradient of temperature or surfactant concentration[1]. This effect is known to play a key role in interfacial transport of fluids[2], formation of tears of wine[3], thinning of soap films[4-7], wetting and dewetting[8-14] behavior of thin liquid films with wide range applications that include lithography[15], microscopic fluidic devices[16-18], spraying of insecticides, paints and inks[19]. Its technological application potential has lead to a vast growth in the literature with reports of both theoretical[20-21] and experimental[21-22] investigations under various conditions and the literature continues to grow. Recently, Pileni and coworkers[23] have demonstrated the self-assembled formation of rings and hexagonal compact network of nanocrystals of different sizes and shapes of various materials, principally driven by the thermally induced hydrodynamic instabilities that are governed by Marangoni effect.

ME plays significant role in the evolution of foams, understanding the property of which is not only a challenging scientific endeavor but also has important consequences in areas like fire retardants, nanoparticles engineering, petroleum products, enhanced oil recovery, and even in the analysis of amniotic fluid and lung surfactants helpful in predicting the lung maturity of a foetus[4]. In general, a soap film has traditionally been used as a model system in understanding the behavior of foams that include thinning of the film and fluid flow. Among other probes, spectroscopic[24-27] investigations in soap films have resulted in the understanding of time dependent changes in film thickness, drainage of various components, microenvironments of the aqueous core of a black soap film and the structure of thin films. On the other hand, there is a lack of data regarding the time dependent thickness behavior of Marangoni convection driven fluid flow in soap films and bubbles and its relationship with the film thickness. We have sought to address the phenomena occurring in soap films by spectroscopic investigations of films in a single soap

bubble. In this regard, our motivation has been to understand the properties of a bubble, which would probably represent the foam better than a film that has traditionally been used. Further, spectroscopic probes can generate unique information regarding time dependent changes in the film thickness, changes in chemical composition of a bubble film and properties of a probe molecule in a constrained environment like a common black film (CBF). Our group has recently developed[28-29] a method of stabilizing a soap bubble necessary for spectroscopic observations. The earlier method involved repeated boiling of an aqueous solution of sodium dodecyl sulfate (SDS) and making a bubble from the solution. UV-visible and FTIR spectroscopic techniques were used to follow time dependent changes in thickness and chemical composition of soap bubbles.

In this thesis, we report the stabilization of a single soap bubble from an aqueous solution of a mixture of SDS and 1-dodecanol. In addition, when such a bubble was placed on top of a pool of soap solution, Marangoni flow driven upward movement of liquid could also be observed. The thickness of this layer of liquid was measured by UV-visible spectroscopic observation using the principle of interferrometry. The same principle allowed us to simultaneously measure the time-dependent film thickness and ME driven flowing fluid layer thickness. We report such measurements for two cases of soap bubble configuration: a vertical bubble and a horizontal bubble. A vertical bubble is a bubble floating on a solution with vertical axis of symmetry (Figure 2.1.4 Top). A horizontal bubble was blown from a soap film placed at the end of a horizontally aligned tube (Figure 2.1.5 Top).

Partial reflections of a beam of light from the surfaces of a thin, semi-transparent film cause interference of light (Figure 2.1.1a). The interference fringes become visually observable when the thickness of the film is on the order of a wavelength of visible light. Thus if a soap film is kept inside the sample compartment of a UV-visible spectrophotometer and the wavelength of light is scanned, a set of maxima and minima occurring at different wavelength is observed (Figure 2.1.1b). The number of such maxima and minima and the separation between two consecutive maxima or minima depend on the

thickness of the bubble film. Thus the film thickness can be monitored from the UV-visible spectra of a film using the following well-known equation[30].

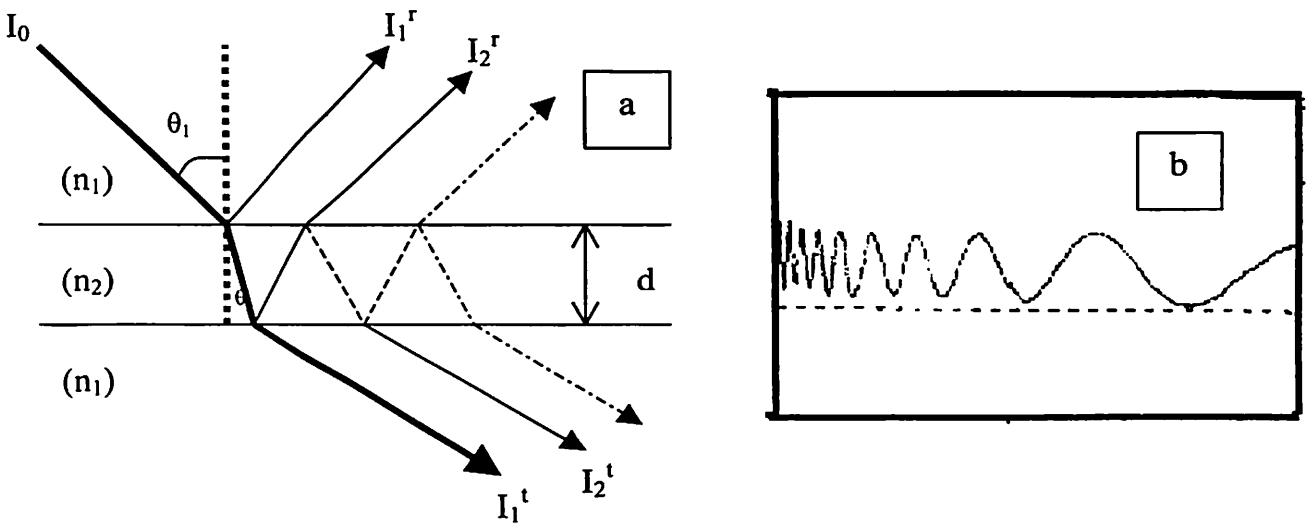

Figure 2.1.1. (a) Origin of interference fringes from a soap bubble film with thickness d with n_1, n_2 being the indices of refraction of air and foam film respectively. (b) Typical absorption spectrum due to Interference of light on a soap bubble film, when scanned in a UV-visible spectrophotometer in the wavelength range 200-1100 nm.

$$\nu = \left[\frac{n(\lambda_1)}{\lambda_1} - \frac{n(\lambda_2)}{\lambda_2}\right] / N_{cyc} \qquad 1$$

$$d = (2\nu)^{-1} \qquad 2$$

Where $n(\lambda_1)$ and $n(\lambda_2)$ are the refractive indices of the film at wavelength λ_1 and λ_2. N_{cyc} is the number of cycles in the interference fringes and d is the thickness of the film. However, in a bubble, with our probe geometry, the light beam traveled through two such films with curved surfaces. Considering the drainage of the liquid from the film surface to be symmetrical around the vertical axis of the bubble, it may be assumed that the thickness of both the films are same at any point of time. Hence the interference pattern arising out of the light passing through two such films would be same as that of the single film. Thus the

thickness obtained by applying the above equations 1 and 2 to the experimentally observed absorption maxima and minima would be the thickness of one such film. We have shown at the end of this part of the chapter (2.1.5 Appendix) that the same equation of thickness measurement can be used for a curved bubble surface film as in our case. In addition, we have assumed the refractive index of the bubble film to be wavelength-independent, which in rigorous sense is not true, but is within the experimental error of our observations.

Our UV-visible spectroscopic observation of a single soap bubble indicated the possibility of simultaneous measurement of ME driven flowing fluid layer thickness along with the time dependent changes of the thickness of the soap films as the spectra consisted of a set of narrowly spaced, weaker absorption maxima and minima superimposed on widely spaced and stronger absorption maxima and minima. The above equation was used to calculate thickness of the film from the widely spaced stronger absorption maxima and minima, while that of ME driven layer thickness was calculated from the narrowly spaced weaker maxima and minima.

We found that the thickness of the upwardly flowing fluid layer was much larger than the film thickness and was independent of the film thickness. The estimated thickness of the layer was about 6.94 ± 0.15 μm for a vertical bubble and 4.75 ± 0.09 μm for a horizontal bubble. Also, the thickness of the layer remained nearly constant throughout the observation period whereas the thickness of the bubble film changed continuously during that time. However, the flow was not observed after some time, although the film thickness was considerably higher than the final low thickness. Further, no such upward fluid movement was observed in a vertical soap film suggesting that liquid from the reservoir flows upward due to surface tension gradient created by stretching of a film to form soap bubble. Finally, the intensity of the interference maxima and minima of absorbance due to moving liquid layer diminished gradually with the thinning of the bubble film indicating change in the refractive index.

2.1.2 Experimental Section

Stabilization of Single Soap Bubbles

0.2 g (0.07 M) sodium dodecyl sulfate (SDS) (Aldrich) and 0.02g (0.01 M) 1-dodecanol were mixed in 10 ml of MilliQ water. The mixture was then gently heated at around 45^0C to obtain a homogeneous solution. 0.5 ml of the solution was poured over an inverted beaker (5 ml) enclosed inside a 250 ml beaker. An air bubble of about 19-20 mm in diameter was blown on the top of the inverted beaker using a pipette tip in presence of high-pressure air. We observed that stable bubbles could not be formed from only SDS solution. We tried to observe stability of a soap bubble at other concentrations of the mixture and we found that the reported concentration suited our experimental requirements the most. We also found that larger and smaller diameter bubbles could also be made stable. However, our experimental geometry and probe beam size limited the size to a value of about 20 mm.

UV-visible spectroscopic observations

A basic experimental setup for the spectroscopic observations of single soap bubbles is shown in Figure 2.1.2. A 250 ml flat top beaker was used for this purpose. Two 20 mm diameter holes were made on the wall of the beaker at the opposite ends. Two 25 mm diameter sapphire windows were glued onto these holes. A small 5 ml beaker was glued at the bottom of the large beaker in an upside down position. For observations with vertical bubbles, 0.5 ml of the solution was poured onto the inverted small beaker and a bubble of about 20 mm size was blown. The larger beaker was immediately covered with a lid. The whole setup was kept inside the sample compartment of a Hitachi U-2001 UV-visible spectrophotometer such that the probe beam passed through the center of the bubble and the wavelength of light was then scanned. To increase the stability of the bubbles the humidity of the chamber was increased by placing a piece of ordinary filter paper soaked with water inside the beaker. Another large beaker with identically placed sapphire windows was used as the reference. Horizontal films and bubbles were made from the horizontal end of a T-shaped quartz tube that was kept hanging from the lid of a 250 ml beaker. For the horizontal bubble, a film was first formed at one horizontal end of the tube by dipping into the soap solution, while the other end of the tube was closed with a sapphire window. The third

opening of the tube was closed with a rubber stopper and used for air blowing or injecting solution. A bubble was formed from the film by air blowing. About 0.5 ml of the soap solution was then injected into the tube such that a drop of the solution remained hanging at the bottom of the bubble. Optical measurements for the horizontal bubbles were performed by putting the larger beaker inside the sample compartment of a Hitachi U-2001 UV-visible spectrophotometer. For calculation of the film thickness as well as flowing fluid layer thickness we have used a value of 1.333 as the refractive index and have assumed that it is independent of the film thickness or fluid layer thickness. The experiments were performed typically in the range of 21-25 ^{0}C.

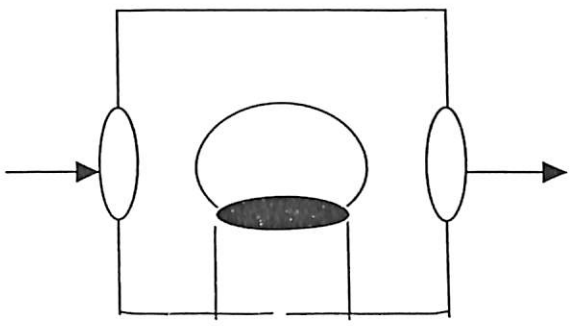

Figure 2.1.2. A pictorial representation of the experimental set up used in our studies. Light is passed through two sapphire windows of the beaker kept inside sample compartment of the UV-visible spectrophotometer. A vertical bubble is made on the top of a smaller inverted beaker placed inside the larger beaker as shown.

2.1.3 Results and Discussion

A vertical Soap Film

In Figure 2.1.3 we present the UV-visible absorption spectra obtained from a single vertical soap film. The soap film was placed on one end of a horizontally aligned quartz tube. The other end of the tube was kept open, thereby removing the possibility of having any curvature of the soap film. The time dependent changes in the thickness of the vertical soap film were observed by scanning over the range of 200-1100 nm. As observed from the set of spectra the thickness decay was gradual and slow. The interference fringes do not appear for the first six minutes from the time of formation of the film. The peaks due to

thickness of the film started appearing in about 7 min from the time of formation as shown in Figure 2.1.3D. The thickness changed from 472 nm at 7-8 min to about 228 nm at about 88 min from the time of the formation of the film. The film then became very thin, and interference fringes no longer could be observed. At this thickness, the film remained stable for hours. It is important to note here that in the case of vertical foam films, there were no observable interference peaks due to Marangoni effect driven fluid flow throughout the period of observation.

A Vertical Bubble

The results obtained with a vertical bubble were observed to be different from the film. Figure 2.1.4 shows a collection of typical time-dependent UV-visible absorption spectra of a vertical bubble. The light beam passed through two films of the bubble. In case of vertical bubbles the interference fringes started appearing from the time of the formation of the bubble. We believe that these fringes occurred due to the ME driven fluid flow as they were observable for a long time with nearly constant thickness of the fluid layer and such fringes did not appear in the case of the vertical film (Figure 2.1.3). For the initial 18 minutes of the bubble formation, interference fringes only due to the ME driven fluid flow was observed. From the 19th minute, the interference fringes due to ME fluid flow could be seen appearing superimposed on the interference fringes occurring due to thickness changes of the film (Figure 2.1.4 D-I). The thickness of the ME fluid layer remained nearly constant with a value varying between 7.16 and 6.81 μm. The fluid flow could also be observed when an ordinary diode laser pointer beam (red) was passed through the bubble and then defocused with a 10 cm focal length lens and projected onto a wall. A fountain of fluid could be seen moving up in the beginning, and with time, drops of fluid were observed moving up along the bubble. The fluid flow was not observed when the bubble film had become thinner and colorless. The spectroscopic observation shown in Figure 2.1.4 D-I was of particular significance as ME fluid layer thickness remained nearly constant with values between 6.90 and 6.81 μm throughout the time interval of 19-50 minutes even though the thickness of the film had decreased from 1781 to 482 nm. This might be due to two parallel processes occurring simultaneously in the bubble film. While the thickness of the film decreased due to drainage of the components, the restoring fluid moved upwards. This could

be observed until the thickness of the film was about 482 nm after which the film thickness continued to reduce due to drainage whereas ME driven fluid movement was not observed. The above observations suggest that flow of fluid up along a symmetrical vertical bubble due to Marangoni convection driven fluid flow runs parallel to film drainage but in the opposite direction up to a film thickness of about 500 nm. Below this film thickness the ME driven fluid flow could not be observed notwithstanding the continuation of the drainage of the film. It is possible that the upward movement of fluid continues, until the film thickness becomes very thin and constant, but could not be observed for a longer time here due to weak signal intensity, whereas the interference peaks due to film thickness remain stronger for a longer period of time. The gradual decrease in intensity of the interference peaks with time due to ME fluid flow is evident in Figure 2.1.4 B through I. It may be argued here that Marangoni convection driven fluid flow might help restore the thickness of the thinning film given the slow rate of decay of the film thickness.

The Horizontal Bubbles

The upward movement of fluid by the surface tension gradient created by the stretching of the film surface to form bubble was further confirmed by performing the time-dependent absorption spectra of the bubble films of two horizontal bubbles one probed along the axis of the bubble and the other perpendicular to it. The UV-visible absorption spectra are shown in Figures 2.1.5 and 2.1.6 for the above two systems respectively. As observed from the spectra, interference fringes both due to ME fluid convection and thickness changes were observed by stretching the film of a vertical film to make horizontal bubble. A drop of solution was kept hanging at the bottom of the bubble (added after its formation) for improved signal of the ME fluid flow. Like the vertical bubble, for both the measurements, the first few absorption spectra consisted of maxima and minima due to ME fluid movement only. The calculated fluid layer thickness values were 4.62, 2.90, and 2.84 μm for spectra in parts A, B, and C of Figure 2.1.5, respectively, and 4.82, 4.89, 4.80, and 4.76 μm for spectra in panels A-D of Figure 2.1.6, respectively. These values are obtained from the observed spectra during the first 6 min of measurement (8 min for the perpendicular to the axis probe case) after the bubble formation. The film thickness peaks started appearing in about 7 min as shown in Figure 2.1.5 (9 min as in Figure 2.1.6). Hereafter the absorption maxima and

minima originating from ME fluid flow were weak, and only rough estimates could be made about the thickness. The estimated thickness values of the ME-driven flowing fluid were about 4.66, 4.70, 4.68, and 4.70 μm (parts D-G of Figure 2.1.5, respectively) while the film thickness went up from 276 to 358 nm. It is interesting to note here that for the axially probed horizontal bubble, the film thickness had already gone down to about 276 nm in about 7 min from the formation of the bubble. The thickness then went up to about 378 nm in about 12 min and then again went down. Similar results were obtained for the bubble probed sideways as shown in Figure 2.1.6. These results are explained based on the fact that in a bubble generated by stretching a horizontal film the initial thickness of the bubble film would be much less than the thickness of the parent film and also less than that in the case when a bubble is blown up along a vertical axis from a pool of solution. On the other hand when a vertical bubble is blown on the top of a solution, upward movement of the fluid from the solution can restore thickness of the bubble film continuously. In case of horizontal bubble, the upward movement of the fluid from the drop, due to the Marangoni convection, helps increase the film thickness after the bubble formation. After the initial increase of the thickness of the film, the drainage of the film dominates over the restoring fluid flow and hence the thickness again decreases gradually. Other observations that require particular attention are the values of thickness of the ME fluid layer in parts B and C of Figure 2.1.5, which are 2.90 and 2.84 μm, respectively. These values are very different from the average value of 4.75 ± 0.09 μm observed for the horizontal bubbles probed both axially and sideways. This may be due to initial stabilization of the bubble film after its expansion. In both the vertical bubble and horizontal bubble probed sideway, ME fluid layer probed has a complete ring to transverse while moving up and then possibly down. On the other hand, the ME fluid layer probed axially transverse half a circle as the water layer reaches glass surfaces once it reaches the top of the bubble. Hence the actual behavior of the fluid layer thickness might be different for the horizontal bubble probed axially and sideway.

2.1.4 Conclusion

In this chapter, I have described a new method of stabilizing single soap bubbles and reported to the results of UV-visible spectroscopic investigations of such bubbles. The

results indicate the soap bubbles were stable for hours needed for the investigation by spectroscopic methods. We also found that the time evolution of gravitational drainage of vertical soap films was similar to commonly observed film drainage. On the other hand for the case of bubbles (both vertical and horizontal) the time evolution had two components. One was the slow gravitational drainage while the other was Marangoni effect driven upward fluid flow. The thickness of this layer was 6.94 ± 0.15 μm for the vertical bubbles and 4.75 ± 0.09 μm for the horizontal bubbles. Also, the upwardly mobile layer occurred with time independent constant thickness while the thickness of the film gradually decreased. After a certain time of evolution the ME driven fluid flow could not be observed while the gravitational drainage continued for a significantly longer time. Among other factors, like the film thickness, the decrease in refractive index[30] of the fluid layer may contribute to the decrease in the transmitted light intensity.

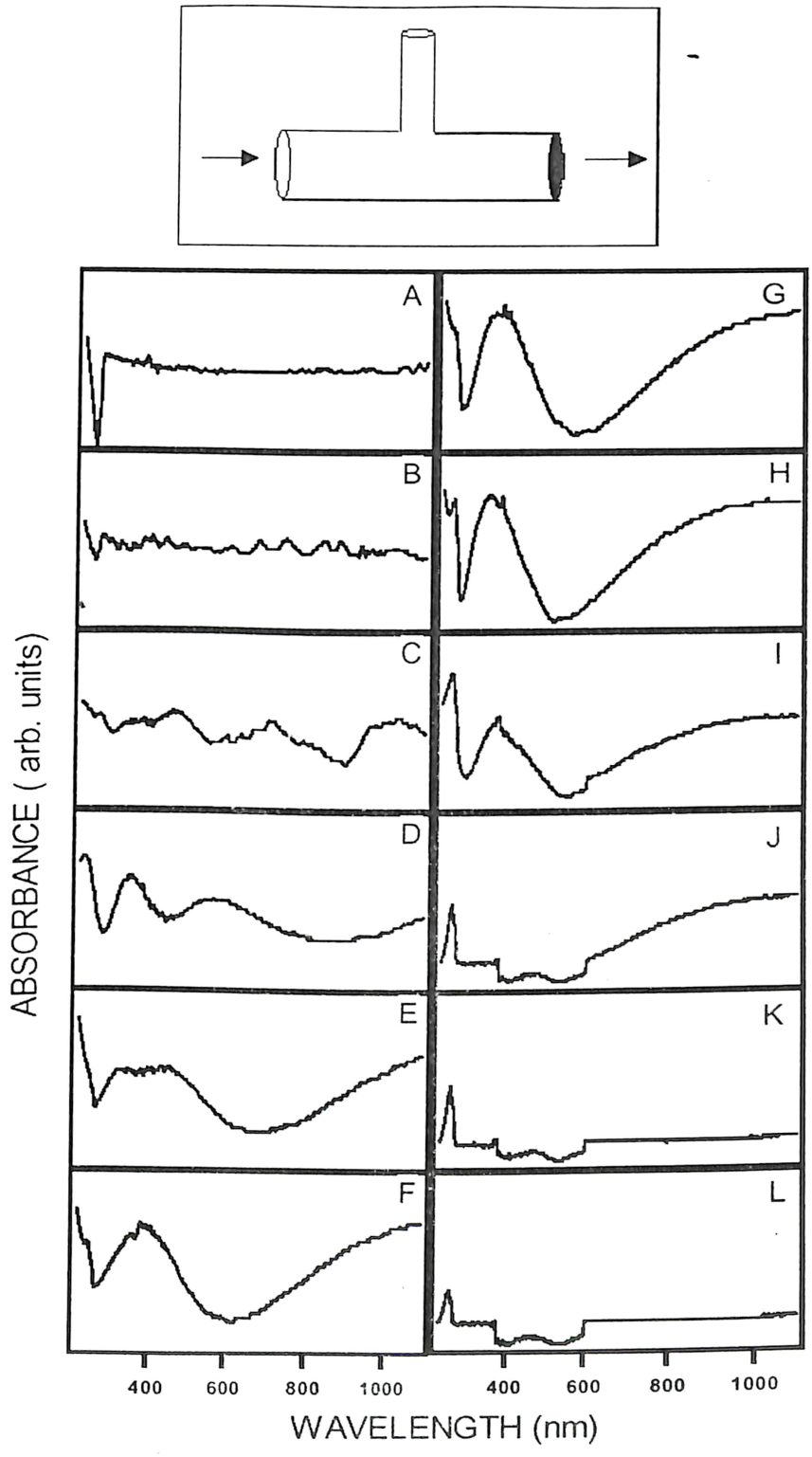

Figure 2.1.3. ***Top****: Schematic representation of the experimental set up containing a vertical soap film.* ***Below:*** *Time – dependent UV - visible spectra of the vertical film: (A) 0-2 min; (B) 5-6 min; d_2 = 624 nm; (C) 7-8 min; d_2 = 472 nm; (D) 9-10 min; d_2 = 396 nm, (E) 11-12 min; d_2 = 270 nm, (F) 13-14 min; d_2 = 254 nm, (G) 17-18 min; d_2 = 242 nm, (H) 29-30 min; d_2 = 240 nm, (I) 88-89 min; d_2 = 228 nm, (J) 90 – 91 min, (K) 92-93 min and (L) = background spectrum after bursting the film after 95 min from the time of formation. d_2 = estimated thickness of the vertical film.*

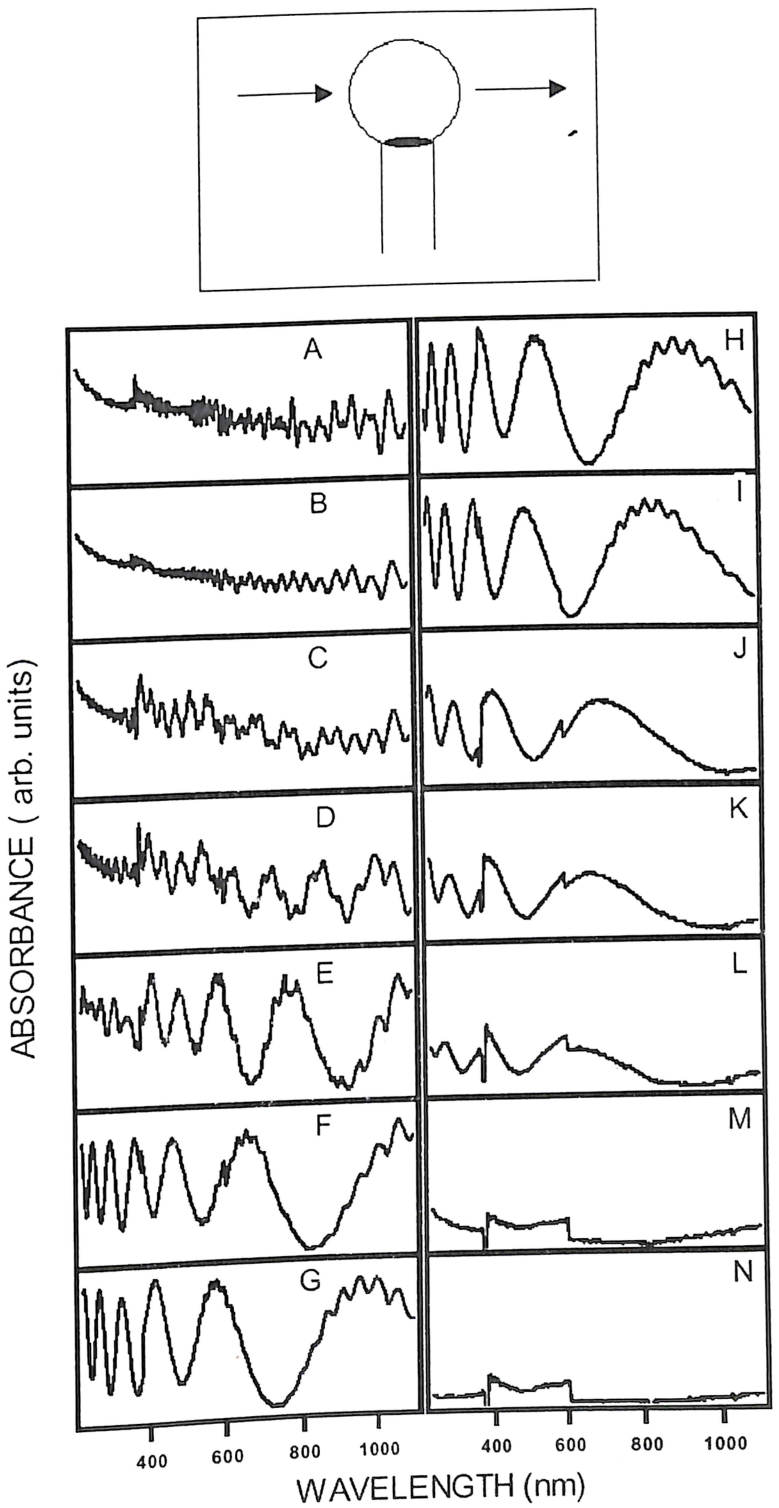

Figure 2.1.4. ***Top****: Schematic representation of the experimental setup containing a Vertical soap bubble.* ***Below****: UV-vis absorption spectra of the vertical bubble: (A) 0-2 min; d_1 = 7.16 μm, (B) 6-8 min; d_1 = 7.11 μm, (C) 16-18 min; d_1 = 7.04 μm, (D) 19-20 min, d_1 = 6.9 μm, d_2 = 1781 nm, (E) 21-22 min; d_1 = 6.81 μm, d_2 = 995 nm, (F) 28-30 min; d_1 = 6.82 μm, d_2 = 647 nm, (G) 34-36 min; d_1 = 6.85 μm, d_2 = 579 μm, (H) 40-41 min; d_1 = 6.82 μm, d_2 = 536 nm, (I) 50-51 min; d_1 = 6.87 μm, d_2 = 482 nm, (J) 62-63 min; d_2 = 408 nm, (K) 64-65 min; d_2 = 378 nm, (L) 66-67 min; d_2 = 364 nm, (M) 68-69 min, (N) background spectra after bursting the vertical bubble after 70 min of formation. d_1= estimated thickness of the water peaks, d_2 = estimated thickness of the bubble film.*

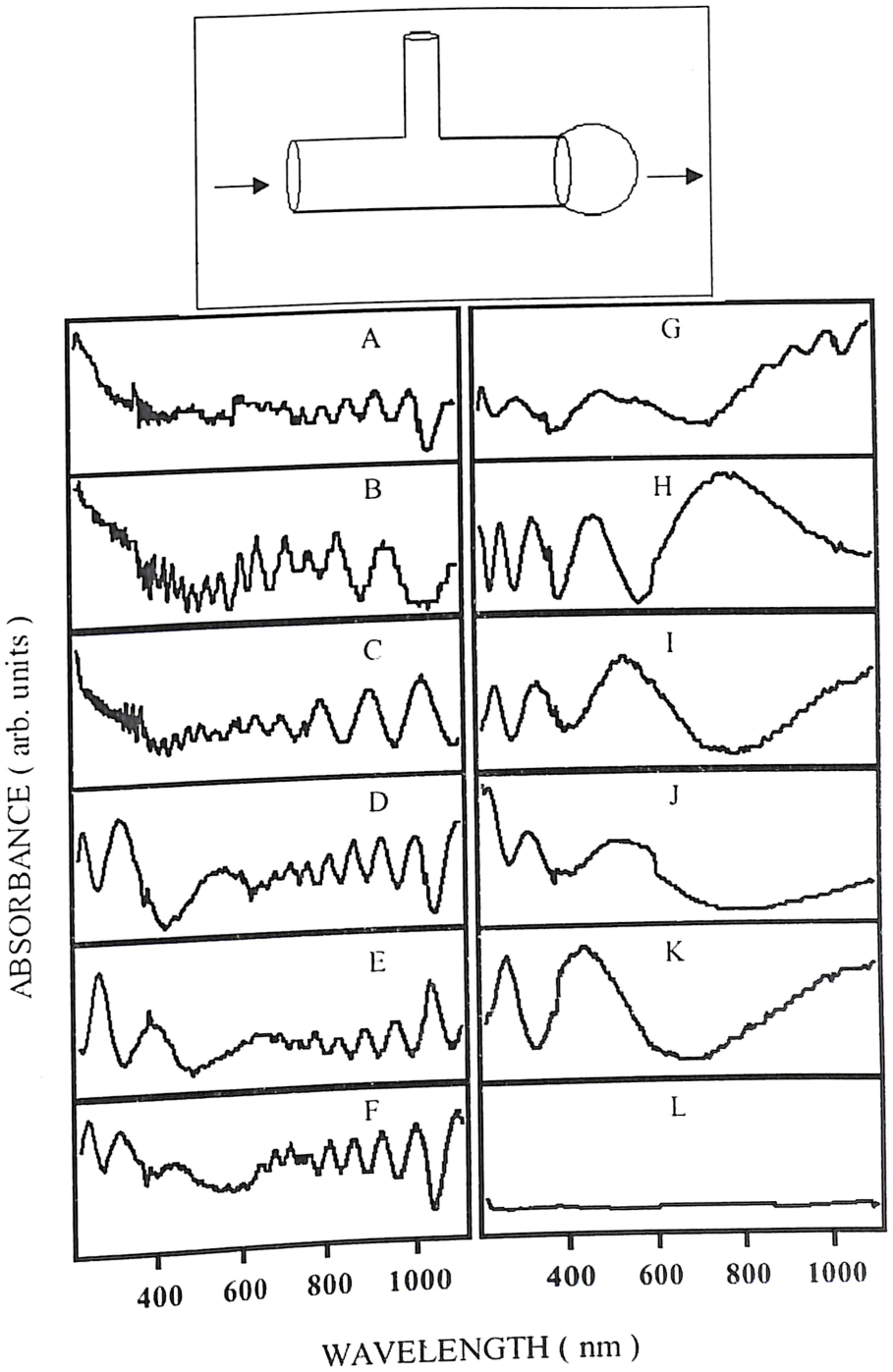

Figure 2.1.5. ***Top:*** *Schematic representation of the experimental setup containing the horizontal bubble probed axially.* ***Below:*** *Time dependent UV-vis absorption spectra of the axially probed horizontal bubble: (A) 0-2 min; d_1 = 4.62 μm, (B) 3-4 min; d_1 = 2.90 μm, (C) 5-6 min; d_1 = 2.84 μm, (D) 7-8 min, d_1 = 4.66 μm, d_2 = 276 nm (E) 9-10 min; d_1 = 4.70 μm, d_2 = 320 nm, (F) 11-12 min; d_1 = 4.68 μm, d_2 = 378 nm (G) 13-14 min; d_1 = 4.70 μm, d_2 = 358 nm, (H) 15-16 min; d_2 = 480 nm, (I) 17-18 min; d_2 = 340 nm, (J) 19-20 min; d_2 = 310 nm, (K) 21-22 min; d_2 = 240 nm, (L) 23-24 min. d_2 = estimated thickness of the fluid layer occurring due to Marangoni Effect, d_1= estimated thickness of the bubble film.*

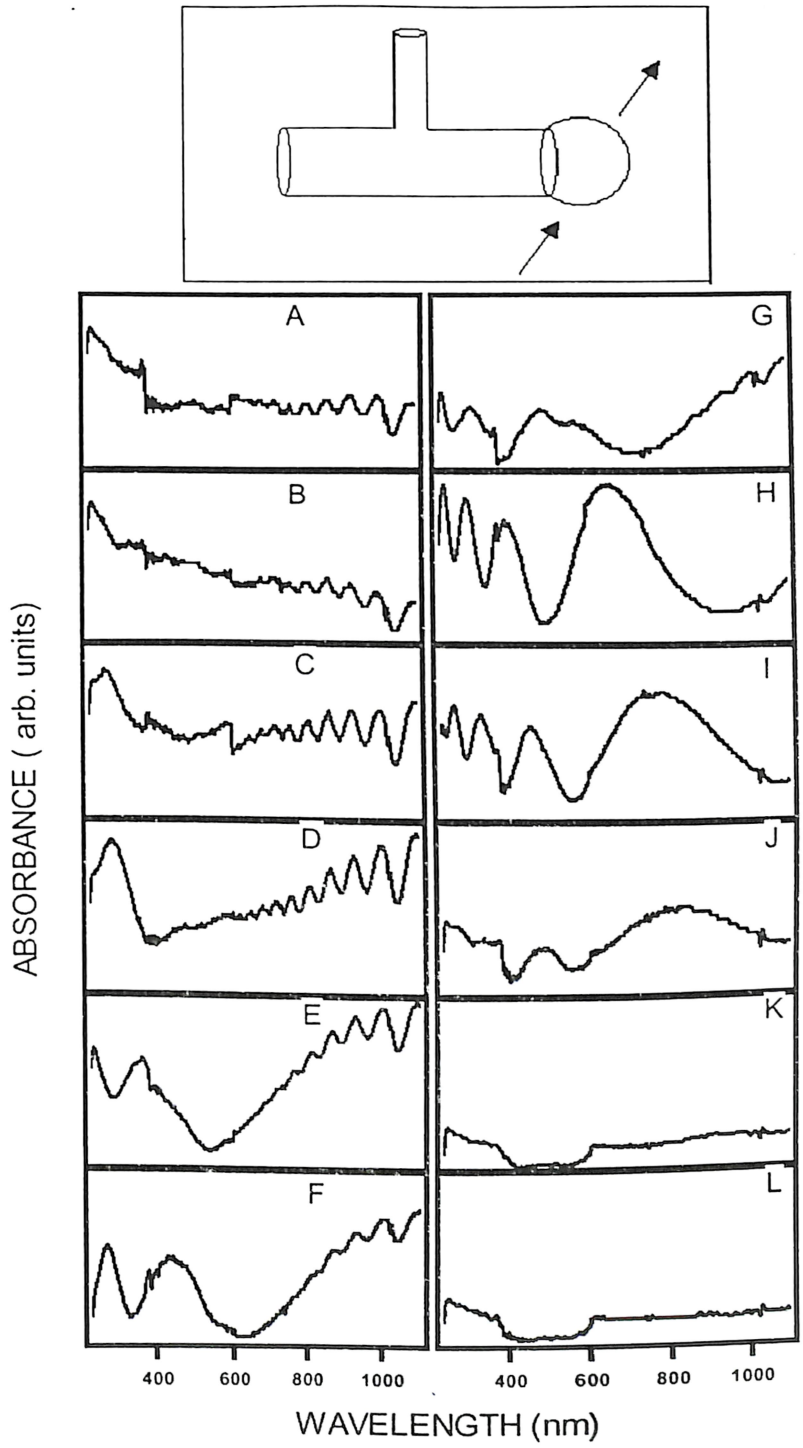

Figure 2.1.6. ***Top:*** *Schematic representation of the experimental set up containing horizontal bubble probed sideway.* ***Below:*** *Time dependent UV-visible absorption spectra of the above horizontal bubble (A) 0-2 min; d_1 = 4.82 μm, (B) 3-4 min; d_1 = 4.89 μm, (C) 5-6 min; d_1 = 4.80 μm (D) 7-8 min; d_1 = 4.76 μm, (E) 9-10 min; d_1 = 4.65 μm; d_2 = 270 nm, (F) 11-12 min; d_1 = 4.68 μm; d_2 = 364 nm, (G) 13-14 min; d_1 = 4.65 μm; d_2 = 386 μm; (H) 15-16 μm; d_2 = 524 nm, (I) 17-18 μm; d_2 = 341 nm, (J) 19 –20 min; d_2 = 244 nm, (K) 21 –22 min, (L) 23-24 min. background spectrum after bursting the bubble. d_1= estimated thickness of the fluid layer occurring due to Marangoni Effect, d_2 = estimated thickness of the bubble film.*

2.1.5 Appendix

When a light beam of parallel rays impinge on a spherical soap bubble where

θ = Angle of incidence

R = Radius of curvature of the sphere

D = Thickness of the spherical film

n(λ) = Refractive index of the film at wavelength λ

H = Height of the incident light beam from the center

N = Number of cycles in the interference fringes

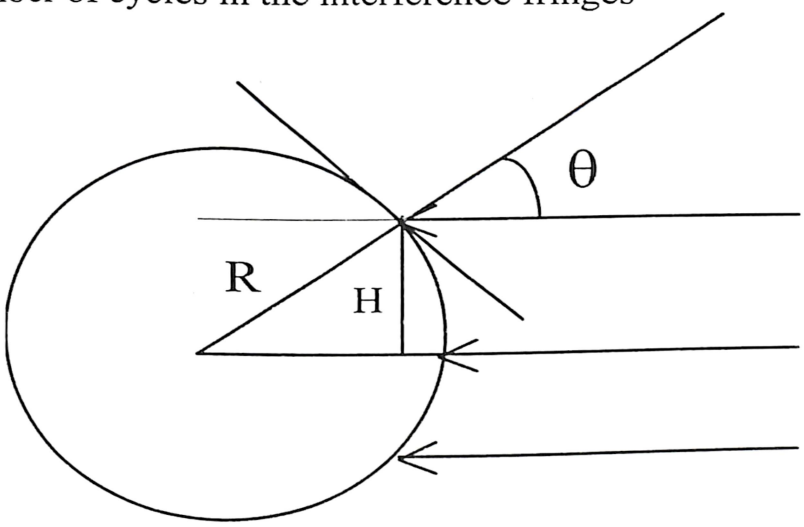

Then $$\theta = 90^0 - \cos^{-1}(H/R) \quad \text{A1}$$

For constructive interference, using the equation of thin parallel films,

$$\frac{2n(\lambda_2)d\cos\theta}{m+1} = \lambda_2 \quad \text{A2}$$

and $$\frac{2n(\lambda_1)d\cos\theta}{m+N+1} = \lambda_1 \quad \text{A3}$$

Therefore, $$d = \frac{N}{2\cos\theta}\left[\frac{n(\lambda_1)}{\lambda_1} - \frac{n(\lambda_2)}{\lambda_2}\right]^{-1} \quad \text{A4}$$

In our experimental apparatus, maximum height of the light beam was about 4 mm (the width of the beam was about 1 mm) and the radius of curvature of the film was about 9.5 mm and hence maximum deviation from normal incidence would be about 24.9^0 corresponding to an error in measurement of about 10% (if the equation corresponding to normal incidence is used instead i.e. equation 2 instead of A4). Considering the variation of angle of incidence at different height of the beam, if we take an average value of H to be 2 mm (angle of incidence 12.2^0), then the average deviation turns out to be 2.3%. This is nearly equal to the error limit of the calculated results of the experiment data.

For example, let us consider the graphs in Figures 2.1.4D and 2.1.4E separated by an average measurement time of 2 minutes. If equation 2 is used the average thickness of film is calculated to be 1767 nm and that of fluid layer is 6.76 μm for graph 2.1.4D while those values are found to be 1808 nm and 6.92 μm if equation A4 is used instead. While the corresponding calculations for 2.1.4E results in a film thickness value of 996 nm and fluid layer thickness value of 6.76 μm if equation 2 is used and 1016 nm and 6.91 μm if equation A4 is used. Also, for the graph 2.1.4D, calculations using equation A4 at various wavelength ranges result in the following film thickness and fluid Layer thickness values for the angle of incidence 12.2^0.

Wavelength Range (nm)	Film Thickness (nm)	Wavelength Range (nm)	Fluid Layer Thickness (μm)
277 – 332	1760	----	----
467 – 585	1790	686 – 773	6.99
776 – 926	1846	974 – 1090	6.92

Thus while using equation 2 or A4 we obtain values close to each other for each graph, the thickness value changes dramatically in 2 minutes of measurement time. Also, the variation of thickness during a single complete scan of wavelength ranges is significant (calculations from Figure 2.1.4D). Hence the use of equation 2 may be sufficient for the

above calculations. However the source of error for the calculation may be due to the assumption that the film has the index of refraction of water and that the film has same refractive index across the entire thickness. We assume that this source of error is negligible in film thickness measurement. In all our calculations above the values of refractive indices were taken from reference.

2.1.6 References:

1. Edwards, D.; Brenner, H.; Wasan D., *Interfacial transport processes and Rheology*, Butterworth-Heinemann: Boston, **1991**
2. (a) Chaudhury, M. K.; Whitesides, G. M., *Science*, **1992**, 256, 1539 (b) Ichimura, K.; Oh, S. K.; Nakagawa, M., *Science*, **2000**, 288, 1624 (c) Brochard, F., Langmuir, 1989, 5, 432 (d) Daniel, S.; Chaudhury, M. K.; Chem, J. C.; *Science*, **2001**, 291, 633 (e) Bain, C. D.; Burnett-Hall, G.; Montgomerie, R., *Nature*, **1994**, 372, 414 (f) Manning-Benson, S.; Bain, C. D.; Darton, R. C., *J. Colloid Interface Sci.* **1997**, 189, 109
3. Grunze, M., *Science*, **1999**, 283, 41
4. Exerowa, D. R.; Krugliakov, P. M. *Foams and Foam Films*: *Theory, Experiment, Application*; Studies in Interface Science; Elsevier: Amsterdam, **1998**; Vol. 5.
5. Prud'Homme, R. K., Khan, S. A., Eds. *Foams*: *Theory, Measurements and Applications*; Surfactant Science Series; Mercel Dekker: New York, **1995**; Vol. 57
6. Adamson, A. W.; Gast, A. P. *Physical Chemistry of Surfaces*, 6th ed.; John Wiley and Sons: New York, **1997**.
7. *Foams*: *Physics, Chemistry and Structure*; Wilson, A. J., Ed.; Springer-Verlag: Berlin, **1989**.
8. Troian, S. M.; Wu, X. L.; Safran, S. A. *Phys. Rev. Lett.* **1989**, 62, 1496.
9. Vanhook, S. J.; Schatz, M. F.; McCormick, W. D.; Swift, J. B.; Swinney, H. L. *Phys. Rev. Lett.* **1995**, 75, 4397.
10. Bestehorn, M. *Phys. Rev. Lett.* **1996**, 76, 46.
11. de Ruijter, M. J.; Blake, T. D.; De Connick, J. *Langmuir* **1999**, 15, 7836.
12. Semal, S.; Voue, M.; De Connick, J. *Langmuir* **1999**, 15, 7848

13. Reiter, G.; Khanna, R. *Langmuir* **2000**, 16, 6351.
14. Bergeron, V.; Bonn, D.; Martin, J. Y.; Vovelle, L. *Nature* **2000**, 405, 772
15. Xia, Y.; Whitesides, G. M. *Angew. Chem., Int. Ed. Engl.* **1998**, 37, 550.
16. Kataoka, D. E.; Troian, S. M. *Nature* **1999**, 402, 794.
17. Delamarche, E.; Benard, A.; Schmidt, H.; Michel, B.; Biebuyck, H. *Science* **1997**, 276, 779.
18. Carre´, A.; Gastel, J. C.; Shanahan, M. E. R. *Nature* **1996**, 379, 432.
19. Golovin, A. A.; Nepomnyashchy, A. A.; Pismen, L. M. *J. Fluid. Mech.* **1997**, 341, 317.
20. Denniston, C.; Yeomans, J. M. *Phys. Chem. Chem. Phys.* **1999**, 1, 2157.
21. Yaminsky, V. V.; Thuresson, K.; Ninham, B. W. *Langmuir* **1999**, 15, 3683
22. Yerushalmi - Rozen, R.; Kerle, T.; Klien, J. *Science* **1999**, 285, 1254.
23. Maillard, M.; Motte, L.; Ngo, A. T.; Pileni, M. P., *J. Phys. Chem.* **2000**, 104, 11871
24. Umemura, J.; Matsumoto, M., Kawai, T.; Takenaka, T. *Can. J. Chem.* **1985**, 63, 1713.
25. Cohen, R.; Exerowa, D.; Kolarov, T.; Yamanaka, T.; Tano, T. *Langmuir* **1997**, 13, 3172.
26. Du, X.; Liang, Y. *Phys. Chem. Chem. Phys.*, **2000**, 2, 137
27. Be´lorgey, O.; Benattar, J. J. *Phys. Rev. Lett.* **1991**, 66, 313.
28. Chattopadhyay, A., *Langmuir*, **1999**, 15, 7881
29. Chattopadhyay, A., *J. Chem. Educ.*, **2000**, 77, 1339
30. Huibers, P. D. T.; Shah, D. O. *Langmuir* **1997**, 13, 5995.
31. Huibers, P. D. T. *Appl. Opt.* **1997**, 36, 3785.

2.2 Visible Spectroscopic Observation of Controlled Fluid Flow up along a Soap Bubble Film from a Pool of Solution

2.2.1 Introduction

Directional flow of fluid across a gradient in concentration plays an key role in many important biological processes such as directional sensing and movement of eucaryotic cells[1,2], biochemical synthetic processes[3], biosensing[4], biomolecular separation[5] drug delivery systems[6] and also study of biological cell motility[7]. The past few years have witnessed a significant growth of research works in the design and fabrication of microfluidic devices, with controlled fluid flow within networks of microchannels, for applications such as in bioassays[8], microreactors and microelectromechanical systems[9]. In addition, the directional fluid flow is also important in phenomena such as wetting and dewetting of a liquid on a solid substrate[10], and the so-called Gibbs-Marangoni effect in foams[11]. Ability to control the directional flow has wide technological applications that include liquid crystal alignment[12] lithography techniques[13], commercial "lab-on-a-chip",[14] processing in food, and the agricultural, pharmaceutical, and cosmetic industries.[15] Parent and Devrotes[2] have demonstrated that chemotactic cells such as guanine nucleotide-binding protein (G-protein) can determine the direction and proximity of an extracellular stimulus (chemoattractants) and concentration gradient as low as 2% between front and back of the cell can direct movement which is very essential for the survival of the microbes and for the effectiveness of the immune system.

There has been a rapid growth in the literature with respect to surface tension driven fluid flow triggered by variations in temperature or composition on a liquid surface along with surface tension heterogeneity on a solid surface owing to their direct technological relevance. On the other hand, study of controlled fluid movement in thin liquid film at the gas liquid interface assumes significance due to technological applications in food, agricultural, pharmaceutical, and cosmetic industries. Traditionally, a soap film has been used as a model for studies in this regard. Surface tension driven Gibbs elasticity of soap films has been measured by Mysels et al.[16] by rapidly changing the surface area of the film.

Marangoni effect driven fluid flow at interfaces under various conditions including movement of fluid particles has been extensively studied.[17]

We were encouraged by our ability to stabilize a single soap bubble along with the spectroscopic observation of Marangoni effect in the bubbles. We were further interested in finding ways to have controlled surface tension gradient driven fluid movement up along the bubble film and we were successful in achieving our objective. The method is based on creating initial surfactant concentration difference between the bubble film and that in a pool of solution where the bubble floats. This was done by having two different solutions, one to make a soap bubble and another one on top of which the bubble would float after transfer. In this a controllable initial surfactant gradient was created between the bubble film and that in the solution. The fluid flow was monitored by time-dependent changes in the visible absorption spectra of a laser dye as it moved in to the bubble film from the solution below. Our results indicate that the rate of flow of fluid from a solution up along the bubble film is governed by small differences in initial surfactant concentration between them. In order for the liquid from solution to move up, the bubble film must have lower surfactant concentration than the solution below. The higher the concentration gradient, the faster is the fluid flow rate. The minimum initial surfactant concentration gradient needed for an upward fluid flow was 2%.

2.2.2 Experimental Section

In order to perform the experiments two different solutions of mixture of surfactants and dye (when appropriate) were necessary. They were prepared from a stock solution containing 0.4 g (69.4 mM) sodium dodecyl sulfate (SDS) (Sigma) and 0.04 g (10.8 mM) of 1-dodecanol (Aldrich) in 20 ml of milliQ water. From the stock solutions 2 ml portions were withdrawn to make solution **A** and **B**. Appropriate amount of the laser dye Rhodamine B (RhB) or Rhodamine 6G (Rh6G) was added to these 2 ml portion for dye incorporation. Difference of concentration between solutions A and B was created by addition of water to either of them. For example to obtain required concentrations in Figure 2.2.4a and 2.2.4b, 40 µl and 100 µl of water respectively were added to 2 ml of above solution in **A**. Solution **A**

was kept in a watch glass and solution **B** was kept on top of the inverted beaker inside the larger beaker (Figure 2.2.1k).

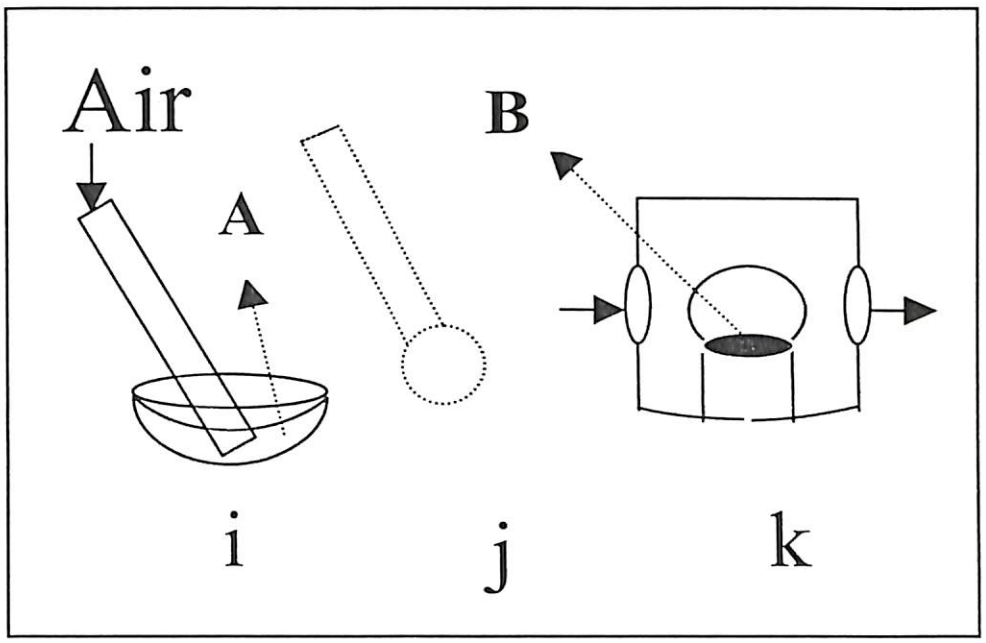

Figure 2.2.1. *A schematic view of bubble transfer and consequent visible spectroscopic probe. (i) A glass tube (5 mm i.d.) connected to a high-pressure air source was dipped into Solution A; (j) the bubble formed was then lifted and (k) transferred to Solution B. The system with the larger beaker with two sapphire optical windows and a cover was kept inside the sample compartment of a Hitachi U2001 UV-visible spectrophotometer for probe.*

An air bubble of about 20 mm diameter was blown at the end of a 5 mm (inside diameter) glass tube by dipping the tube into **A** and then lifting it immediately while air was being blown. The bubble was then transferred to **B** following which time dependent visible spectra were recorded. Figure 2.2.1 schematically describes the bubble formation and transfer method. For recording of the time-dependent visible spectra of the dye in the bubble film, the larger beaker containing the bubble was kept inside the sample compartment of a Hitachi U2001 UV-visible spectrophotometer and wavelengths of light were scanned.

2.2.3 Results and Discussion

When a soap bubble was placed inside a UV-visible spectrophotometer and the wavelength was scanned, absorption maxima and minima due to interference of light started appearing when the film thickness became of the order of the wavelength of the probe light. This had become a problem for our experiment especially when the interference fringes resulted in strong absorption maxima and minima, as compared to relatively weak absorption maxima and minima due to the fluid movement along the thin bubble film surface. We circumvented the problem by focusing on the observation of the fluid flow within the first few minutes of bubble formation and transfer. During this time the thickness of the bubble film was generally higher than the probe wavelength and hence absorption due to interference of light was low. We have taken advantage of this and report the results of the first few minutes of studies for each case. In Figure 2.2.2 we demonstrate the feasibility of this approach by showing the time-dependent spectra of RhB as it moved through the film during the first 10 min of evolution.

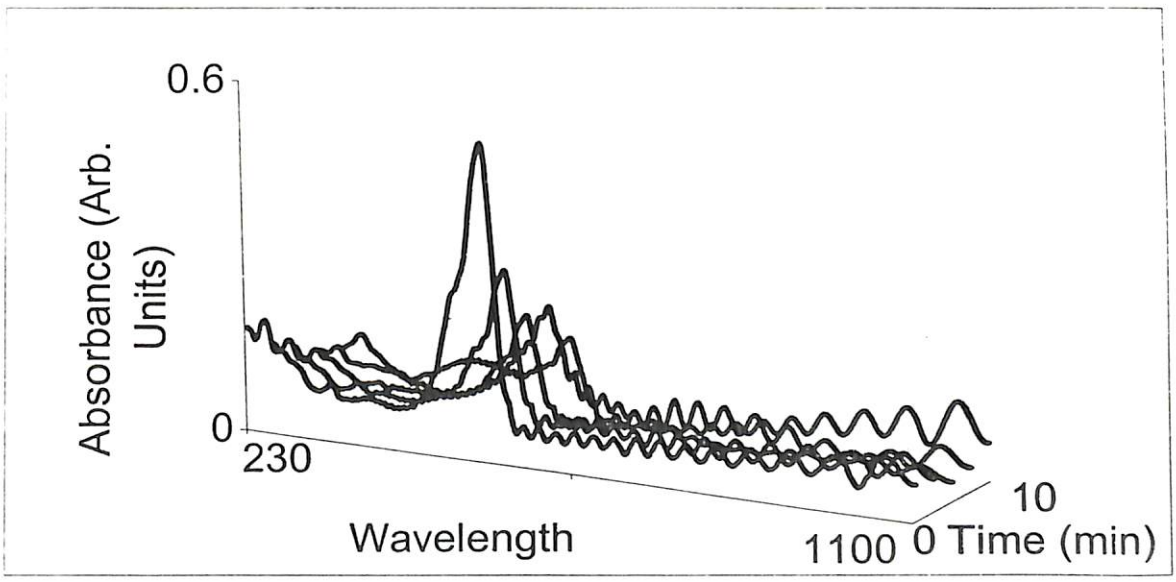

Figure 2.2.2. *Time evolution of UV-Visible absorption spectra of RhB in a soap bubble (made directly from* ***B*** *only) during first 10 min. Shown here is the 230 – 1100 nm of wavelength range to emphasize the ability of the present method to differentiate the absorption changes from the background interference fringes during the first few minutes.* ***B*** *contained 69.4 mM of SDS, 10.8 mM 1-dodecanol and 33.4 mM RhB.*

It may be pointed out here that even in the above measurement there is the presence of peaks due to weak interference fringes, due to the Marangoni convection driven upward fluid movement as described in chapter 2.1. Despite that, the peak due to the dye is prominent and the decay of dye concentration (absorbance), due to drainage from the film, with time could easily be made out from the graphs. In fact the measurements we report below are for the first six minutes and thus considerably less than the above time and hence the problems due to interference may be ignored in this context.

The time-dependent visible absorption spectra of Rhodamine B as it appeared and did not appear in the film, are shown in Figure 2.2.3a and 2.2.3b respectively. Here solution **A** contained surfactants and no dye, while **B** contained surfactants with the dye.

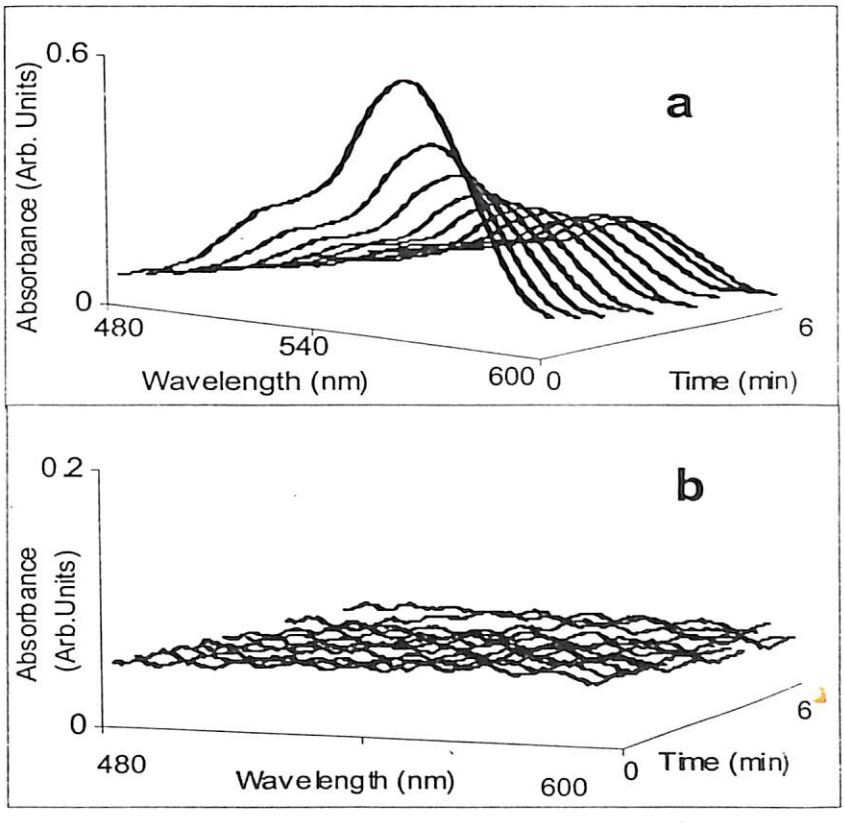

Figure 2.2.3. *Time evolution of UV-Visible absorption spectra of RhB in a soap bubble as it moved from solution **B** to the film. The film had no initial dye content. Shown here are the absorbances in the 480 – 600 nm of wavelength range during the first 6 min of spectra recording.* ***a.*** *Fast upward movement of RhB from the solution to the bubble and subsequent decay. The surfactant concentration in **B** was same as in Figure 2.2.2 while **A** was diluted by 50%. The dye movement was much faster than the probe time and hence the initial zero of absorbance could not be observed.* ***b.*** *No movement of dye from **B** to the bubble. Both solutions **B** and **A** had equal initial concentration of surfactants as in Figure 2.2.2.*

For the spectra in Figure 2.2.3a, the initial concentration of surfactants in **A** were 50% as less as those in **B**. As a bubble was made from **A** and then transferred to **B**, the initial gradient of surfactant concentrations between solutions **A** and **B** resulted in the fast upward movement of dye from **B** up along the bubble film. This is clearly shown in Figure 2.2.3a. The initial upward flow of dye-containing solution was faster than one minute and hence the zero of absorbance in the spectra could not be observed. With time, the absorption intensity went down as a consequence of film (and hence the dye) drainage. It may be pointed out here that the most intense peak due to dye absorption appeared at the beginning and after that the intensity only went down and never went up again. In another case when the initial concentrations of surfactants in **A** and **B** were kept equal and a bubble was made from **A** and subsequently transferred to **B** and probed, no dye peak could be observed during the entire period of scanning. This is shown in Figure 2.2.3b. Although we have reported in Figure 2.2.3b our observation for about six minutes, there was no significant change in the spectral characteristics with respect to the dye absorption for more than an hour of observation. This observation suggests that when the initial concentrations of surfactants are same there is no movement of fluid up along the film from the solution. We also note here that when the initial surfactant concentration in **A** was kept higher than **B**, then also we did not observe any movement of dye up along the film. The above observations indicate that in order for a fluid movement to occur from a solution up along the bubble film the initial surfactant concentration in the solution (**B**) must be higher than that in the film (made from **A**). Again when the surfactant concentration gradient between the bubble film and the solution was high, fast upward movement of fluid could be observed.

Our next question was whether one could have further control on the rate of fluid flow up along the film as a function of concentration gradient of surfactants between **A** and **B**. In fact we did observe controlled fluid movement when we had started with solution **A** selectively diluted with respect to **B**. The results are shown in Figure 2.2.4a and 2.2.4b. As clear from Figure 2.2.4a, there was a controlled movement of fluid along the bubble film in the upward direction and it took about 2-3 min for the maximum absorbance to appear when the difference in initial surfactant concentration was about 2%. After that the peak intensity gradually decayed due to gravitational drainage. On the other hand, when the gradient in

concentration was about 5%, the upward fluidic movement was relatively faster and it took about 1-2 min for the maximum of absorbance to appear followed by a slow decay in the intensity (Figure 2.2.4b).

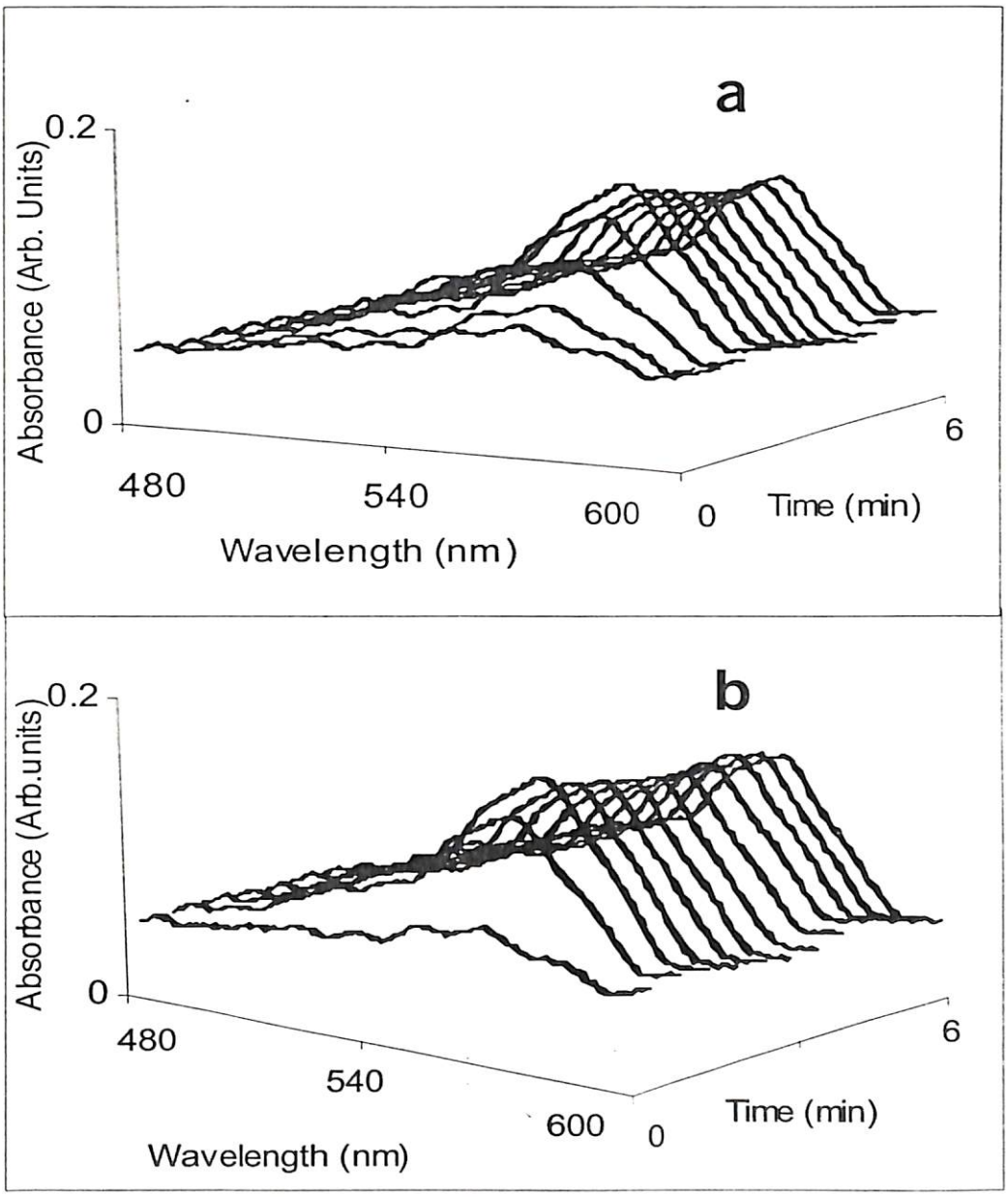

Figure 2.2.4. ***a.*** *Relatively Slower upward movement of RhB up along the bubble film that had no initial dye present.* ***B*** *had 69.4 mM SDS, 10.8 mM 1-Dodecanol and 33.4 mM RhB and* ***A*** *contained 2% diluted surfactants of* ***B*** *and no dyes.* ***b.*** *Relatively faster movement of RhB up along the film that initially had no dye-content.* ***B*** *had the same surfactant and dye concentrations as in* ***a*** *while* ***A*** *contained 5% diluted surfactants of* ***B*** *and no dyes.*

Our next question was whether the gravitational drainage of the film occurred in concurrence with the upward fluid flow. To test this we used two dye system: one in the bubble and the other in the solution that had absorption maxima at different but closely spaced wavelengths so that rapid scanning could be achieved to follow the movement. We used Rhodamine B and Rhodamine 6G for this purpose. First we had the surfactant concentration in both **A** and **B** kept the same with Rh6G in the bubble and RhB in the solution below and performed the experiment as before. We observed that a slow decay of the Rh6G dye peak intensity with time while no peak due to RhB was observed (Figure 2.2.5a).

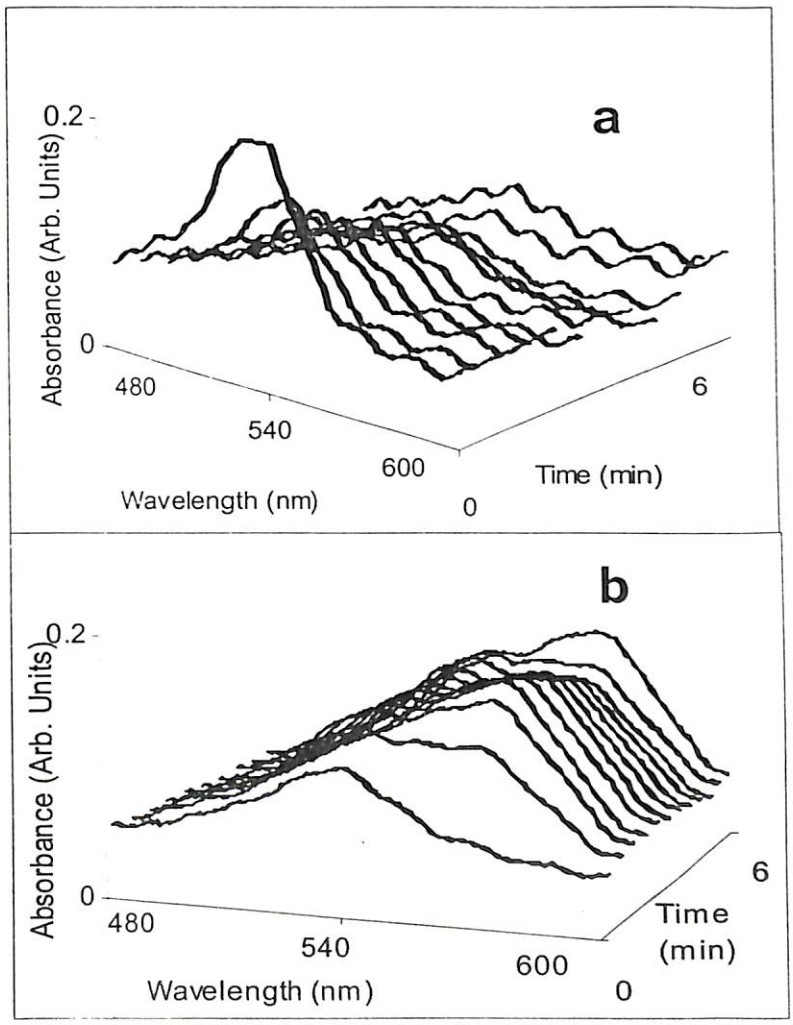

Figure 2.2.5. ***a.*** *Gradual decay of Rh6G absorption from the bubble while no movement of RhB (33.4 mM) could be observed which was present in* ***B****. Both solutions* ***A*** *and* ***B*** *had equal initial surfactant concentrations and that of* ***B*** *in Figure 2.2.3b. In addition,* ***B*** *contained 36.5 mM Rh6G.* ***d.*** *Slow upward movement of RhB from* ***B*** *to the film and simultaneous gradual decay of Rh6G from the film. Both* ***A*** *and* ***B*** *had same initial surfactant concentrations as in Figure 2.2.4a.* ***A*** *contained 36.5 mM Rh6G and* ***B*** *contained 33.4 mM RhB.*

This observation is similar to what we had observed with no dye initially in the bubble as in Figure 2.2.3b. In addition, the gradual decay of Rh6G dye from the film could also be observed. This suggests that the initial concentration gradient between the film and the bulk solution is critical for upward fluid flow and gravitational drainage-induced generation of concentration gradient does not induce any upward movement of fluid. Further shown in Figure 2.2.5b are gradual decay of Rh6G dye peak intensity in the bubble film and simultaneous slow increase in the RhB absorption peak intensity due to upward fluid movement from solution **B**. The concentration of surfactants in **A** was about 2% less than that in **B**. The above observation indicates that gravitational film drainage and initial upward fluid flow due to surfactant concentration gradients occur concurrently in our system. The apparent variation in peak intensity toward the end of the scan above was due to interference fringes which had changed the background absorption and the shoulder peak of RhB appearing nearly at the same wavelength as that of Rh6G and hence the net absorbance values.

When a soap bubble is made by stretching the surface of a film, the initial concentration of surfactants in the bubble film might not necessarily be the same as that in the solution but there ought to be a correlation between them. Also, when the bubble is transferred so as to float on top of another solution, the concentrations of surfactants in the bubble film after transfer might not be the same as that in the parent solution. In addition, the exact nature of processes occurring in a soap bubble when it is formed from a solution and then transferred to another solution is not known. Even then, in a series of observation that we have reported here it is clear that there is a definite correlation between the surfactant concentration in the parent solution and that in the bubble floating on top of another solution. Marangoni effect driven fluid flow from higher surfactant concentration region to lower concentration region is known to occur in soap films. Our present observations indicate that when a bubble is transferred to another solution, fluid may flow up along the bubble film, depending upon the initial surfactant concentration gradient between the solution and the film. When the concentration of surfactants in the solution was higher than that in the film, fluid flow up along the bubble film could be observed. When the concentration in the solution was equal or lower than the film fluid movement had not been

observed. This is based on the assumption that surfactant concentration of the parent solution is maintained in the bubble that might not be exactly possible. Even then, the concentration gradient between the two solutions is probably maintained in the film and the solution below. Thus, higher concentration gradient induces faster rate of upward fluid flow. It may also be pointed out here that even though the initial concentration of surfactants in the bubble film may not have been the same as that in the bulk solution from which the bubble was made (**A**), the flow of fluid up along the film can greatly be influenced by the surfactant concentration difference between **B** and **A**.

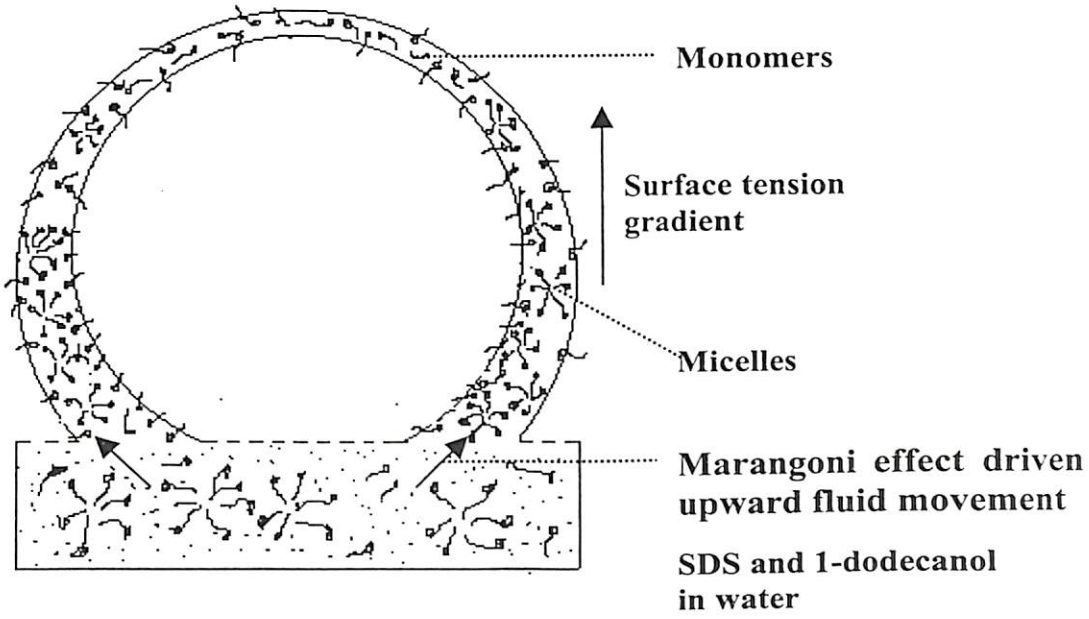

Figure 2.2.6. A schematic representation of the Marangoni effect driven fluid flow up along a soap bubble film floating on the water surface.

Both the dyes we have used are water-soluble and do not have any known tensioactivity. Hence they can be considered as water-soluble probe molecules only. Also, both solutions **A** and **B** were at the same temperature (room temperature) and hence it is expected that there was no thermal gradient between the bubble and the solution below. Thus the upward fluid flow is driven by surface tension gradient created by sudden stretch of the bubble film. When a bubble is transferred from the tip of the glass tube to a water surface, the bottom of the bubble opens up to float on the surface and the top film of the

bubble must merge to complete the sphere. This creates a sudden change in surfactant concentration gradient in the bubble film and thus drives the fluid flow from the surface of the solution below.[18] A schematic illustration for the upward fluid movement guided by the surfactant concentration gradient is shown in Figure 2.2.6. We have also observed that for larger bubble sizes, the upward fluid flow rate was higher than reported above. The larger bubbles are considerably thinner to begin with and hence the interference fringes that interfere with our measurement are quite strong. The smaller ones were difficult to probe in our experimental geometry.

2.2.4. Conclusion

In a series of experiments with controlled surfactant concentration gradient between bubble film and that in a solution onto which the bubble floated, we have been able to demonstrate that controlled fluid movement could be observed. Our essential conclusions are that when a bubble floats on a soap solution Marangoni effect drive fluid flow could be observed if the surfactant concentration in the bubble film (due to that from the parent solution) was less than that in the solution. If the concentrations of the parent solutions are equal no upward fluid flow could be observed. The upward fluid flow along the soap bubble surface from the solution below could be observed with a concentration gradient as low as 2% between the parent solutions. Further increase in the concentration gradient increases the flow rate dramatically. We also observed that the upward movement of the fluid occurred in concurrence with gravitational drainage that leads to the time-dependent changes in the film thickness. Here we have presented the spectra only for the first few minutes of total time evolution as peaks due to interference fringes becomes dominant after that. Also, no further increase in the absorbance values were observed after the reported period.

2.2.5. References

1. Dekker: L. V.; Segal, A. W., *Science,* **2000**, 287, 982.
2. Parent, C. A.; Devreotes, P. N., *Science,* **1999**, 284, 765.
3. (a) Whitesides, G. M.; Stroock, A. D., *Physics Today*, **2001**, 45 (b) Takayama, S.; McDonald, J. C.; Ostuni, E.; Liang, M. N.; Kenis, P. J. A.; Ismagilov, R. F.;

Whitesides, G. M. *Proc. Natl. Acad. Sci. USA*, **1999**, 96, 5545 (c) Pollack, L.; Tate, M. W.; Darnton, N. C.; Knight, J. B.; Gruner, S. M.; Eaton, W.A.; Austin, R. H., *Proc. Natl. Acad. Sci. USA*, **1999**, 96, 10115 (d) Wang, J.; Ibanez, A.; Chatrathi, M. P.; Escarpa, A. *Anal. Chem.*, **2001**, 73, 5323

4. (a) Freemantle, M. *Chem. Eng. News,* **1999**, 77, 27 (b) Unger, M. A.; Chou, H. P.; Thorsen, T.; Scherer, A.; Quake, S. R. *Science*, **2000**, 288, 113
5. (a) Hadd, A. G.; Jacobson, S. C.; Ramsey, J. M., *Anal. Chem.*, **1999**, 71, 5206 (b) Li, P. C. H.; Harrison, D. J., *Anal. Chem.*, **1997**, 69, 1564
6. Santini Jr., J. T.; Richards, A. C.; Scheidt, R.; Cima, M. J.; Langer, R., *Angew. Chem. Int. Ed.,* **2000**, 39, 2396
7. (a) Carter, S. B., *Nature,* **1967**, 213, 256 (b) Dubertret, B.; Skourides, P.; Norris, D. J.; Noireaux, V.; Brivanlou, A. H.; Libchaber, A. *Science*, **2002**, 298, 1759
8. (a) Hadd, A. G.; Raymond, D. E.; Haliwell, J. W.; Jacobson, S. C.; Ramsey, S. C., *Anal. Chem.*, **1997**, 69, 1407 (b) Lagally, E. T.; Medintz, I.; Mathies, R. A., *Anal. Chem.,* **2001**, 72, 2995 (c) Delamarche, E.; Bernard, A.; Schmid, H.; Michel, B.; Biebuyck, H., *Science,* **1997**, 276, 779 (d) Gallardo, B. S.; Gupta, V. K.; Eagerton, F. D.; Jong, L. I.; Craig, V. S.; Shah, R. R.; Abbott, N. L., *Science* **1999**, 283, 57.
9. (a) Lee, J.; Kim, C. J., *J. Microelectromech. Syst.*, **2000**, 9, 171. (b) Liu, R. H.; Stremler, M. A.; Sharp, K. V.; Olsen, M. G.; Santiago, J. G.; Adrian, R. J.; Aref, H.; Beebe, D. J. *J. Microelectromech. Syst.* **2000**, 9, 190 (c) Thorsen, T.; Maerkl, S. J., Quake, S. R., *Science*, **2002**, 298, 580 (d) Jeon, N. L.; Dertinger, S. K. W.; Chiu, D. T.; Choi, I. S.; Stroock, A. D.; Whitesides, G. M. *Langmuir* **2000**, 16, 8311. (e) Caelen, I.; Bernard, A.; Juncker, D.; Michel, B.; Heinzelmann, H.; Delamarche, E., *Langmuir,* **2000**, 16, 9125. (f) Schasfoort, R. B. M.; Schlautmann, S.; Hendrikse, J.; van den Berg, A., *Science,* **1999**, 286, 942. (g) Zhao, B.; Moore, J. S.; Beebe, D. J., *Science,* **2001**, 291, 1023. (h) Ichimura, K.; Oh; S. K.; Nakagawa, M., *Science*, **2000**, 288, 1624 (i) Song, H.; Tice, J. D.; Ismagilov, R. F., *Angew. Chem. Int. Ed.* **2003**, 42, 768
10. (a) Kargupta, K.; Konnur, R.; Sharma, A., *Langmuir,* **2000**, 16, 10243 (b) Decamps, C.; De Coninck, J., *Langmuir,* **2000**, 16, 10150. (c) Daniel, S.; Chaudhury, M. K.; Chen, J. C., *Science*, **2001**, 291, 633.

11. Exerowa, D.; Kruglyakov, P. M. *Foams and Foam Films Theory, Experiment, Application*; Elsevier: New York, **1998**.
12. Ichimura, K.; Suzuki, Y.; Seki, T.; Hosoki, A.; Aoki, K., *Langmuir,* **1988**, 4, 1214
13. Kenis, P. J. A.; Ismagilov, R. F.; Takayama, S.; Whitesides, G. M.; Li, S.; White, H. S., *Acc. Chem. Res.*, **2000**, 33, 841
14. (a) Kataoka, D. E.; Troian, S. M., *Nature,* **1999**, 402, 794 (b) Gau, H.; Herminghaus, S.; Lenz, P.; Lipowsky, R., *Science,* **1999**, 283, 46. (c) Gleiche, M.; Chi, L. F.; Fuchs, H., *Nature,* **2000**, 403, 173.
15. Wen, L.; Papadopoulos, K. D., *Langmuir,* **2000**, 16, 7612.
16. Mysels, K. J.; Cox, M. C.; Skewis, J. D., *J. Phys. Chem.* **1961**, 65, 1107
17. Kralchevsky, P. A.; Danov, K. D.; Denkov, N. D. In *Handbook of Surface and Colloid Chemistry*; Birdi, K. S., Ed.; CRC Press: New York, **1997**; pp 333-494.
18. Schramm, L. L.; Wassmuth, F. In *FOAMS Fundamentals and Applications in the Petroleum Industry*; Schramm, L. L., Ed.; Advances in Chemistry Series 242, American Chemical Society: Washington, DC, **1994**; pp 17-18.

CHAPTER 3

SYNTHESIS OF Au-NANOPARTICLES, Au NANOPARTICLE- POLYANILINE COMPOSITE AND SURFACE DEPOSITION OF Au NANOPARTICLES

3.1 A Simple Method of Electroless Deposition of Au-Nanoparticles on Two and Three-Dimensional Surfaces of Various Materials

3.1.1 Introduction

The "Gold - Rush" for creating materials that have characteristic sizes of nanometer length, in at least one dimension, has led to a "Nanoboom" in the discovery of a large number of methods to synthesize nanomaterials and generation of nanostructures, with appropriate features designed for modern electronics, optical, electromechanical and other applications.[1] Development of synthetic protocols for nanomaterials over a range of chemical compositions, sizes and shapes continues to be a fast developing area of research owing to the huge application potential associated with them. The growing interest in this direction has been fueled by the unusual physical and chemical properties exhibited by the nanomaterials that are quite different from their bulk counterparts[2]. With the reduced size and dimensionality of a material, the electronic properties change dramatically as the density of states and the spatial length scale of the electronic motion are reduced[3]. The synthesis of gold nanoparticles has, in particular, received considerable attention owing to its potential applications in catalysis, single electron tunneling, nonlinear optical devices and DNA sequencing[4]. Gold nanoparticles generated in aqueous medium has been one of the cornerstones in nanotechnology due to their immense contributions towards the development of biological applications such as drug delivery, gene transfer and recognition, biological markers etc[5].

One of the chief objectives of nanotechnology is the miniaturization of sensors and actuators for chemical, mechanical and biological applications.[6] To achieve this objective the primary requirement is to have metal or semiconductor nanoparticles (NPs) deposited on surfaces. These are useful as electrodes or functionalized surfaces for appropriate applications such as sensors and catalysts. Attainment of these objectives using simplest possible ways with adaptability as required by the applications is a prime condition for future development in this direction. A constant and growing endeavor has been to find

newer methods of synthesis of nanomaterials under different experimental conditions, guided by their application potential.[7]

The traditional method of vapor deposition of Au metal on various surfaces suffers from the inherent disadvantage of depositing bulk - metal - like materials on selective surfaces. Thus the main advantage of having Au NPs on non-functionalized surfaces has not been possible to be implemented using this method. On the other hand a significant amount of work has been carried out with regard to deposition of metal or semiconductor NPs on various surfaces. The popular among them have been the photolithographic patterning,[8] electrophoretic approach,[9] chemical deposition using appropriate functionalization of the surface for accommodating the required NPs[10] and by functionalization of the NPs themselves.[11] Langmuir – Blodgett (LB) film or self – assembled films of monolayer of nanoclusters using efficient cross-linking molecules have also been deposited on surfaces.[12] Non–aqueous Au colloids have also been used to deposit Au films on various substrates by evaporative solvent removal.[13] To the best of our knowledge none of the methods have used deposition of non-functionalized Au NPs from aqueous solution onto glass, quartz or plastic surfaces. This is important as metal nanoparticles without being capped by a stabilizer when deposited on a surface could be used as catalysts, electrode materials and as the base for designing sensors.

Here we report a new method of synthesis of colloidal Au NPs in aqueous solution and their deposition on glass, quartz and polymer surface such as Overhead Projector Paper (OHP) surfaces. The shape of the surfaces may be just ordinary two - dimensional like that of a circular disk or rectangular or three - dimensional that is the inside walls of a quartz optical cuvette or that of laboratory glass sample vials. For the synthesis of Au NPs we have used the method of reduction of $HAuCl_4$ in aqueous solution by H_2O_2 as the reducing agent. We have also been able to deposit Au NPs, generated in aqueous medium, on various surfaces without the use of a capping agent or pre-functionalization of surface such that the deposited Au NPs have to the potential to be used for fabrication of microelectronic devices. The use of glass and plastic substrates for deposition of Au NPs has the final motivation for use of these materials as inexpensive alternative substrates in microelectronics.

It is well known[14] that an otherwise typically oxidizing species like H_2O_2 in presence of NaOH reduces $HAuCl_4$ to metallic gold, due to higher reduction potential (Au^{3+} / Au^0) of the latter, as shown in equation 1.

$$2[AuCl_4]^- + 3H_2O_2 + 6OH^- \rightarrow 2Au + 3O_2 + 8Cl^- + 6H_2O \qquad 1$$

The precipitated metal is reported to appear brownish – black by reflected light and bluish – green by transmitted light. That is the case for bulk metal. However, we have found that just a mixture of H_2O_2 and $HAuCl_4$ with controlled concentration in aqueous medium in absence of base produces purple colored colloidal Au NPs with characteristic UV-visible absorption. Further, when previously treated glass or quartz substrates were kept in contact with the nanoparticle solution, deposition of Au nanoclusters had occurred on the surfaces of these materials. Thus it is possible to have uncapped nanoparticle immobilization on the hydrophilic glass surface by using a simple dipping method. We also found that the same deposition occurred on an OHP paper. A schematic diagram is shown in figure 3.1.1.

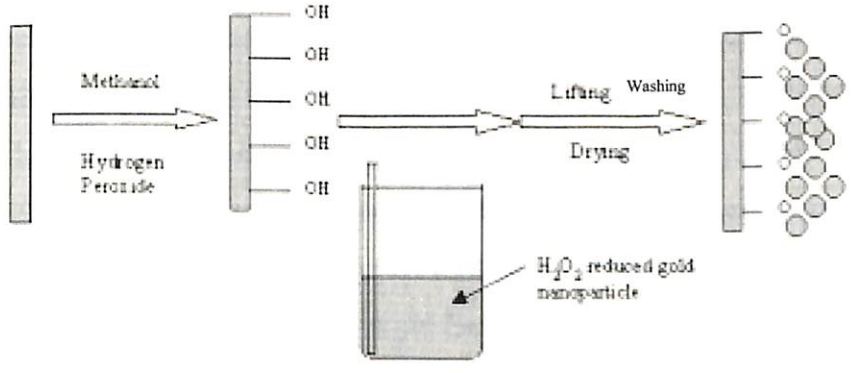

*Figure **3.1.1**. A schematic diagram of the present method of Au NP deposition on glass surfaces.*

In addition, when the solution was kept in an optical cuvette or a 15 ml laboratory glass vial deposition also occurred on the inside walls of them. We have used UV-visible absorption spectroscopy, transmission electron microscopy and scanning electron microscopy for the characterization of the NPs. Also, powder X-ray Diffraction method[15], optical micrographs and UV-visible absorption spectra of the samples exhibit gradual deposition of NPs on to the surfaces.

3.1.2 Experimental Section

The Au NPs were prepared as described below. To a 10 ml aqueous solution of 1 x 10^{-3} M $HAuCl_4$ [17% w/w $HAuCl_4$ in dilute HCl solution, aldrich], 400 µl of 30% H_2O_2 (v/v) was added slowly. The initial $HAuCl_4$ solution had a pH ca. 4, and we observed that addition of H_2O_2 to a basic solution of $HAuCl_4$ (pH was adjusted using NaOH) lead to the precipitation of metallic Au. However addition of H_2O_2 to an acidic solution of $HAuCl_4$ and constant stirring for about 5 min lead to the formation of purple colored Au NP solution with a characteristic visible absorption band where the maximum absorption occurred at about 530 nm. However for deposition of Au NPs on non-functionalized glass surfaces we found that preparation of Au NPs in aqueous medium using microwave radiation yielded better deposition. For this purpose 400 µl of 30% H_2O_2 was added to a 4 x 10^{-4} M solution of $HAuCl_4$. The mixture was kept inside a commercially available microwave oven (Samsung model CE118KF) that was set at 100% power for 1 minute. The purple colored Au NP solution was formed immediately with a characteristic visible absorption band at 530 nm. The colloidal solution was transferred to a 25 ml beaker and previously cleaned microscope glass slides were placed, standing vertically, inside the solution onto which gradual deposition of NPs occurred. Within a few hours of keeping the slide the NPs deposited on the slide could be observed by naked eye. The slides were kept dipped in the solution for a desired time and then cleaned with running distilled water. They were air–dried and then used for further analysis. We observed that without the use of microwave radiation, during the preparation of NPs, the deposition on surfaces required higher starting concentration of $HAuCl_4$. The deposited Au NPs on the walls of the container were neither soluble in HNO_3 nor HCl alone. There were soluble only in aqua regia. For UV-visible spectroscopy, we have used a Hitachi U2001 spectrophotometer. For XRD study the Au NPs deposited slides were placed horizontally inside the sample chamber of a Seifert powder X–Ray diffractometer (XRD 3003 TT) with Cu-Kα source (wavelength 1.54 Å). Optical micrographs of the NP deposited glass slides were recorded by using a Carl Zeiss Axiotech microscope. For transmission electron microscopic measurement of the Au NPs prepared by peroxide reduction we used sodium dodecyl sulfate (SDS) micelles as the stabilizing agent. Typically, to 10 ml of 1.2 x 10^{-2} M aqueous SDS solution $HAuCl_4$ was added so that the final concentration of $HAuCl_4$ was 4 x 10^{-4} M and to it 400 µl of 30% H_2O_2 was added and

the solution was kept inside the microwave oven for 1 min at 100% power. TEM measurements were performed by casting one drop of the colloidal solution onto a carbon grid which was then vacuum dried for observation. A JEOL JEM 200CX TEM with operating voltage at 200 kV was used for the measurements. The scanning electron micrographs of the Au NPs coated glass plates were recorded by a Hitachi S-4500 microscope operating at 80 kV operating voltage.

Glass slides were made ready for Au NP deposition in the following way. Microscope slides of 25 mm x 75 mm size were broken into smaller pieces, washed with water followed by boiling in methanol for about 30 minutes. The glass slides were then kept in boiling hydrogen peroxide solution (10 ml of 30% H_2O_2), which contained a few drops of ammonia, for about 30 minutes[16]. The slides after removal were kept immersed in water until used.

3.1.3 Results and Discussions

It is well known that formation of metal nanoparticles in a colloidal solution leads to strong coloration of the solution. The intensity and color of the solution depend on the nature of the metal particles as well as their shapes and sizes. Typically, formation of spherical metal NPs leads to unique color generation that is specific to the metal. Also, spherical metal NPs in a solution have unique UV-visible absorption spectrum with the maximum absorption peak position and the width representing the nature of the metal and their size distribution. For example, spherical Au NPs generally have a single and strong absorption peak at around 530 nm and the peak position shifts towards red or blue depending upon the particle size of the nanoparticles. In our case with the reaction of $HAuCl_4$ with H_2O_2 we observed strong purple or violet coloration of the solution. Characteristic visible absorption spectrum of the aqueous solution is shown in Figure 3.1.2. The surface plasmon resonance absorption of the NPs appeared as a single peak at 530 nm. The peak position and the shape of the curve indicated the formation of Au NPs. To find out the particle sizes and their distribution we pursued TEM measurements. For this measurement we synthesized the NPs in the presence of SDS at above its critical micellar concentration (1.2×10^{-2} M), which is a usual procedure for stabilization of the NPs. A

typical picture is shown in Figure 3.1.3. As clear from the figure, the particle sizes varied between 10nm and 30 nm with the majority of the particles formed with diameter in the range of 15 to 25 nm. Further confirmation of Au NP formation came from XRD studies with various surface deposited particles from the solution. We shall discuss this in the next section.

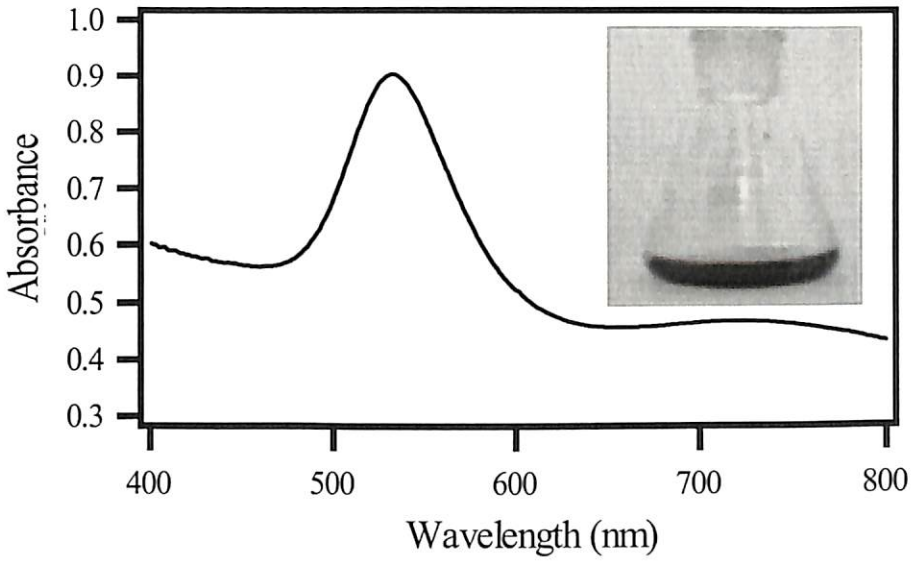

*Figure **3.1.2**. UV-visible absorption spectrum of the Au nanoparticles synthesized by our method in aqueous medium. The photograph is of purple colored Au nanoparticles in a conical flask. (see color plate, page 131)*

The reduction of $HAuCl_4$ to Au NPs by reducing agents such as citrates, $NaBH_4$, alcohol, hydrazine both in aqueous and organic solvents is well established. However, for the first time we have shown that H_2O_2 being itself an otherwise oxidizing agent can also be used in the reduction of $HAuCl_4$ for the generation of Au NPs in acidic medium. The standard potentials for the two processes are:

$$H_2O_2 + 2H^+ + 2e^- \longrightarrow 2\,H_2O \quad + 1.78\ (E^0/V) \qquad 2$$

$$Au^{3+} + 3e^- \longrightarrow Au \quad + 1.40\ (E^0/V) \qquad 3$$

Thus the formation of the Au NPs cannot be explained by simple redox chemistry. We do not know the exact mechanism of formation of Au NPs. However, our observations clearly demonstrated that it is possible to generate Au NPs with narrow particle size distribution in aqueous solution using H_2O_2 as the reducing agent. This is potentially useful as one could use the same H_2O_2 for oxidation of another species simultaneously with Au NP formation leading possibly to important and environmentally friendly way of generating materials like nanoparticle-polymer composite, deposition of surfaces for microelectronics application etc. which we shall discuss in the subsequent sections.

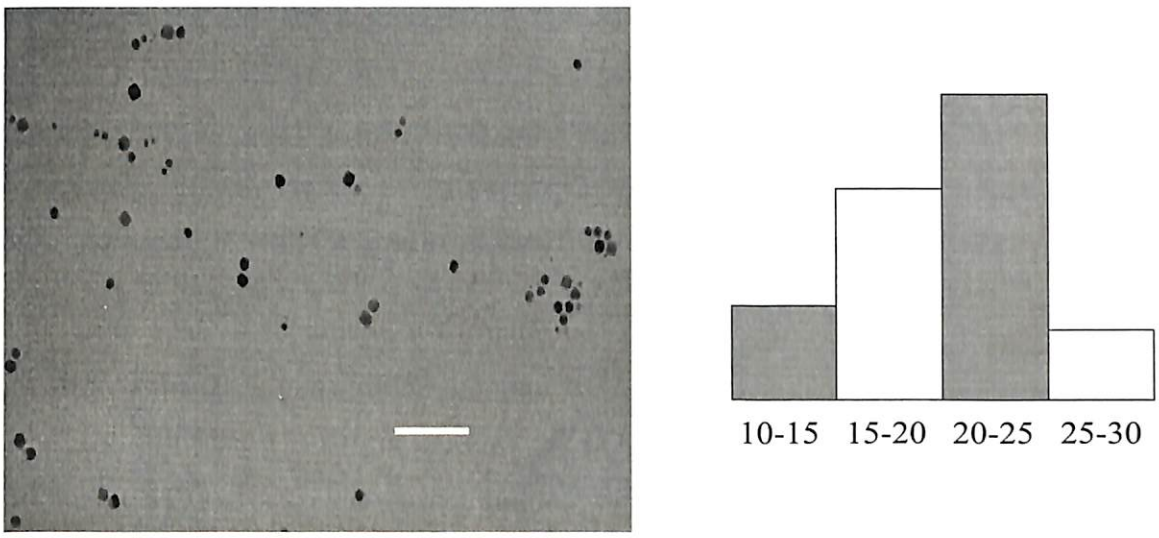

*Figure **3.1.3**. TEM micrograph and particle size distribution of the Au nanoparticles synthesized by H_2O_2 reduction of $HAuCl_4$. Scale bar =200 nm.*

While pursuing the synthesis of Au NPs we observed that the walls of the glass container were getting colored (same as the solution) after the formation of particles in the solution after keeping for sometime. We then decided to pursue the nature of deposition on the walls. We considered four systems: a glass slide, a quartz optical cuvette, a quartz disk and a polymer surface in form of Overhead Projector paper (OHP). We synthesized Au NPs in the cuvette and kept the solution for a long time (about 24 hr), while in the case of glass slide, quartz disk and OHP paper we dipped them into a solution of Au NPs synthesized using the above method for 24 hr. In all cases we observed purple coloration of the surfaces

that confirmed the deposition of the nanoparticles on the unfunctionalized surfaces. Three photographs of the coated quartz cuvette (inside walls), quartz disk and OHP paper are shown in Figures 3.1.4A and 3.1.4B and 3.1.4C respectively. Photographs were taken after washing and air - drying the substrates. Corresponding visible absorption spectra are shown in Figures 3.1.4D and 3.1.4E and 3.1.4F respectively. As evident from the figures, all the absorption spectra showed a single peak characteristic of that of Au NPs occurring at around 550 nm. The peak generally observed due to transverse plasmon resonance band of Au NPs[17], is red-shifted by 20 nm compared to those observed in the solution. However the general nature of the peak is the same as the solution peak. This might occur possibly due to aggregation of the Au NPs leading to the formation of islands on the deposited surface. We would like to mention here that the deposited particles were stable for months without any observable change. Again, deposited particles were stable enough to have withstood the washing cycle. It may further be mentioned here that when the same solution was kept in a Borosil glass sample vial, the inside wall of the vial was coated with Au NPs.

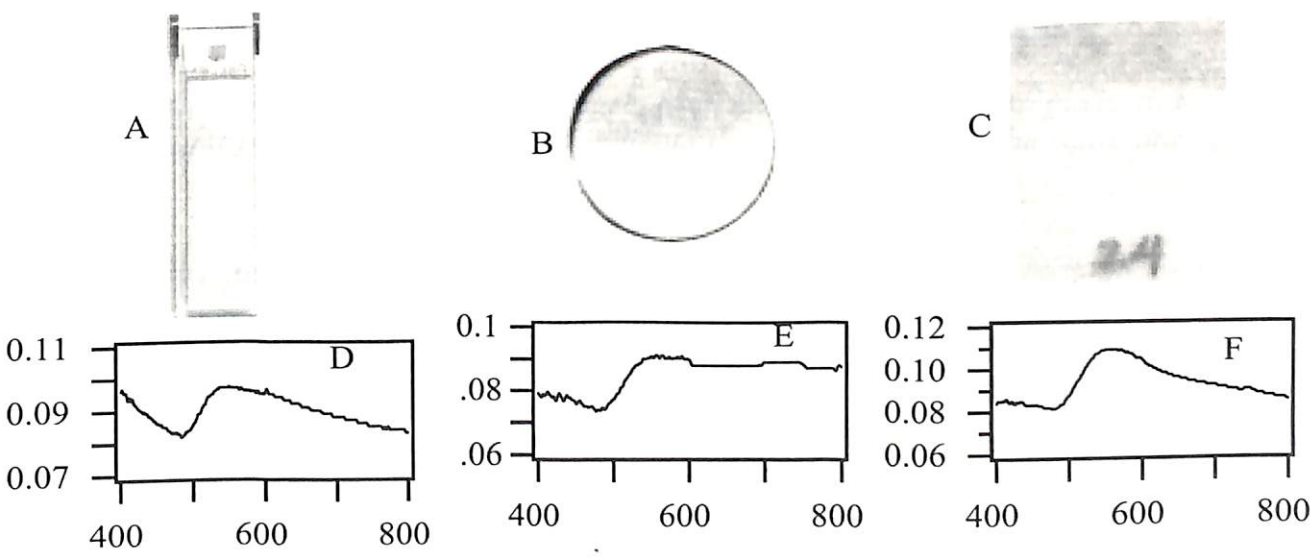

*Figure **3.1.4**. Photographs of Au NP– coated (A) quartz cuvette, (B) quartz disk and (C) OHP paper and their corresponding visible absorption spectra in (D), (E) and (F) respectively.* *(see color plate, page 131)*

Further confirmation of deposition of Au NPs on glass slides came from scanning electron microscopic observation of deposited particles. As shown in Figure 3.1.5, for a deposition time of 1 hr, the particles deposited still had sizes in the range of tens of nanometer. As can be seen from the picture, there were nearly uniform-sized particle depositions on the surface with island formation at a few places.

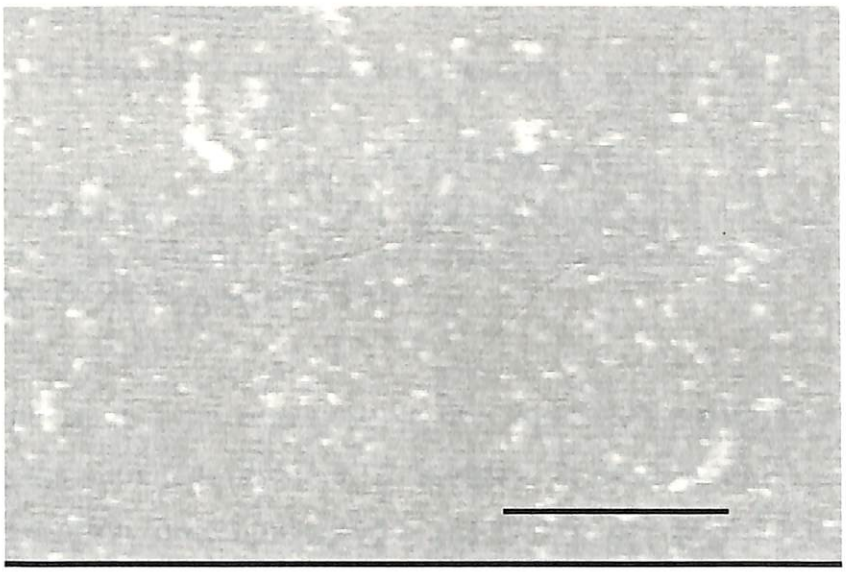

*Figure **3.1.5**. Scanning electron micrograph of Au NPs deposited on glass slide for 1 hr. The bright particles on the surface indicate the deposited NPs. The scale bar is 500 nm.*

We have also studied time dependent deposition of nanoparticles on glass slides kept in the Au - NP solution. Six different glass slides were immersed in the nanoparticle solution. The slides were lifted one after another at the reported time, washed and then dried. Figure 3.1.6 represent the UV-visible spectra of the Au NPs deposited on glass slides for different time-span of deposition. The slides were lifted from the solution, washed and air-dried after certain time intervals. It was observed that the intensity of the plasmon resonance band increased with increased time of deposition. The increase of intensity in the plasmon resonance band for the Au nanoparticles indicated that although the amount of Au NPs increased with time, the nanoparticle character was retained even after immobilization of the Au NPs on the glass surface. On the other hand bulk metal formation was not observed.

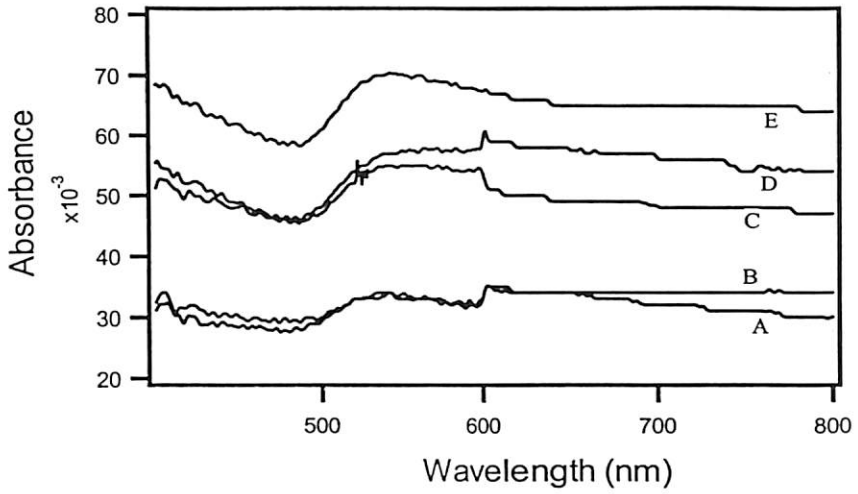

*Figure **3.1.6.** Time dependence in the deposition of Au – NPs on glass slides as observed by UV – vis absorption. The time allowed for deposition was (A) 4 hrs; (B) 8 hrs; (C) 12 hrs; (D) 24 hrs and (E) 30 hrs.*

Further, the optical micrographs for the deposited particles and powder X-ray diffraction graphs are shown in Figure 3.1.7. Increase in the amount of Au NPs in the form of islands with deposition time could easily be assessed using optical microscope. The color here is an artefact. The x-Ray diffraction signal intensity appearing at 38.5° (2Θ) were taken as proportional to the amount of Au NP deposited of the slides. We observed that with time the deposition was increasing as was evident from XRD pattern intensity and visible absorption spectra of the slides. The increase in the amount of deposition continued for about 24 hr. After that there was no significant increase in the XRD pattern intensity. The reason for not observing further increase in the deposition after about 24 hr may be due to gradual settling of the colloidal particles from the parent solution. This means that there were not sufficient NPs present in the solution to be deposited in the slide. Hence no significant increase in Au NP deposition was observed. The XRD patterns are characteristic of that of a [111] fcc lattice of Au cluster with interatomic distance of 0.29 nm. This is equal to the reported distance between Au atoms in bulk[3a]. The average particle size determination of the Au NPs deposited on the glass plate was performed applying the Debye-Scherrer equation to the XRD data and that was found to be 32 nm.

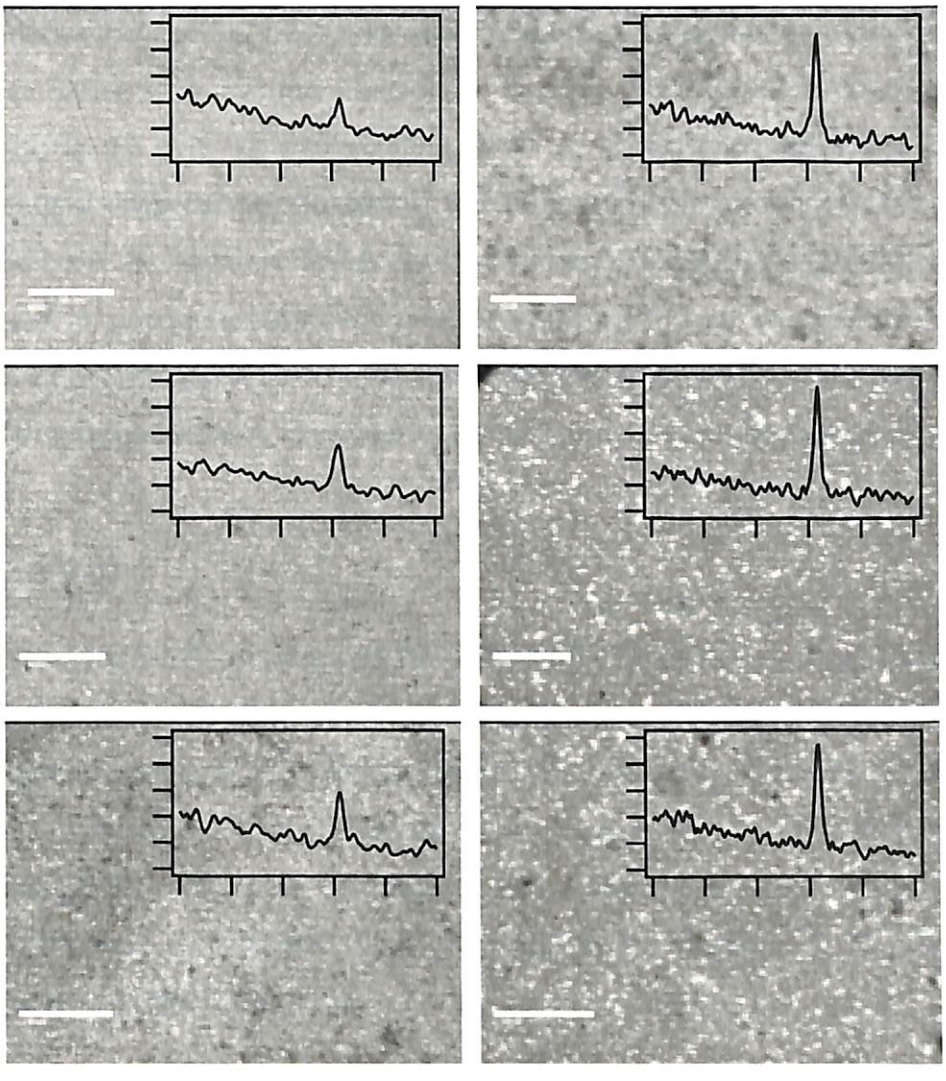

*Figure **3.1.7**. Time dependence of deposition of Au NPs on glass slides as observed by optical microscopic and XRD measurements. Scale bar in optical micrographs is 10 μm. XRD measurements of Au NPs deposited slides were performed by placing the slides horizontally inside the sample chamber of a Seifert powder X–Ray diffractometer (XRD 3003 TT) with Cu-Kα source (wavelength 1.54 Å) (see color plate, page 132)*

3.1.4 Conclusion

In this work we have reported a new method of preparation of colloidal Au NPs by reduction of $HAuCl_4$ using H_2O_2 as the reducing agent in acidic condition. We have also reported the deposition of Au NPs on two-dimensional glass, quartz and plastic surfaces. We have also been able to obtain deposition on three-dimensional surfaces such as in the inside walls of an optical cuvette and glass sample vials. It is reported that when a glass

surface is kept in contact with H_2O_2 the result is the formation of Si-OH at the interface[6b,15]. The Si-OH present at the interface may react with Au NP assembly to accommodate them at the interface. Thus it has become possible to deposit Au NPs on various substrates without either modifying the NPs for surface deposition or significant surface modification of the substrate using a different attachment in the form of molecules typically used for surface deposition of NPs. In addition, this particular way of depositing nanoparticle is attractive as it is performed in an aqueous solution thereby avoiding the environmental factors associated with the use of organic solvents. Further, the requirement of surface modification using the principle of electrophoresis or electrolytic deposition has been avoided in the present case.

3.1.5 References

1. (a) Service, R. F., *Science*, **1999**, 286, 442 (b) Service, R. F. *Science*, **2000**, 290, 1524 (c) Gittins, D. L.; Bethell, D.; Schiffrin, D. J.; Nichols, R. J. *Nature* **2000,** 408, 67 (d) Craighead, H. G. *Science*, **2000**, 290, 1532 (e) Klein, D. L.; Roth R.; Lim, A. K. L.; Alivisatos, A. P.; McEuen, P. L. *Nature*, **1997**, 389, 699 (f) Jarrold, M. F. *Science*, **1991**, 252, 1085 (g) Ingram, R. S.; Hostetler, M. J.; Murray, R. W.; Schaff, T. G.; Khoury, J.; Whetten, R. L.; Bigioni, T. P.; Guthrie, D. K.; First, P. N., *J. Am. Chem. Soc.*, **1997**, 119, 9279

2. (a) Lu, L.; Sui, M. L.; Lu, K. *Science,* **2000,** 287, 1463 (b) Alivisatos, A. P. *Science,* **1996**, 271, 933

3. (a) Link, S.; El-Sayed, M. A. *J. Phys. Chem. B,* **1999**, 103, 8410 (b) Henglein, A. *J. Phys. Chem.*, **1993**, *97*, 8457. (c) Alivisatos, A. P. *J. Phys. Chem.*, **1996**, 100, 13226.

4. (a) Andres, R. P.; Bein, T.; Dorogi, M.; Feng, S.; Henderson, J. I.; Kubiak, C. P.; Mahoney, W.; Osifchin, R. G.; Reifenberger, R. *Science,* **1996**, 272, 1323 (b) Galletto, P.; Brevet, P. F.; Girault, H. H.; Antoine, R.; Broyer, M. *J. Phys. Chem. B,* **1999**, 103, 8706 (c) Mirkin, C. A.; Letsinger, R. L.; Mucic, R. C.; Storhoff, J. J. *Nature,* **1996**, 382, 607

5. Niemeyer, C. M. *Angew. Chem., Int. Ed.,* **2001**, 40, 4128.

6. (a) Jager, E. D. H.; Smela, E.; Inganas, O. *Science*, **2000**, 290, 1540 (b) Shipway, A. N.; Katz, E.; Willner, I. *CHEMPHYSCHEM,* **2000**, 1, 18 (c) Holtz, J. H.; Asher, S. A. *Nature* **1997**, 389, 829 (d) Velev, O. D.; Kaler, E. W. *Langmuir,* **1999**, 15, 3693

7. (a) Puntes, V. F.; Krishnan, K. M.; Alivisatos, A. P. *Science,* **2001**, 291, 2115 (b) Nikppbakht, B.; Wang, Z. L.; El-Sayed, M. A. *J. Phys. Chem. B,* **2000**, 104, 8635 (c) Mirkin, C. A. *Inorg. Chem.,* **2000**, 39, 2258 (d) Zhang, G.; Niu, A.; Peng, S.; Jiang, M.; Tu, Y.; Li, M.; Wu, C. *Acc. Chem. Res.,* **2001**, 34, 249 (e) Barth, J. V.; Weckesser, J.; Cai, C.; Günter, P., Bürgi, L.; Jeandupeuz, O.; Kern, K. *Angew. Chem. Int. Ed.,* **2000**, 39, 1230 (f) Liu, C.; Zhang, Z. J. *Chem. Mater.,* **2001**, 13, 2092 (g) Zhou, Y.; Itoh, H.; Uemura, T.; Naka, K.; Chujo, Y. *Chem. Commun.,* **2001,** 613 (h) Jana, N. R.; Gearheart, L.; Murphy, C. J. *Chem. Commun.,* **2001**, 617

8. Hayward, R. C.; Saville, D. A.; Aksay, I. A. *Nature,* **2000**, 404, 56

9. Chandrasekharan, N.; Kamat, P. V. *Nano Lett.,* **2001**, 1, 67

10. (a) Harnisch, J. A.; Pris, A. D.; Porter, M. D. *J. Am. Chem. Soc.,* **2001**, 123, 5829 (b) Schmit, J.; Mächtle, P.; Eck, D.; Möhwald, H.; Helm, C. A. *Langmuir,* **1999**, 15, 3256 (c) He, H. X.; Zhang, H.; Li, Q. G.; Zhu, T.; Li, S. F. Y.; Liu, Z. F. *Langmuir,* **2000**, 16, 3846 (d) Doron, A.; Joselevich, E.; Schlittner, A.; Willner, I. *Thin Solid Films,* **1999**, 340, 183

11. (a) Gu, Z. Z.; Horie, R.; Kubo, S.; Yamada, Y.; Fujishima, A.; Sato, O. *Angew. Chem. Int. Ed.,* **2002**, 41, 1153 (b) Mayya, K. S.; Sastry, M. *Langmuir,* **1999**, 15, 1902 (c) Bharathi, S.; Nogami, M.; Lev, O. *Langmuir,* **2001**, 17, 2602

12. (a) Chen, S. *Adv. Mater.,* **2000**, 12, 186 (b) Andres, R. P.; Bielefeld, J. D.; Henderson, J. I.; Janes, D. B.; Kolagunta, V. R.; Kubiak, C. P.; Mahoney, W. J.; Osifchin, R. G. *Science,* **1996**, 273, 1690 (c) Collier, C. P.; Saykally, R. J.; Shiang, J. J.; Henrichs, S. E.; Heath, J. R. *Science,* **1997**, 277, 1978. (d) Chung, S.W.; Markovich, G.; Heath, J. R. *J. Phys. Chem. B,* **1998**, 102, 6685 (e) Kim, F.; Kwan, S.; Akana, J.; Yang, P. *J. Am. Chem. Soc.,* **2000**, 122, 4360

13. (a) Klabunde, K. J.; Youngers, G.; Zuckerman, E. J.; Tan, B. J.; Antrim, S.; Sherwood, P. M. *Eur. Solid State Inorg. Chem.* **1992**, 29, 227 (b) Rabinivitch, S.; Horner, R. H.; Klabunde, K. J.; Hooker, P. *Metalsmith*, 1994, 14, 41 (c) Klabunde, K. J. *U. S. Patent* 1989, **4,877**, 647

14. *Vogel's Qualitative Inorganic Analysis Sixth Edition*, Revised by Svehla, G. **1987,** Orient Longman, pp 253.

15. Whetten, R. L.; Shafigullin, M. N.; Khoury, J. T.; Schaaff, T. G.; Vezmar, I.; Alvarez, M. M.; Wilkinson, A. *Acc. Chem. Res.,* **1999**, 32, 397

16. Ung, T.; Liz-Marzán, L. M.; Mulvaney, P. *J. Phys. Chem. B,* **2001**, 105, 3441

17. Kumar, A.; Mandale, A. B.; Sastry, M. *Langmuir*, **2000**, 16, 6921

3.2 Synthesis of Au Nanoparticle-Conductive Polyaniline Composite using H_2O_2 as both Reducing and Oxidizing Agent

3.2.1. Introduction

Conducting polymers termed as the "fourth generation of polymeric materials" [1], have brought revolutionary improvement in the application of materials in modern technology. They have application potentials in optical and microelectronic devices, chemical sensors, catalyses, drug delivery and energy storage systems[2-15]. The electrically conducting polymers with their unique redox properties, when doped appropriately, can have electrical conductivity over the full range from insulator to metallic regime[1]. Polyaniline (PANI) is an important class of electronically conducting polymers. Extensive studies have been carried out to understand the mechanism[16] and applications for the unusual chemical, electrical and optical properties associated with the polymer in both insulating and conducting forms. The attractive properties of PANI include tunable electrical conductivity, comparatively lower density than metal, good environmental stability and ease of preparation from commonly available chemicals. PANI holds a unique position among conducting polymeric materials, as highly conducting doped form can be achieved by completely two different processes- protonic acid doping and oxidative doping[17]. In case of PANI, doping with a strong acid preferencially protonates the imine nitrogens, leading to an increase in conductivity[18-19]. The positive charge created along the backbone by protonation is counterbalanced by negatively charged counter-ions created from the doping acid, which causes physical rearrangement of the polyaniline chain to accommodate them. Thus the counter-ions play an important role in order to improvise solubility, processibility and conductivity by using functionalized protonic acids.

On a separate front, there has been growing interest in the development of inorganic/organic composites in the past few years due to wide range of potential applications associated with them[20-22]. These hybrids constitute a class of advanced composite materials with unusual properties, which can be used in many applications such as optics, electronics, sensors and actuators. The formation of hybrids of conducting

polymers and inorganic solids[23-26] has the goal of obtaining composite materials with synergic or complementary behaviors of the polymer and the inorganic matrices. The properties of the designed composite will depend both on the characteristics of the polymers and the nature of the inorganic matrix. The unique properties of the hybrid materials is expected to be more pronounced if at least one of the fractions occurs in the nanometer level. The nano-dimensional materials of metals, metal oxides, alloys and semi conducting particles offer superior optical, electronic, magnetic and catalytic behavior compared to their bulk counterparts[27-28]. This has lead to constant search for improvisation of methodologies for the generation of nanomaterials incorporated polymer matrices in the form of colloids, films and bulk materials using various techniques including molecular self-assembly, sol–gel synthesis, electrochemical and photochemical deposition.[29–34] Polyaniline–carbon nanotube composites with enhanced electronic properties[35-36] has been synthesized. The traditional methods involve synthesis of polymer and nanoparticles separately followed by mixing to obtain a composite. However, none of the above methods has demonstrated the ability to synthesize nanoparticle and polymer using the same reagent in aqueous solution for generating nanoparticles and polymer in the form of a composite. This is important as it reduces the number of steps in a complex set of sequential reactions leading to the formation of a composite. In addition, a more uniform and molecularly defined composite material could be obtained in this way.

In this work we report a novel method for the generation of Au nanoparticle-conducting polyaniline (Au NP-PANI) composite obtained in a straightforward way with reactions in aqueous medium. In the previous work we described the generation of Au NPs from its parent metal salt $HAuCl_4$ in aqueous medium by using H_2O_2 as a reducing agent. Again H_2O_2 has been used traditionally as an oxidizing agent for the polymerization reactions especially for the synthesis of PANI. The present method is a combination of the two processes and it involves formation of Au NPs from $HAuCl_4$ in aqueous solution followed by polymerization of aniline to form PANI. Thus it was possible for the formation of Au NP-conductive PANI composite using a single pot reaction. The composite was analyzed using various spectroscopic techniques. Gel permeable chromatographic results confirmed the molecular weight of the polymer formed to be around 2500 dalton. Powder

X-ray diffraction studies were performed to confirm the presence of Au NPs in the polymer matrix. The room temperature electrical conductivity measurements by four-probe method showed in increase in electrical conductivity of the polymer by more than two orders of magnitude upon incorporation of a small amount of Au NPs.

3.2.2 Experimental Section

Au NPs were prepared in aqueous medium by the reduction of $HAuCl_4$ using H_2O_2 as the reducing agent that has already been discussed earlier. Briefly, to 5 ml of 4.5×10^{-4} M $HAuCl_4$ solution prepared in milliQ water, about 400 µl of 30% H_2O_2 was added and stirred for 5 minutes at room temperature. The color of the solution changed gradually from pale yellow to purple indicating the formation of Au NPs in aqueous medium. The Au NPs thus formed showed plasmon resonance absorption maximum at 530 nm.

In a separate vial, 100 µl of distilled aniline was dissolved in 5 ml of 1 M HCl solution in aqueous medium. The whole of the solution was added to the Au NP solution in separate batches (500 µl in a batch) over a period of 10 min under constant stirring at room temperature. It was observed that with the addition of anilinium chloride solution with the Au NP solution, the characteristic purple color of the Au nanoparticles disappeared to form a colorless solution. The polymerization reaction was then allowed to take place under constant stirring for 12 hr. The color of the solution turns from colorless to light green to dark green black and the reaction was stopped. A dark green colored precipitated was collected at the bottom of the flask. In a separate experiment polyaniline was synthesized without the addition of Au NPs using the same experimental condition, by the addition of 100 µl of distilled aniline in 10 ml of 1M HCl aqueous solution followed by addition of 400 µl of H_2O_2 constant stirring.

The time dependent formation of PANI and composite in presence and absence of Au NPs were studied by the addition of the reagents of the same amount inside a 3 ml quartz cuvette with constant stirring at room temperature. The cuvette was placed inside the sample compartment of a Hitachi spectrophotometer (model U2001) and UV-visible spectra at different time intervals were recorded.

The PANI and Au NP-PANI composite were washed several times with distilled water and methanol to remove unreacted chemicals and aniline monomers. They were then allowed to dry under vacuum at room temperature for 24 hr.

Gel permeation chromatography was performed only for the PANI by dissolving in HPLC grade THF solution. FTIR spectrum for the composite was recorded in a KBr pallet by using a nicolet (model Impact 410) spectrophotometer. The presence of Au-NPs inside PANI was confirmed from the XRD patterns recorded using a Seifert powder X-ray diffractometer (XRD TT 3003) with Cu-Kα source (wavelength 1.54 Å). The electrical conductivities of PANI and the composite were measured by a four-probe van-der-Pauw technique.

3.2.3 Results and Discussion

The overall reaction for the synthesis of the Au NP-PANI composite is shown in the following schematic diagram (Figure 3.2.1). The reactions leading to the synthesis of the composite involves two steps, the first step involves the generation of Au NP from the parent metal salt, $HAuCl_4$, in aqueous medium using H_2O_2 as the reducing agent, as discussed earlier (Chapter 3.1). Addition of anilinium chloride to the solution leads to the formation of the composite, where excess H_2O_2 in the solution acts as the oxidizing agent required for the polymerization reaction.

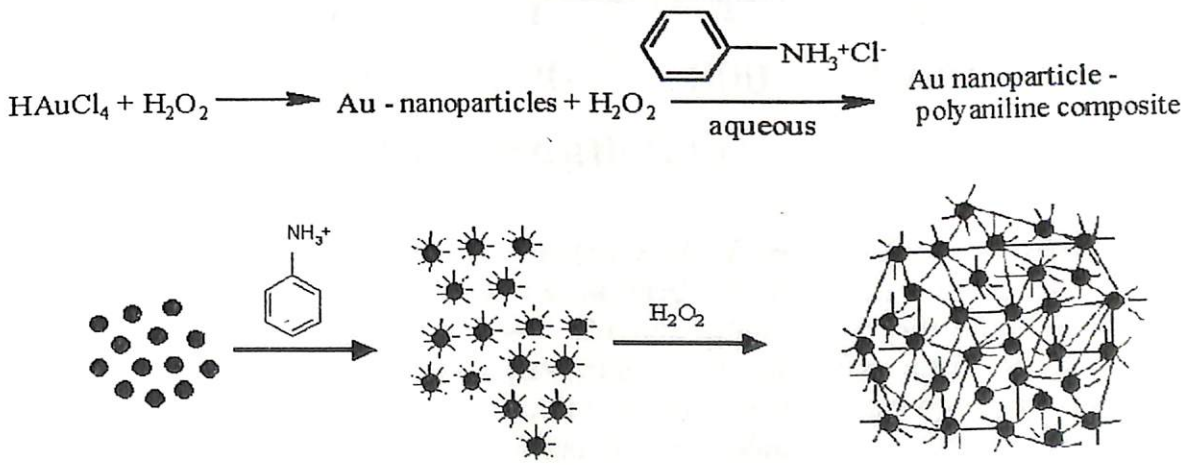

Figure 3.2.1. Schematic representation of the overall reaction leading to the formation of Au NP-PANI composite.

The time dependent progress of the reaction leading to the formation of the composite was monitored by UV-visible spectroscopy the results of which are shown in Figure 3.2.2.

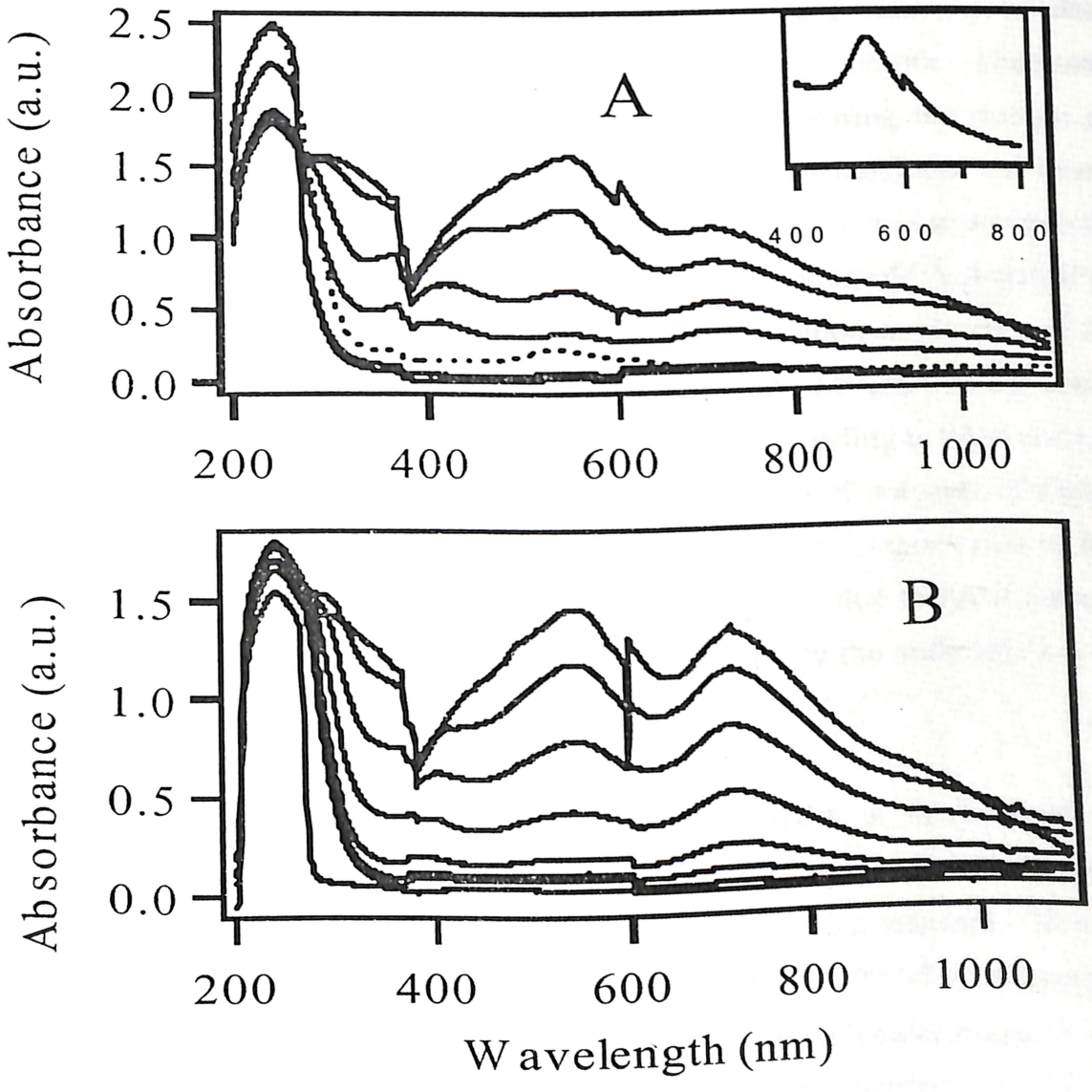

*Figure **3.2.2** (A) Time-dependent UV-Vis spectra of the formation PANI in presence of Au nanoparticle at about 25^{0}C and recorded at several time intervals during the first 250 min. The first scan (bottom) was recorded 20 min after the completion of aniline addition. The PANI peaks can be seen appearing at 50 min after addition of aniline. Dashed line is the UV – Vis absorption spectrum of Au NPs prepared by using H_2O_2 and was recorded before addition of aniline. Inset is the explanded view of the same. (B) Time dependent growth of PANI in absence of Au – NPs recorded at several time intervals during first 220 min of scan. The polyaniline peaks can be seen appearing 40 min after addition of aniline.*

The Au-NP synthesized in aqueous medium by the reduction of $HAuCl_4$ showed a characteristic plasmon resonance band with maxima at 530 nm. With the addition of the anilinium ions to the Au NP, the plasmon resonance band disappeared and then the characteristic absorption peaks for the conductive form of PANI appeared at 730 nm, 520 nm and 440nm. As cleared from the figure (3.2.2 A) strong peaks due to conductive PANI started appearing in about 50 min of addition of anilinium chloride. The intensity of the peaks continued to grow with time. We stopped monitoring the reaction once green precipitation started to appear in about 4 hrs. We also monitored the time-dependent progress of PANI formation in absence of Au NPs by UV-visible spectroscopy. It was observed that the characteristic peaks indicating the formation of PANI started to appear in about 40 min a little sooner compared to the polymerization in presence of Au NP. The results are shown in Figure 3.2.2 B indicating the growth of PANI with characteristic peaks. It is worth noting that the exact shape of the peaks corresponding to PANI and PANI-Au-NP composite varied a little indicating the possible formation of polymers of slightly different molecular weight. In addition, it is important to note the disappearance of Au NP peaks upon addition of anilinium chloride and before the peaks due to PANI started appearing. This is probably due to surface passivation of Au NPs by the anilinium ions reducing the intensity of the plasmon resonance peak.

The molecular weight distributions and dispersity of the conductive polyaniline materials were determined by dissolving them in THF followed by gel permeation chromatography measurement. Polystyrene was used as the standard. However we have measured the molecular weight of the polymer only for the PANI synthesized in absence of the Au NPs. Figure 3.2.3 depicts the chromatograph and molecular weight distribution graph obtained for the PANI formed. The result of the molecular distributions is given in the table below. The molecular weight of the polymer synthesized was found to be 2561 with a polydispersity of 1.0045 with respect to polystyrene as a standard. The unimodal chromatogram of the PANI suggested the formation of polymer species having similar chain length with molecular size distributions within a narrow range as indicated by the polydispersity being close to unity.

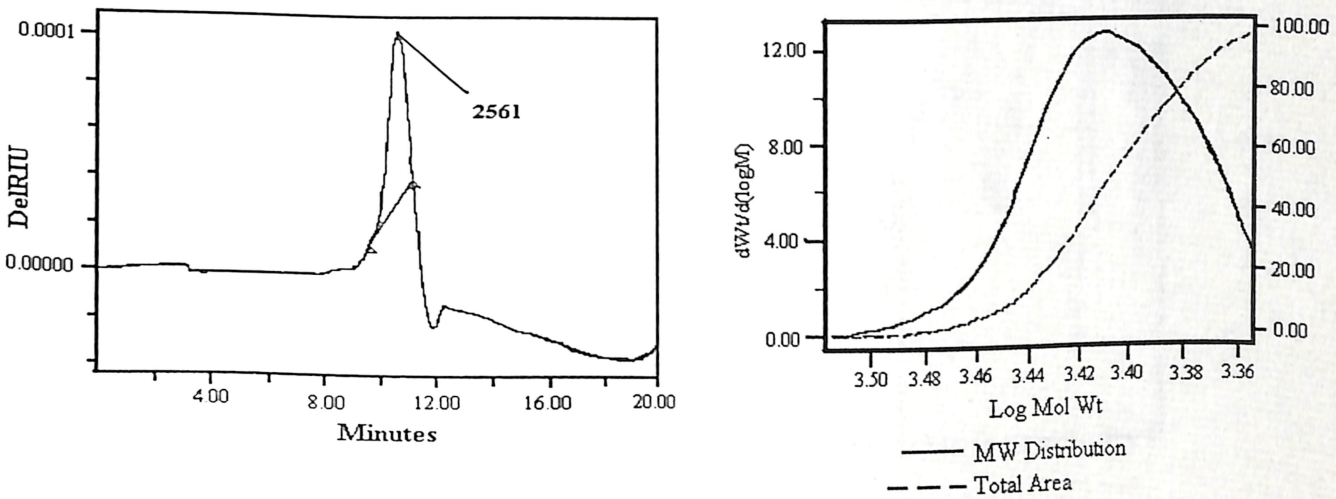

GPC results:

M_n	M_W	MP	M_Z	M_{Z+1}	Polydispersity
2557	2569	2561	2581	2593	1.004504

Figure 3.2.3. Gel-permeation chromatogram (left) and molecular weight distribution graph (right) for the PANI formed in absence of Au NPs by the present method. The result of the molecular weight distribution is shown in the table.

Further confirmation of the nature of polymer came from FTIR spectroscopic investigation of the composite. Figure 3.2.4 shows the FTIR spectra of the Au-NP-PANI composite. The spectrum exhibits the presence of benzoid and quinoid ring vibrations at 1490 and 1570 cm^{-1} respectively[37]. The spectrum of PANI only was similar to this. As commonly observed for the emeraldine salt form of polyaniline, the quinoid band at 1570 cm^{-1} is less intense than that of the benzoid band at 1490 cm^{-1}. The weak and broad band near 3400 cm^{-1} is assigned to the N-H stretching mode. The strong band at 1150 cm^{-1} was described by MacDiarmid[37] as the "electronic like band" and is considered to be a measure of degree of delocalization of electrons and thus a characteristic peak of conductive PANI. The absorbance band at 688 cm^{-1} is due to N-H bending vibrations of the emeraldine salt. In brief the FTIR spectrum indicated the formation of emeraldine salt form of PANI.

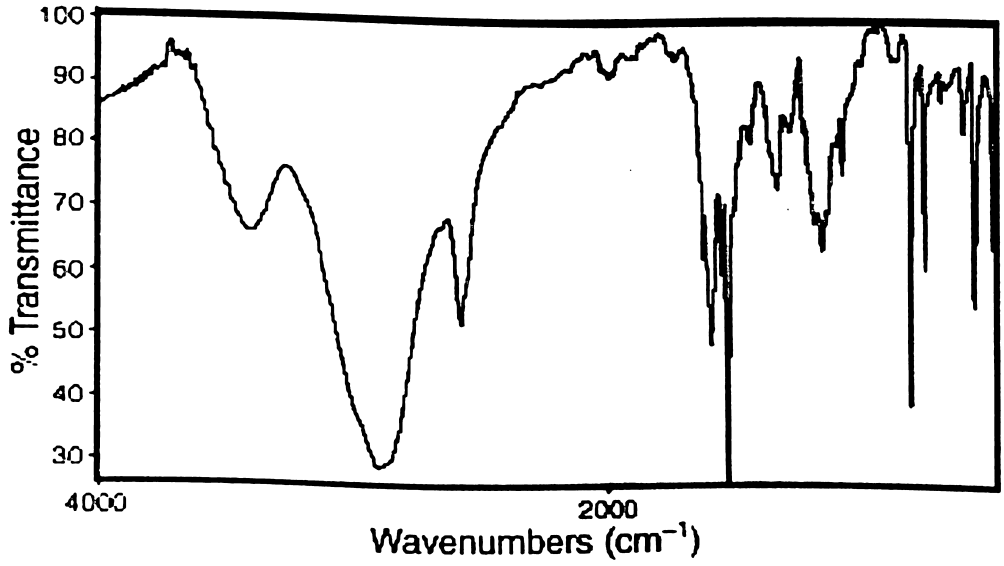

Figure 3.2.4. FTIR spectra of the Au-NP-PANI composite recorded in a KBr pellet.

The ^{1}H NMR spectrum of the composite, as shown in Fig. 3.2.5, contained multiplets in the range δ 7.25–7.5. This indicates formation of a structure with the combination of benzenoid and quinoid forms of the 'emeraldine salt', the primary doped form of PANI, in which two structures coexist: the polaronic form and the bipolaronic structure[35].

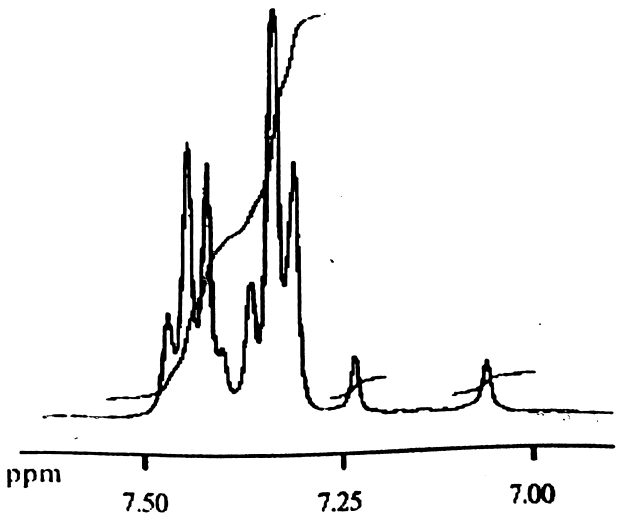

Figure 3.2.5. ^{1}H NMR of Au NP-PANI composite in DMSO.

The incorporation of the Au NPs and their particle size distribution inside the PANI matrix were determined by powder X-ray diffraction (XRD) measurements. For enhanced intensity of the peaks corresponding to the Au NPs we prepared the composite with higher concentration of Au NPs. This was done by the preparation of Au NPs in aqueous medium with addition of 400 μl of H_2O_2 to 20 ml of 4.5 x 10^{-4} M $HAuCl_4$ solution. To the Au NPs thus synthesized, we added anilinium ion solution prepared by addition of 100 μl of aniline with 5 ml of 1M HCl solution. The green precipitate of the composite was washed several times with water and methanol and dried under vacuum. The X-ray diffraction pattern as shown in figure 3.2.6 shows intense peaks at 2θ values of 38.5^0, 43.2^0 and 64.8^0 clearly depicting the three principal Braggs reflections from (111), (200), (220) planes of Au and also in agreement with the previously reported values for the Au NP.[38] An estimation of the mean size of Au NPs in the composite was performed from the width of the (111) Bragg reflection using Debye-Scherrer equation[39]. This method of estimation for the average particle size distribution of nanoparticles using is known to provide sometimes better estimate of particle sizes than electron microscopy. The average size of the Au NPs in the composite was found to be *ca.* 26 nm.

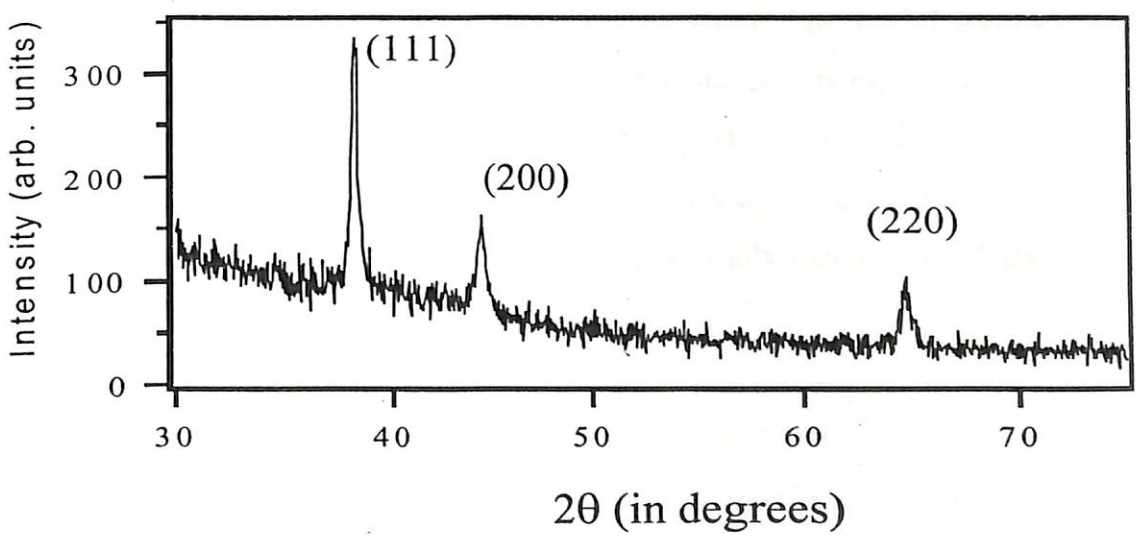

Figure 3.2.6. Powder XRD pattern recorded from an Au NP–PANI composite (for better signals, here the $HAuCl_4$ to aniline ratio was higher than in other cases) deposited on a glass slide. The principal Bragg reflections are identified. A Seifert powder X-Ray diffractometer (XRD 3003 TT) with Cu-K source (wavelength 1.54 Å) was used for recording the above data at room temperature.

The electrical conductivity of the Au NP–PANI composite in the solid state was measured by four-probe method using van der Pauw technique.[40] This technique allows resistivity measurement on arbitrarily shaped but flat homogeneous and samples free from holes. For measuring the conductivity of the Au-NP-PANI composite and only PANI, thin films of the composite and PANI were deposited on mica sheets. The conductivity of a film of the composite, was found to be 0.3 Scm^{-1}, whereas that of PANI in absence of Au NPs was found to be 2.4 x 10^{-3} Scm^{-1}. Thus there was about a two orders of magnitude increase in conductivity upon incorporation of Au NPs in the conductive form of PANI prepared using the present method.

3.2.4 Conclusion

We have introduced herein a simple and novel method of synthesis of Au NPs incorporated in conductive PANI in the form of a composite synthesized in a pot. H_2O_2 was used to reduce $HAuCl_4$ to Au NPs as well as oxidize aniline. The method is important as it decreases the number of sequential steps and avoids the problem of inhomogeneous mixing using the traditional method. The composite showed enhanced electrical conductivity compared to the PANI prepared by the same method. The PANI formed in the composite was the emeraldine form as characterized by various spectroscopic methods. The Au in the composite was in the form of NPs with average particle size of about 26 nm. The increase in conductivity of PANI, with incorporation of only a low concentration of NPs prepared in aqueous solution, may find important application in advanced technology.

3.2.5 References

1. Heeger, A. J. *Angew. Chem. Int. Ed.* **2001**, 40, 2591
2. Shipway, A. N.; Katz E.; Willner, I.; *ChemPhysChe*m, **2000**, 1, 18.
3. Kraft, A. *ChemPhysChe*m, **2001**, 2, 163.
4. Holtz J. H.; Asher, S. A., *Nature*, **1997**, 389, 829.
5. Pernaut J. M.; Reynolds, J. R., *J. Phys. Chem.* B, **2000**, 104, 4080.
6. He, H.; Zhu, J.; Tao, N. J.; Nagahara, L. A.; Amlani I.; Tsui, R., *J. Am. Chem. Soc.*, **2001**, 123, 7730.

7. Kong, J.; Franklin, N. R.; Zhou, C.; Chapline, M. G.; Peng, S.; Cho, K.; Dai, H. *Science* **2000**, *287*, 622.
8. Martin, C. R. *Science* **1994**, *266*, 1961.
9. Nishizawa, M.; Matuse, T.; Uchida, I. *Anal. Chem.* **1992**, 64, 2642
10. Burroughes, J. H.; Jones, C. A.; friend, R. H. *Nature*, **1988**, 335, 137
11. Sirringhaus, H.; Tessler, N.; Friend, R. H. *Science*, **1998**, 280, 1741
12. Wohlgenannt, M.; Tandon, K.; Mazumdar, S.; Ramasesha, S.; Vardeny, Z. V. *Nature*, **2001**, 409, 494
13. Yu, G.; Gao, J.; Hummelen, J. C.; Wudl, F.; Heeger, A. J. *Science*, **1995**, 270, 1789
14. Shah, A.; Torres, P.; Tscharner, R., Wyrsch, N.; Keppner, H. *Science*, **1999**, 285, 692
15. Genies, E. M.; Lapkowski, M. *Synth. Met.* **1988**, 24, 69
16. Stafstorm, S.; Bredas, J. L.; Epstein, A. J.; Woo, H. S.; Tanner, D. B.; Huang, W. S.; MacDiarmid, A. G. *Phys. Rev. Lett.* **1987**, 59, 1464
17. MacDiarmid, A. G. *Angew. Chem. Int. Ed.* **2001**, 40, 2581
18. Chiang, J. C.; MacDiarmid, A. G. *Synth. Met.* **1986**, 13, 193
19. Reghu, M.; Cao, Y.; Moses, D.; Heeger, A. J. *phys. Rev. B* **1993**, 47, 1758
20. Boury, B.; Corriu, R. J. P. *Adv. Mater.* **2000**, *12*, 989.
21. Backov, R.; Bonnet, B.; Jones, D. J.; Rozie`re, J. *Chem. Mater.* **1997**, 9, 1812.
22. Giannelis, E. P. *Adv. Mater.* **1996**, 8, 29.
23. Kerr, T. A.; Wu, H.; Nazar, L. F. *Chem. Mater.* **1996**, 8, 2005.
24. Lira-Cantu, M.; Gomez-Romero, P. *Chem. Mater.* **1998**, *10*, 698.
25. Maeda, S.; Armes, S. P. *Chem. Mater.* **1995**, 7, 171.
26. Xia, H.; Wang, Q. *Chem. Mater.* **2002**, *14*, 2158.
27. Templeton, A. C.; Pietron, J. J.; Murray, R. W.; Mulvaney, P., *J. Phys. Chem. B*, **2000**, *104*, 564.
28. Chandrasekharan, N.; Kamat, P. V., *J. Phys. Chem. B*, **2000**, 104, 10851.
29. Zhou, Y.; Itoh, H.; Uemura, T.; Naka K.; Chujo, Y., *Chem. Commun.*, **2001**, 613.
30. Corbierre, M. K.; Cameron, N. S.; Sutton, M.; Mochrie, S. G. J.; Lurio, L. B.; Rühm A.; Lennox, R. B., *J. Am. Chem. Soc.*, **2001**, 123, 10411.
31. Manners, I., *Science*, **2001**, 294, 1664.

32. Breimer, M. A.; Yevgeny, G.; Sy S.; Sadik, O. A.; *Nano Lett.*, **2001**, 1, 305.
33. Lu, Y.; Yang, Y.; Sellinger, A.; Lu, M.; Huang, J.; Fan, H.; Haddad, R.; Lopez, G.; Burns, A. R.; Sasaki, D. Y.; Shelnutt J.; Brinker, C. J., *Nature*, **2001**, 410, 913.
34. Boal, A. K.; Ilhan, F.; DeRouchey, J. E.; Albrecht, T. T.; Russel T. P.; Rotello, V. M., *Nature*, **2000**, 404, 746.
35. Cochet, M.; Maser, W. K.; Benito, A. M.; Callejas, M. A.; Martinez, M. T.; Benoit, J. M.; Schreiber J.; Chauvet, O., *Chem. Commun.*, **2001**, 1450.
36. Zengin, H.; Zhou, W.; Jin, J.; Czerw, R.; Smith Jr., D. J.; Echegoyen, L.; Carroll, D. L.; Foulger, S. H.; Ballato, J., *Adv. Mater.* **2002**, 14, 1480
37. Sun, Y.; MacDiarmid A. G.; Epstein, A. J., *J. Chem. Soc., Chem. Commun.*, **1990**, 529.
38. Mukherjee, P.; Ahmad, A.; Mandal, D.; Senapati, S.; Sainkar, S. R.; Khan, M. I.; Ramani, R.; Parischa, R.; Ajayakumar, P. V.; Alam, M.; Sastry M.; Kumar, R., *Angew. Chem., Int. Ed.*, **2001**, 40, 3585.
39. Klug H. P.; Alexander, L. E., *X-Ray Diffraction Procedure*, John Wiley & Sons: New York, **1974**, p. 656.
40. *Low Level Measurements*, ed. Yeager J.; Hrusch-Tupta, M. A., Keithly, 5th edn., **1998**, pp. 4–27.

3.3 Synthesis of Nanometer Size Colloidal Conducting Polyaniline and Au Nanoparticle-Polyaniline Composite Particles in Aqueous Medium

3.3.1 Introduction

Polyaniline (PANI) is an electrically conducting polymer having properties that can be exploited in various applications such as microporous electrically conducting materials, anticorrosion protection of metals, molecular sensor, supporting material for catalysts[1]. Among the conducting polymers, PANI has been studied extensively due to its good environmental stability and also because its electrical properties can be modified by the oxidation state of the main chain or degree of protonation[2]. However the processibility of conductive form of PANI has been reduced due to its insolubility in aqueous medium and most of the common organic solvents[3].

The preparation of PANI in colloidal form is one of the attractive alternatives to overcome the poor processability of PANI due to its insolubility in common organic solvents and water. There have been numerous reports on the preparation of PANI dispersions containing 100–300 nm sized particles. Usually, they are produced with suitable polymeric stabilizers[4], such as poly(vinyl alcohol), poly(N-vinylpyrrolidone), poly(vinyl methyl ether), cellulose ethers or sophisticated tailor-made copolymer architectures. In another approach, dispersed particles in the nanometer dimension of the conductive polymers, such as polypyrrole, were synthesized by controlling the rate of polymerization at low temperature[5]. PANI and polypyrrole nanotubes and nanofibers have also been synthesized through self assembly[6] using various oxidizing agents such as camphor sulphonic acids (CSA), β-napthalenesulphonic acid (β-NSA) which also function as the stabilizing agents. Their use as chiral sensor has also been demonstrated[7]. Conductive polymer nanotubes[8] used for effective separation of biomolecules, have also been synthesized in various membranes, such as alumina, carbonate or porous carbon membranes with uniform pour sizes.

On the other hand core-shell nanoparticles consisting of metal nanoparticles as the core and polymer as the shell[9] or polymer nanoparticles as the core and metal nanoparticles deposited on the polymer surface[10] have attracted interest because of their potential applications in catalysis, controlled delivery, artificial shells, light fillers, low dielectric constant materials, acoustic insulation and photonic crystals. In this regard, conducting polymer particles have gained wide attention due to their inherent application potentials. A significant volume of efforts has been made for the synthesis of core shell nanoparticles with conducting polymers as the core or the shell. In addition, synthesis of metal nanoparticle-conducting polymer composite with sizes in the nanometer domain has been performed. Most of these methodologies apply self-assembled process[11] or Layer-by-layer[12] (LBL) techniques. Synthesis of ordered PANI inverse opals appropriate for the photonic applications have also been reported by Caruso and coworkers[13] using ordered colloidal assemblies as the template.

In this chapter, we report a new microemulsion based method to form dispersed aqueous PANI as well as Au-NP-PANI composite with nanometer size particles. The method is based on controlling the sizes of the PANI and Au-NP-PANI composite particles by introducing the aniline monomer from the vapor phase while the reaction is performed in aqueous solution. Microemulsion, defined as a thermodynamically stable and isotropic, transparent solution of two immiscible liquids consisting of oil, water and surfactant molecules, has been employed as a polymerization medium to obtain metal particles and polymers in the nanometer dimension[14]. In our work, the introduction of aniline from the vapor phase to an aqueous acidic micellar solution containing the oxidizing agent resulted in the formation of nanometer size PANI particles. In the previous work we reported the synthesis of Au-NP-PANI composite using H_2O_2 both as oxidizing as well as reducing agent. Here we extended the same idea for the formation of the composite with nanometer size particles. We have used sodium dodecyl sulfate (SDS) as the surfactant. It is well known that ordinary micelles such as SDS are too small to serve as hosts for large domains, and they usually dissolve molecules as monomers. Thus the shape of the micelles prevents the formation of large linear oligomers in the subsequent acid-catalyzed polymerization[15]. The formation of the PANI particles were confirmed by UV-visible and IR spectroscopy.

Transmission electron microscopy (TEM) and X-ray diffraction (XRD) studies were performed to have an insight about the particle sizes and incorporation of Au NPs in the composite. Our observations suggest that nanoparticles of PANI and Au-NP-PANI composite could be obtained using the present method where particle sizes were below 100 nm diameter. Also, TEM micrographs showed the evidence of formation of Au-core-PANI-shell composite.

3.3.2. Experimental Section

Materials: Aniline (Merck) was distilled under vacuum prior to use. Sodium dodecyl sulfate (SDS) and 30% H_2O_2 solution were from Merck. $HAuCl_4$ (17% w/w in HCl solution) was obtained from Aldrich and used without further purification. For all the experiments MilliQ water was used.

Preparation of dispersed PANI particles: 1.2×10^{-2} M (1.5 cmc) SDS solution was prepared by dissolving 0.17 g of SDS in 45 ml of water in a 250 ml stoppered conical flask. The solution was magnetically stirred until all the surfactants were solubilized. To the solution conc. HCl (11.2 M) were added, so that the total concentration of acid in the solution was 1 M. 600 µl of H_2O_2 were then added to the acidic surfactant solution. 2ml of distilled aniline was taken separately in a 3 ml sample vial and the vial was kept hanging from the top of the conical flask so that only the aniline vapor can go to the solution and no liquid aniline comes in contact with the solution. The reaction was allowed to take place for about 12 hr, while the solution being continuously stirred, whereupon the color of the solution turned light green to dark green starting from a colorless solution. The reaction was stopped as soon as the dark green polymers were obtained, which is indicative of the formation of emeraldine salt form of polyaniline. This was done by removing the vial with aniline and quickly stoppering the flask. The solution remained in the dispersed state for months without any observable precipitation. In order to obtain the polymer, the dispersed solution was first centrifuged; the precipitate was washed for several times with methanol and dried under vacuum prior to analytical measurements. The reaction was carried out at room temperature, which varied between 20 and 30°C.

Preparation of dispersed Au-NP-PANI composite: In a conical flask 45 ml of 1.2 x 10^{-2} M SDS solution was prepared in water. From a stock solution of $HAuCl_4$ 600 µl of was added to the micellar solution so that the total concentration of $HAuCl_4$ in the solution became 4.5 x 10^{-4} M. To the solution 600 µl of H_2O_2 were added and magnetically stirred for 5 min whereupon Au nanoparticles were generated with the characteristic purple-red color. To the solution conc. HCl was added so that the final conc. of HCl became 1 M. The purple color of the Au nanoparticles faded away upon addition of HCl to the solution. The aniline was introduced from the vapor phase in a separate vial and the stopper of the conical flask was sealed. The reaction was allowed to take place with magnetically stirring for about 10 hr until the color of the solution turned dark green. The reaction was stopped by removing the aniline containing vial from the conical flask. In order to obtain the composite, the dispersed solution was first centrifuged; the precipitate was washed for several times with methanol and dried under vacuum prior to further studies. The reaction her also was carried out at room temperature, which varied between 20 and 30°C.

Analytical studies: UV-visible spectra of the dispersed particles as synthesized were recorded in a Hitachi UV-visible spectrophotometer (model U2001). IR spectra of the cleaned and dried precipitates were recorded in KBr pallets, using a Perkin-Elmer FTIR (Spectrum one) spectrometer. X-ray diffraction studies were performed by depositing the colloidal particles on a glass slide followed by drying in vacuum. A Seifert powder X-Ray diffractometer (XRD 3003 TT) with Cu-K source (wavelength 1.54 Å) was used for recording the above data at room temperature. The transmission electron microscopic studies of the samples were performed, by depositing the colloidal particles on a copper grid and then drying in vacuum. A Jeol electron microscope (JEM 100 CX II) operated at 80 kV accelerating voltage was used for these measurements.

3.3.3. Results and discussion

In an earlier section we have described that when anilinium chloride was added to a solution of Au NPs, prepared by using H_2O_2 as the reducing agent, precipitate consisting of Au-NP-PANI composite was obtained. The composite had better electrical conductivity

than the polymer alone. Encouraged by the success we worked further to develop a method where the polymer as well as the composite would remain in the aqueous solution as dispersed particles. One of the ways to achieve this could be by slowly supplying aniline / anilinium ions. We have earlier prepared PANI by vapor phase introduction of aniline in a different experimental condition. We wanted to try the same method of introducing aniline from the vapor phase in the present study. We observed that under the present experimental conditions polymer could also be generated by introducing aniline from the vapor phase to the reaction medium, thereby having control over supply of one of the essential reactants. In other words, the reaction beginning and termination could be controlled externally. In this way, we observed that PANI as well as composite of Au NP and PANI could be produced in the form of stable dispersion in aqueous medium.

As a first characterization of the product formation we show, in Figure 3.3.1, the UV-visible spectra of the PANI and Au-PANI composite dispersed in aqueous medium. Shown in the inset is the characteristic visible spectrum of Au NPs synthesized by the reduction of $HAuCl_4$ with H_2O_2 as the reducing agent recorded in the wavelength range 800-400 nm in aqueous SDS solution (1.2×10^{-2}M). The UV-visible spectrum of dispersed PANI particles synthesized in absence of Au showed peaks at 760 and 435 nm, characteristic of the emeraldine form of PANI. In the case of Au NP-PANI composite, Au NPs were first synthesized in aqueous micellar medium, which showed a plasmon resonance band at 530 nm. When conc. HCl was added to the Au NP solution, the intensity of the plasmon resonance band had diminished. Upon introduction of aniline from the vapor phase the color of the solution changed from colorless to light green to dark green. The solution absorption spectrum exhibited peaks at 790 and 435 nm characteristic of the formation of emeraldine PANI. The plasmon resonance band of the Au NPs was not observed in the composite spectrum. The longitudinal band in case of the composite appeared red-shifted by about 30 nm compared to only PANI prepared in absence of Au NPs. The longitudinal band shift, could be due to formation of PANI of a different molecular weight or could also be a signature of the level of protonation of PANI in the composite.

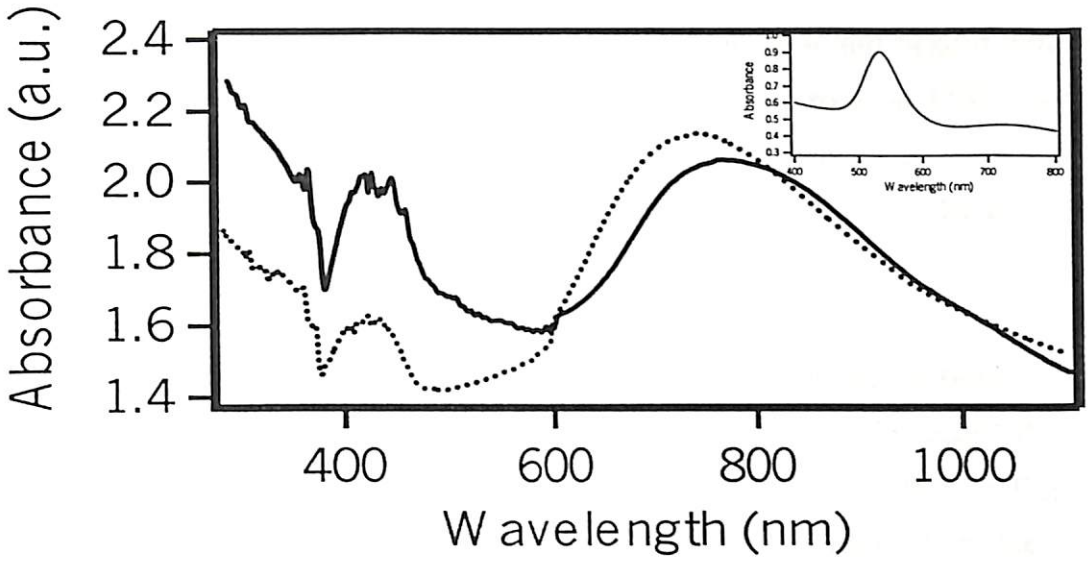

*Figure **3.3.1**. UV-visible spectra of colloidal PANI (dotted) and Au NP-PANI composite (solid) in aqueous SDS solution prepared by the present method using H_2O_2 both as oxidizing and reducing agent. Inset shows the UV-visible spectrum of Au NPs synthesized in aqueous SDS solution using H_2O_2 as the reducing agent.*

We have also recorded the FTIR spectra of PANI and Au-NP-PANI composite and the results are shown in Figure 3.3.2. Both the spectra are identical indicating that there is no structural difference between PANI alone and PANI in the Au NP-PANI composite.

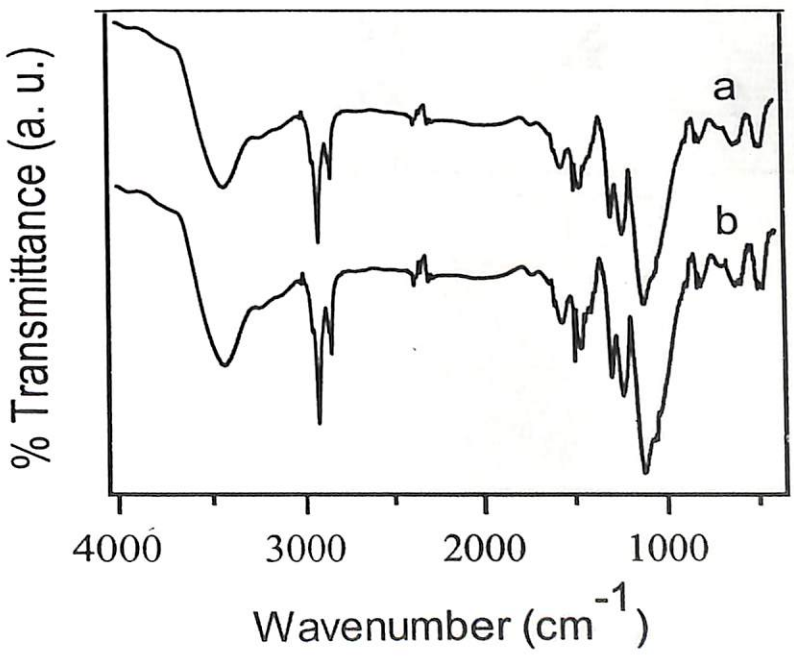

*Figure **3.3.2**. FTIR spectra of (a) PANI (b) Au NP-PANI composite in KBr pellets.*

The peaks at 1590 and 1500 cm^{-1} depict the quinoid and bezoid deformations of the emeraldine form of polyaniline. In both cases the quinoid band at 1590 cm^{-1} is less intense than that of the benzoid band at 1500 cm^{-1}. The intense peak at 1150 cm^{-1} suggests the formation of the conductive form of PANI, as it is a measure for the delocalization of the electrons in the polymer backbone.

We further pursued the investigation to learn about the particle sizes of PANI and Au-NP-PANI composite as formed in the aqueous solution. We recorded TEM pictures of the samples dried on a copper grid. The micrographs are shown in Figure 3.3.3. The micrograph in Figure 3.3.3a indicates that PANI was generated in the form of largely spherical particles with a wide distribution of particle sizes with average particle diameters below 100 nm.

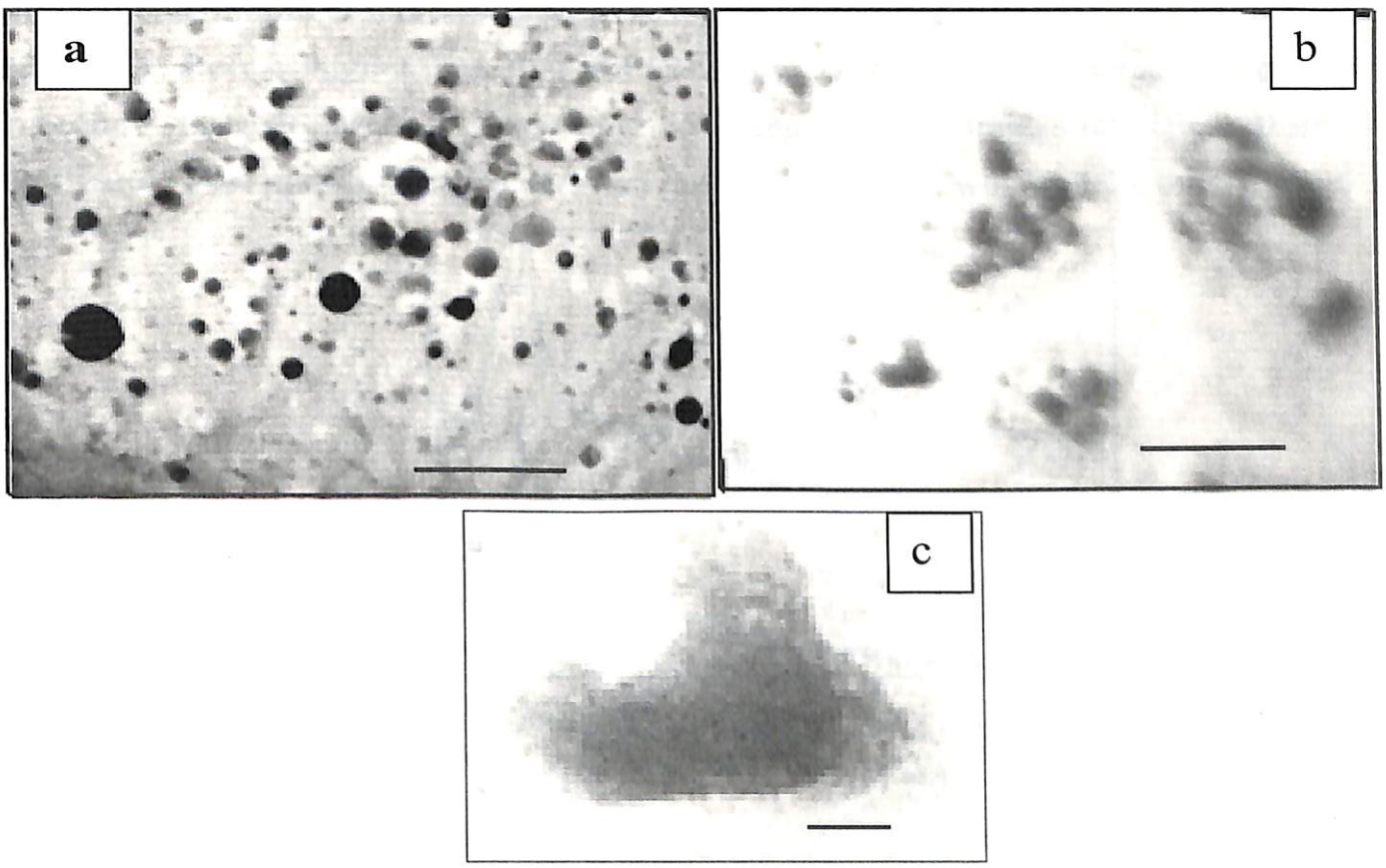

Figure 3.3.3. (a) Transmission Electron micrograph of colloidal PANI particles prepared by the present method. Scale bar is 200 nm. (b) TEM of Au NP-PANI composite with scale bar at 200 nm (c) Au NP / PANI core shell nanoparticle. Scale bar is 20 nm.

On the other hand the TEM studies of Au-NP-PANI composite (Figure 3.3.3b) revealed the formation of aggregated particles, with PANI layer formation around aggregated NPs, resulting in greater than 100 nm diameter clusters of well-separated composite particles. A closer look into the TEM micrograph depicts the formation of Au-NP-PANI core-shell nano composites with assembled Au-NP distinguishable by dark cores surrounded by grayish shells of PANI (Figure 3.3.3c).

Further, the presence of Au NPs in the dispersed composite was further confirmed by powder X-ray diffraction studies (shown in 3.3.4). In the case of PANI (only) particles, two broad bands appeared at 2Θ values of 22^0 and 26^0 indicative of low level of crystalline phase in the polymer[16]. In Au-NP-PANI composite, the peak appearing at 23^0 is sharper and stronger implying that the molecular chains of the PANI prepared in the micellar medium are in a much more ordered state in presence of Au NPs and the crystallinity of the PANI in the composite was higher than that in PANI only. Further, three strong bands appeared with maximum intensity at 38.5^0, 43.4^0 and 65.1^0 representing Bragg's reflections from (111), (200) and (220) planes. This means that the Au NPs had growth in all the three planes.

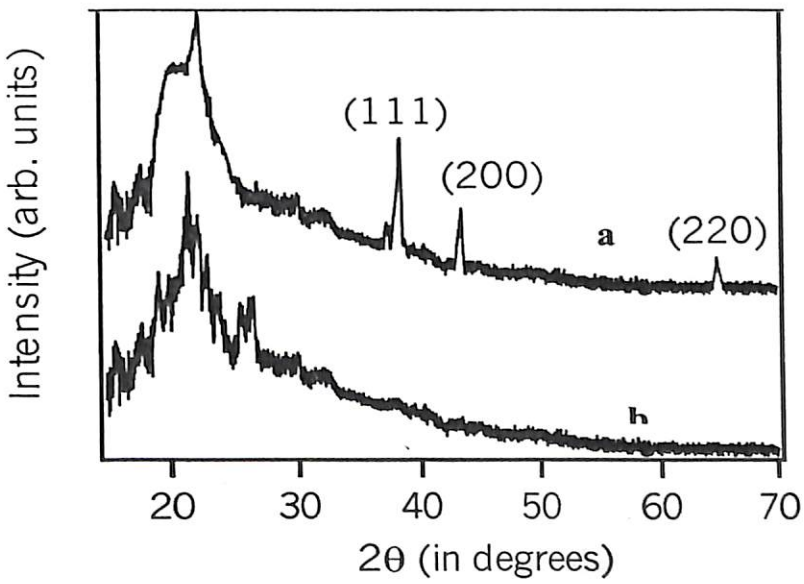

Figure 3.3.4. Powder X-ray diffraction spectra of (a) Au NP-PANI composite particles and (b) PANI particles. The spectra were recorded by depositing the colloidal solutions on a glass plate. The principal Bragg's reflections are identified for the Au nanoparticles. A seifert X-ray diffractometer (XRD 3003 TT) with Cu Kα source (wavelength 1.54 Å) was used for recording the above data at room temperature.

Finally, we have been able to achieve PANI and Au-NP-PANI composite formation in the form of nanometer sized particle dispersion in aqueous medium. In this regard, we have taken advantage of two factors. First is the vapor phase introduction of aniline, which means a slow release of a reagent and also termination of the reaction is controllable by removing the vial containing aniline. The second factor, which is equally important, is the use of SDS micelles in the reaction medium. It is well known that hydrophobic molecules are dissolved in the hydrophobic core of micelles, whereas the polar molecules are solubilized at the micelle-water interface. In case of anilinium ion, it has been reported that anilinium cations are adsorbed at the micellar surface by electrostatic interaction with anionic parts of SDS molecules fully exposed to the aqueous phase[17]. Thus we assume that the aniline monomers were solubilized at the micelle-water interface, which is schematically shown in Figure 3.3.5. The polymerization might have taken place while anilunium ions were at the interface leading to spherical particle formation. The large size and their variation in the polymer particles generated indicate a large number of such micelles with dissolved anilinium ions might have come together at the time of formation. And the number of such micelles varied widely leading to the variation of sizes of the polymer particles generated in the medium.

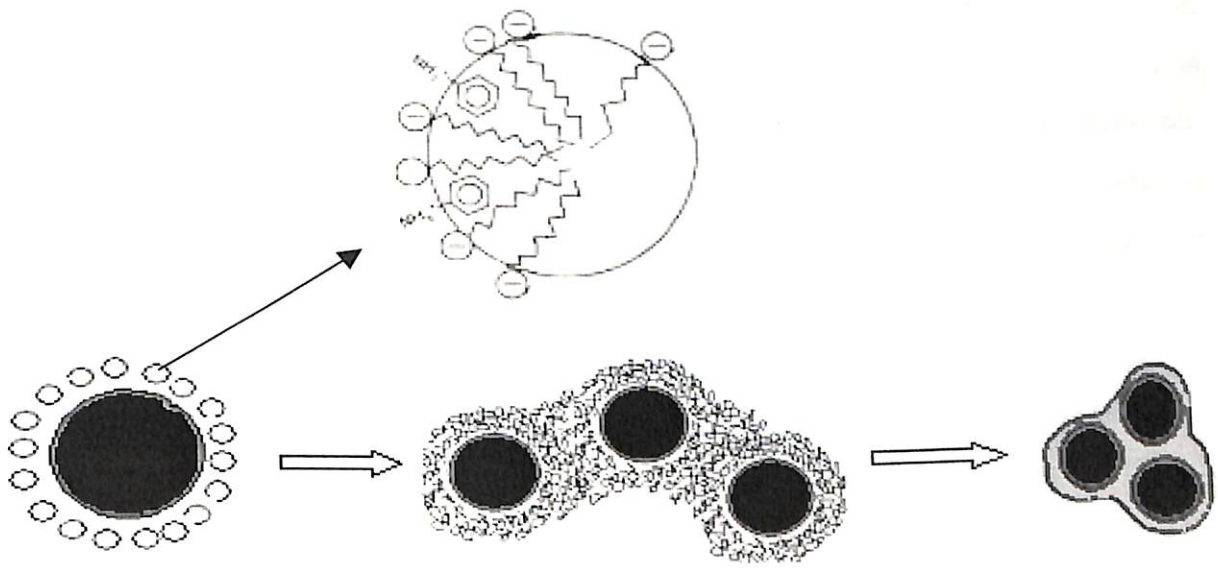

*Figure **3.3.5**. (top) A pictorial representation for the dissolution of anilinium ions at the micelle-water interface (bottom) Schematic representation for the formation of Au NP-PANI composite particles at the nanometer dimension. Each circle surrounding the Au-NP corresponds to diagram in the section "top".*

We propose the following mechanism of formation of Au-NP-PANI composite in the present case. Au NPs are surrounded by anilinium ions in the medium. A number of such particles come together leading to polymerization and thus composite formation. The number of such particles in a composite is decided by the number of available Au NP surrounded by anilinium ions. As the concentration of anilinium ions in the solution is low the polymerization with such particles is more favored than polymerization process from free anilinium ions. In addition, SDS micelles act as stabilizer of Au NPs as well as help dissolve anilinium ions. This means agglomeration of Au-NPs with simultaneous polymerization of from anilinium ions would be favored at lower anilinium concentration. This is because Au NPs have been stabilized by the micelles first before introduction of anilinium ions. Anilinium ions would go to the micelles and polymerize in presence of a number of Au NPs resulting in composite particle formation. The proposed mechanism of formation of the Au-NP-PANI composite particles with the nanometer dimension by the present method has been shown schematically in figure 3.3.5.

3.3.4. Conclusion

Herein we have reported the generation of conducting PANI and Au-NP-PANI composite nanometer size particles dispersed in aqueous medium. The controlled polymerization had been achieved using sodium dodecyl sulfate surfactants as the micellar medium and controlling the monomer concentration by introducing aniline from the vapor phase. Polymerization of aniline using H_2O_2 as the oxidizing agent in acidic solution resulted in the formation of nanometer size spherical particles well separated from each other. In case of composite, H_2O_2 was used both as the oxidizing as well as reducing agent. The result was the formation of aggregated particles, with the PANI shell formed around aggregated Au NPs. Both the colloidal PANI and the composite particles were formed with emeraldine PANI.

3.3.5 References

1. (a) *Handbook of Conducting Polymers*, ed. Skotheim, T. A.; Elsenbaumer, R. L.; Reynolds, J. R., Marcel Dekker: New York **1997**, Vols. 1 & 2 (b) *Handbook of*

Organic Conductive Molecules and Polymers, ed. Nalwa, H. S.; Wiley: Chichester, UK **1997**, Vols. 1-4

2. a) MacDiarmid, A. G. *Synth. Met.* **1997**, 84, 27. (b) MacDiarmid, A. G.; Chiang, J. C.; Richter, A. F.; Epstein, A. J. *Synth. Met.* **1987**, 18, 285. (c) Chinn, D.; Dubow, J.; Liess, M.; Josowicz, M.; Janata, J. *Chem. Mater.* **1995**, 7, 1504. (d) MacDiarmid, A. G.; Epstein, A. J. *In Science and Applications of Conducting Polymers*; Salaneck, W. R., Clark, D. T., Samuelsen, E. J., Eds., Adam Hilger: Bristol, England, **1990**. (e) Cao, Y.; Li, S.; Xue, Z.; Guo, D. *Synth. Met.* **1986,** 16, 305. (e) Westerweele, W.; Smith, P.; Heeger, A. J. *Adv. Mater.* **1995**, 7, 788. (f) Paul, E. W.; Rico, A. J.; Wrighton, M. S. *J. Phys. Chem.* **1985**, 89, 1441.
3. (a) Genies, E. M.; Boyle, A.; Lapkowski, M.; Tsintavis, C. *Synth. Met.* **1990**, 36, 139. (b) MacDiarmid, A. G.; Chiang, J. C.; Richter, A. F. *Synth. Met.* **1987**, 18, 285.
4. (a) Armes S. P.; Vincent, B., *J. Chem. Soc., Chem. Commun.*, **1987**, 288; (b) Armes S. P.; Aldissi, M., *J. Chem. Soc., Chem. Commun.*, **1989**, 88; (c) Cawdery, N.; Obey T. M.; Vincent, B. *J. Chem. Soc., Chem. Commun.*, **1988**, 1198. (d) Vincent B.; Waterson, J., *J. Chem. Soc., Chem. Commun.*, **1990**, 683. (e) Stejskal, J.; Kratochvil, P., *Langmuir* **1996**, 12, 3389. (f) Arms, S.P.; Aldissi, M.; Agnew, S.F.; Gottesfeld, S. *Langmuir* **1990**, 6, 1745. (g) Banerjee, P.; Bhattacharyya, S. N.; Mandal, B.M., *Langmuir*, **1995**, 11, 2414. (h) Chattopadhyay, D.; Banerjee, S.; Chakravorty, D.; Mandal, B.M., *Langmuir*, **1998**, 14, 1544.
5. (a) Jang, J.; Oh, J. H.; Stucky, G. D. *Angew. Chem. Int. Ed.* **2002**, 41, 4016 (b) Jang, J.; Oh, J. H. *Chem. Commun.* **2002**, 2200
6. (a) Wei, Z.; Zhang, Z.; Wan, M. *Langmuir* **2002**, 18, 917. (b) Huang, L. M.; Wang, Z. B.; Wang, H. T.; Cheng, X. L.; Mitra, A.; Yan, Y. X.; *J. Mater. Chem.* **2002**, 12, 388. (c) Huang, K.; Wan, M., *Chem. Mater.* **2002**, 14, 3486. (d) Huang, J.; Virji, S.; Weiller, B. H.; Kaner, R. B., *J. Am. Chem. Soc.* **2003**, 125, 314
7. Huang, J.; Egan, V. M.; Guo, H.; Yoon, J-Y, briseno, A. L.; Rauda, I. E.; Garrell, R. L.; Knobler, C. M.; Zhou, F.; Kaner, R. B. *Adv. Mater.* **2003**, 15, 1158
8. (a) Wu, C. G.; Bein, T. *Science* **1994**, 264, 1757. (b) Martin, C. R. *Chem. Mater.* **1996**, 8, 1739 (c) Martin, C. R., *Acc. Chem. Res.* **1995**, 28, 61 (d) Parthasarathy, R.;

Martin, C. R., *Nature*, **1994**, 369, 298 (d) Lei, Z.; Zhang, H.; Ma, S.; Ke, Y.; Li, J.; Li, F., *Chem. Commun.* **2002**, 676

9. (a) Liu, Y. C.; Chuang, T. C. *J. Phys. Chem. B*, **2003**, 107, 12383 (b) Shin, H. J.; Hwang, I. W.; Hwang, Y. N.; Kim, D.; Han, S. H.; Lee, J. S.; Cho, G. *J. Phys. Chem. B*, **2003**, 107, 4699 (c) Choi, S. J.; Park, S. M., *Adv. Mater.*, **2000**, 12, 1547 (d) Marinakos, S. M.; Anderson, M. F.; Ryan, J. A.; Martin, L. D.; Feldheim, D. L., *J. Phys. Chem. B*, **2001**, 105, 8872 (e) Cao, H.; Xu, Z.; Sang, H.; Sheng, D.; Tie, C., *Adv. Mater.* **2001**, 13, 121
10. (a) Brown, K. R.; Natan, M. J. *Langmuir*, **1998**, 14, 726 (b) Jackson, J. B.; Halas, N. J. *J. Phys. Chem. B*, **2001**, 105, 2743 (c) Ji, T.; Lirtsman, V. G.; Avny, Y.; Davidov, D. *Adv. Mater.* **2001**, 13, 1253 (d) Kaltenpoth, G.; Himmelhaus, M.; Slansky, L.; Caruso, F.; Grunze, M. *Adv. Mater.* **2003**, 15, 1113 (e) Freeman, R. G.; Grabar, K. C.; Allison, K. J.; Bright, R. M.; Davies, J. A.; Guthrie, A. P.; Hommer, M. B.; Jackson, M. A., Smith, P. C.; Walter, D. G.; Natan, M. J. *Science*, **1995**, 267, 1629
11. (a) Zhang, L.; Wan, M. *J. Phys. Chem. B*, **2003**, 107, 6748 (b) Watson, K. J.; Zhu, J.; Nguyen S. T.; Mirkin, C. A. *J. Am. Chem. Soc.*, **1999**, 121, 462.
12. Oldenburg. S. J.; Averitt, R. D.; Westcott, S. L.; Halas, N. J. *Chem. Phys. Lett.*, **1998**, 288, 143
13. Wang, D.; Caruso, F., *Adv. Mater.*, **2001**, 13, 350
14. (a) Kuramoto, N.; Genies, E. M. *Synth. Met.*, **1995**, 68, 191. (b) Kinlen, P. J.; Liu, J.; Ding, Y.; Graham, C. R.; Remsen, E. E., *Macromolecules,* **1998**, 31, 1735. (c) Riede, A.; Helmstedt, M.; Riede, V.; Stejskal, J., *Langmuir,* **1998**, 14, 6767. (d) Premachandran, R.; Banerjee, S.; John, V. T.; McPherson, G. L.; Akkara, J. A.; Kaplan, D. L., *Chem. Mater.*, **1997**, 9, 1342. (e) Cason, J. P.; Miller, M. E.; Thompson, J. B.; Roberts, C. B., *J. Phys. Chem. B*, **2001**, 105, 2297
15. Li, G.; Fudickar, W.; Skupin, M.; Klyszcz, A.; Draeger, C.; Lauer, M.; Fuhrhop, J. H. *Angew. Chem. Int. Ed.*, **2002**, 41, 1828
16. Yan, F.; Xue, G. *J. Mater. Chem.*, **1999**, 9, 3035
17. Kuramoto N. Tomita A. *Polymer,* **1997**, 38, 3055

CHAPTER 4

STARCH AS A TEMPLATE FOR SOLUBILIZATION OF POLYANILINE IN AQUEOUS MEDIUM AND SHAPE-SELECTIVE SYNTHESIS OF Au-NANOPARTICLES

4.1 Reversible Encapsulation of Nanometer size Polyaniline and Au nanoparticle-Polyaniline Composite in Starch

4.1.1 Introduction

Polyaniline (PANI) is a well-studied electrically conducting organic polymer with the potential of a variety of applications such as in batteries[1], microelectronics[2], displays[3], antistatic coatings[4], electromagnetic shielding materials[5], sensors[6] and actuators[7]. In addition, its good environmental and thermal stability and the ability to have tunable conductivity by appropriate doping make PANI an ideal active material for such applications. Even though the potential is immense, the applications remain quite below the potential due to its poor solubility in most organic solvents and insolubility in water. Several strategies have been developed to overcome such problems. For example, the protocols that have been used to make water soluble PANI are the generation of sulfonated PANI[8], phosphonic acid doped PANI[9] and enzymatic synthesis of PANI / sulfonated polystyrene complex[10]. In different systems, there are several other methods that have been employed to facilitate application of PANI in various forms, such as water dispersion of PANI nanofibers[11], self-assembled PANI Nanotubes[12] formation, polymerization of aniline inside macroporus carbon[13], rod-like inclusion complex formation of cyclodextrin and PANI[14], direct assembly of large arrays of PANI nanowires[15]. Notwithstanding the advancement mentioned above, for the realization of the full potential of PANI, biocompatibility of the polymer is essential. One strategy that could possibly be used is the reversible complex formation with a biopolymer, where the complex would be soluble in water and PANI can be delivered under appropriate releasing condition. In an ideal situation, the mechanical properties of PANI could also be enhanced by forming complex with another polymer such as carbohydrates. This would be similar to the case of a methylcellulose and polypyrrole composite[16] that has been synthesized with enhanced mechanical properties of the conducting polymer. Thus it makes all the more sense that we search for methods of inclusion of PANI in biopolymers to harness the electrical conductivity of PANI and mechanical properties of the biopolymer.

On a different domain there has been a increasing interest in the generation of organic[17] and inorganic[18] supramolecular assemblies for encapsulation of guest

molecules with intended application in solubilization[19], catalysis[20], controlled delivery[21] and to grow materials with the structural motif of the host[22]. There are several choices that are available in this regard. For examples, one of them is amphiphiles, which form three-dimensional fluid structures like micelles and vesicles, while the other would be starch[23] forming helical structures of controllable sizes in aiding the solubilization of hydrophobic molecules inside their hydrophobic core while the outer hydrophilic layer helps in getting dissolved in water. Several forms of Cyclodextrins, an important class of carbohydrates, have been playing the role of host to a number of important chemical compounds and chemical reactions with their fixed sizes and shapes. The linear analog starch offers a unique advantage in this regard. First of all it is a biopolymer and thus very safe. It is known to form a helical structure with a hydrophobic core that can accommodate hydrophobic moieties while the molecule itself can be dissolved in water. In addition, amylose is reported to form helical structure of variable pocket sizes according to the size of the host. Stoddart and coworkers have recently taken advantage of this property in dissolving and purifying carbon nanotubes in water[24].

We were interested in finding a simple and useful way of solubilizing PANI in water such that its recovery could easily be achieved. As explained in the background above one of the favorable and flexible molecules of choice is starch. We have selected starch for its flexible pocket size in forming helix with a hydrophobic guest molecule, solubility in water and the ability of an enzyme to digest starch for the recovery of the polymer at appropriate site and reaction condition. There were two polymers in our hands. One is the PANI synthesized as bulk precipitate insoluble in water, while the other is starch soluble in water with possible hydrophobic core. We were also interested in the investigation of the nature of incorporation of PANI in starch (in terms of particle sizes) starting with a bulk PANI. In this chapter, we introduce the idea and report the results of solubilization of PANI in water by encapsulation in starch. In addition, we show that PANI-Au-nanoparticles (NP) composite, which we have reported in the previous chapter, could also be encapsulated using the same method. We have shown in an earlier experiment that PANI-Au NP composite has significantly (at least 100 fold) higher electrical conductivity than the PANI alone when synthesized using our method. Further, in general, composite represents higher level of functional superiority compared to its constituents by themselves. Thus finding ways of processing PANI-Au-NP composite is equally, if not more, important as for the polymer itself. We have found that the PANI-Au-NP composite, like PANI, is also insoluble in water and typical

organic solvents. Hence we have pursued the solubilization study of PANI-Au-NP composite in starch in the present set of experiments. In the present method, the encapsulation has been achieved by dissolving PANI as well as Au-nanoparticles-PANI composite in aqueous solutions of starchin the presence of ultrasonic waves. The additional fortuitous advantage of our method is that for encapsulation the starch molecules do not necessarily need pre-organization by small molecules like I_2 thereby making the process straightforward and single step. We also show that this encapsulation is completely reversible and both PANI and the composite could be recovered by introducing molecular iodine in the aqueous solution of either of them. Interestingly, we observed that PANI could also liberate I_2 from starch–iodine complex while the polymer itself got encapsulated inside starch. Further, PANI could be liberated from starch-PANI composite by hydrolyzing starch using an enzyme (diastage). Our observations with transmission electron microscopic measurements suggest that PANI and the PANI-Au-NP composite were dispersed in starch solution in the form of particles having average diameters on the order of 10-20 nm.

4.1.2 Experimental Section

Preparation of conducting polyaniline

The green colored emeraldine salt form of PANI was prepared by polymerization of aniline in acidic medium using H_2O_2 as the oxidizing agent. Typically, to a 1.25 X 10^{-2} M (~ 1.5 cmc) sodium dodecyl sulfate (SDS) solution prepared in milliQ water, conc. HCl was added so that the final concentration of acid was 0.1 M and the final volume was 50 ml. The solution was constantly stirred to which 200 µl of distilled aniline and 500 µl of 30% H_2O_2 were added. The green colored PANI was obtained as a precipitate in about 12 hrs. The PANI precipitate was separated by decantation and was then cleaned by washing with distilled water for several times. The excess surfactants were removed by washing PANI with methanol followed by centrifugation and decantation in several cycles. The final green precipitate was dried in vacuum. UV-visible, FTIR spectroscopic measurements were performed to confirm the formation of emeraldine salt of PANI. In an earlier experiment[25] (see Chapter 3.2) we have found that the average molecular weight of PANI synthesized by this method was 2500 dalton (obtained from gel permeation chromatography data).

Solubilization of polyaniline in starch solution and further precipitation by I_2

Starch solution was prepared by dissolving 0.2g of starch in 100ml of boiling water. The solution was cooled to room temperature. To 20 ml of the starch solution, 12mg of PANI was added and it was then kept inside an ultrasonicator bath (ELMA, Model Transonic 460 / H, 35 KHz) for 20 min upon which the solution turned green. On the other hand we observed that PANI could not be dissolved in starch solution with stirring or just leaving the solution overnight. It was further observed that more amount of PANI could be dissolved if more concentrated starch solution was used (saturated water soluble starch concentration is $10gl^{-1}$). We however performed our experiments with the above solution only.

To the PANI containing starch solution 10 mg of iodine was added and kept overnight. The solution colored turned blue and green color precipitate was obtained at the bottom of the vial. The blue color solution was then carefully decanted, and the green color precipitate was washed with water. 2 ml of chloroform ($CHCl_3$) was then added to the precipitate, which was dispersed in aqueous solution and shaken properly to remove the excess iodine. The green color precipitate was dried in vacuum for further analysis.

In a separate experiment, to the above amount of blue colored starch-iodine solution, 10mg of PANI was added and the mixture was kept in an ultrasonicator bath for 20 min. The blue colored solution then turned green indicating the dissolution of PANI. 2 ml of $CHCl_3$ was added to the solution and then was shaken vigorously for mixing. The $CHCl_3$ layer turned blue indicating transfer of I_2. The green colored aqueous layer was decanted and water of the solution was removed by vacuum drying and the green colored solid obtained was used for further analysis.

Preparation of conducting polyaniline-Au nanoparticles composite

In the earlier chapter we have reported the preparation of conducting PANI-Au-NP composite using H_2O_2 as both oxidizing as well as reducing agent. Typically, to 50 ml of 2.5 X 10^{-2} M SDS solution, $HAuCl_4$ solution was added so that the final concentration of $HAuCl_4$ became 4 X 10^{-4} M. To that solution 500 µl of 30% H_2O_2 was

added with constant stirring. Purple colored Au nanoparticles, with UV-visible absorbance at 520 nm, were formed in 5 min. In another beaker 200 µl of aniline was dissolved in 50 ml of 0.2 M HCl solution. Both the solutions were mixed together and stirred for 12 hrs. The solution initially turned green which finally yielded a green colored precipitate while at the came time the parent solution turned colorless. The precipitate was first separated by decantation and then washed with milliQ water followed by methanol for several times to remove surfactant. After several cycles of centrifugation and decantation, the precipitate was air-dried. The dissolution of the composite in starch solution was performed in the same way as for the PANI only with the same amount of PANI-Au-NP composite in the place of PANI. The powder X-ray diffraction of the air-dried composite was performed using a MAC Science diffractometer (model MXP^{JVA}) with CuKα doublet (1.54052 & 1.544390 Å).

Enzyme hydrolysis of starch-wrapped polyaniline

For this study we have used the fungal diastage enzyme with amylase activity 1:2000. 10 mg of the enzyme was dissolved in 5 ml of milliQ water. Separately, 3 ml of starch-PANI composite was kept in a 3 ml cuvette and 50 µl of the enzyme solution was added to the composite solution. The solution was then kept inside the sample compartment of a Hitachi U2001 UV-vis spectrophotometer to monitor the absorption spectrum with time in the range of 200 nm to 1100 nm. When the solution turned colorless and at the same time a green colored precipitate was obtained the recording was stopped. It took about 10 hrs at 25°C for the precipitation to occur The precipitate was washed with water and then vacuum dried which was used for further analysis by FTIR spectroscopy.

4.1.3. Results and Discussions

First of all we want to emphasize here that for the solubilization of PANI in aqueous starch solution the presence of ultrasonic wave was necessary. In absence of the ultrasonic wave despite stirring with a conventional stirrer there was no discernible solubilization of PANI. On the other hand, when PANI was dispersed in aqueous solution of starch using ultrasonic irradiation, a green solution could be obtained that is characteristic of the conductive polyaniline. This is shown in Figure 4.1.1A. The UV-

visible absorption spectrum of the solution with characteristic peaks at 800 and 440 nm as shown in Figure 4.1.1A' confirmed the presence of PANI (emeraldine form) in the solution.

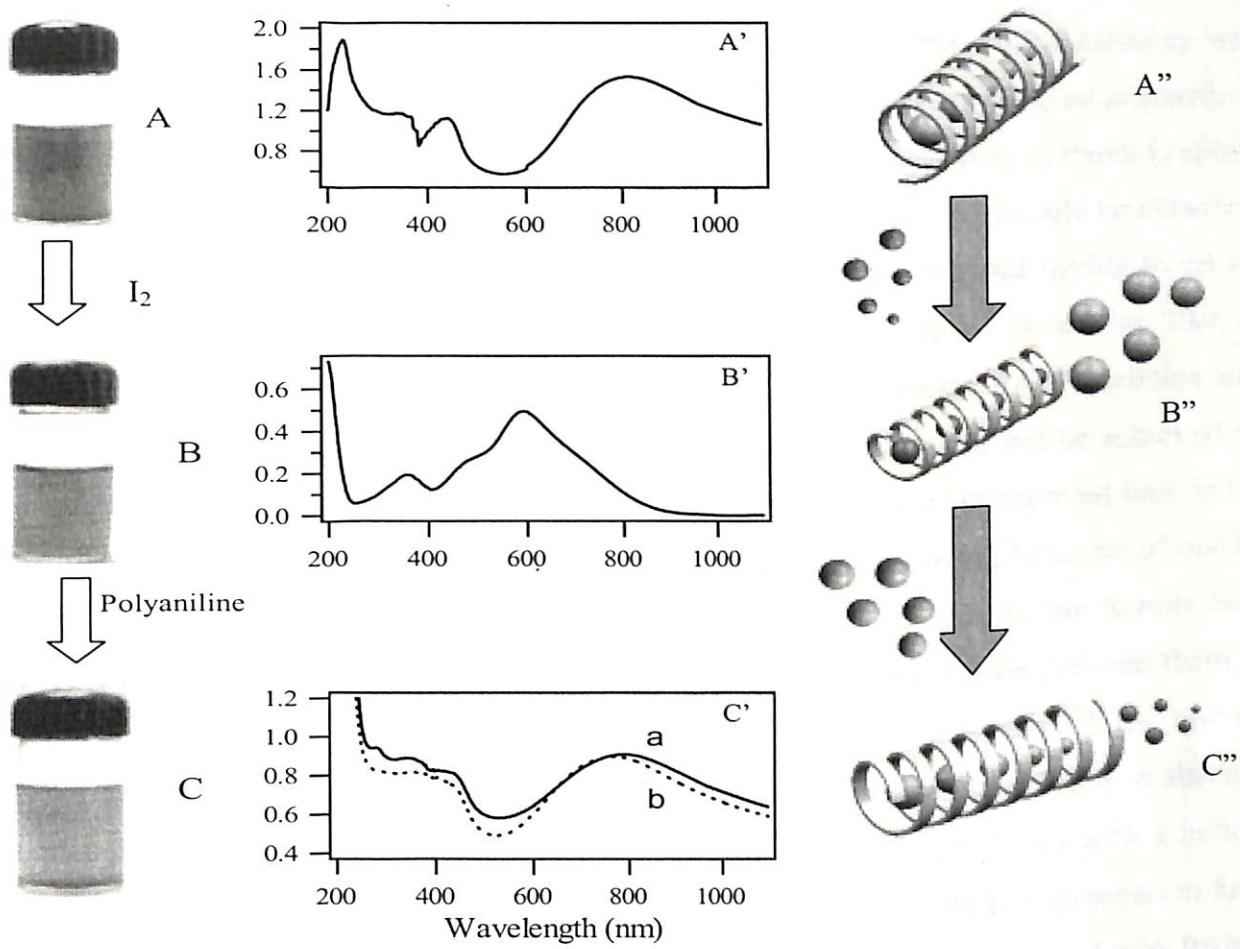

Figure 4.1.1. *Photographs of (A) starch solubilized PANI, (B) I_2 in starch replacing PANI and (C) PANI again in starch replacing I_2. (A') and (B') are UV-vis absorption spectra of sample in (A) and (B) respectively. (C') (a) UV-vis absorption spectra of sample in C and (b) after treatment of the solution by $CHCl_3$. (A''), (B") and (C") are schematic representation of a model of the processes in (A), (B) and (C) respectively.* *(see color plate, page 133)*

When molecular iodine was added to the starch-PANI solution in the presence of ultrasonic waves, the solution color turned blue (Figure 4.1.1B) with a peak at 600 nm, which is again typical of starch-iodine complex (Figure 4.1.1B'). In other words, upon interaction of starch-PANI solution with I_2 the absorption peaks due to PANI vanished

and the peak due to starch-I_2 appeared instead. WE observed the precipitation of green colored PANI particles out of the solution. Interestingly, when PANI was again introduced in starch-I_2 solution in presence of ultrasonic wave, the characteristic green color solution of PANI-starch with absorption maxima at 800 nm and 440 nm reappeared (Figure 4.1.1C and C'), while the blue color as well as UV-visible peak due to starch-I_2 had vanished. Based on the above observations we propose that PANI particles were being encapsulated in much the same way, as I_2 is known to be encapsulated in starch. A model representation of reversible encapsulation of PANI as well as I_2 in starch is shown in Figures 4.1.1A", B" and C". It is important to note here that PANI could be dissolved in an aqueous solution of starch under ambient condition and without having to go via initial structural motif formation of starch in presence of small molecules like I_2. Ultrasonic waves probably serve two purposes here - to disperse PANI particles into water and also to help dissolve the particles in starch, which could not be achieved by ordinary stirrer. Also, an important and integral aspect of the work reported here is the reversible binding of PANI and I_2 to starch, which is evidenced by replacement of one by the other in presence of excess of one component. Further, it is important to note here that during the exchange process of I_2 and PANI there is no interaction between them as clear from the UV-visible absorption spectra of PANI shown in Figure 4.1.1A' and C' that are identical. Moreover, the fact that excess I_2 could also replace PANI in absence of ultrasonic waves indicate that PANI-starch composite probably forms with a helical structure of starch similar to that of starch-I_2 complex. We would like to mention here that similar results were obtained when the above experiments were repeated with PANI-Au-NP composite instead of PANI only. From the results of works reported in the last chapter we know that the formation of PANI-Au-NP composite in water occurs with green color solution with characteristic absorbance of PANI at 440 nm and 800 nm which are the same as those of PANI in starch only and hence we do not show here the spectrum due to PANI-Au-NP-starch composite. Also, the absorption spectrum of Au-NP becomes too weak to be measured after addition of aniline even before the formation of Au-NP-PANI composite. However, the presence of Au nanoparticles in the composite was confirmed by powder X-ray diffraction observations where the principal Braggs reflections of Au in the solidified composite were observed (discussed later).

We were interested in finding out whether there was any reaction between PANI and I_2 taken place during the reversible replacement of PANI by I_2. Simply put, did we recover unaltered PANI when replaced by I_2 from the complex with starch? This is

specially relevant with respect to small blue shift of the PANI peak when the recovered PANI starch solution was treated with $CHCl_3$ to remove possible excess iodine that is shown in Figure 4.1.1C'(b). To find an answer to this question we performed the following experiment. Solid PANI kept in a 10 ml beaker was placed inside an iodine chamber. The chamber was heated to 70°C for 10 min. The setup was brought to room temperature and PANI with I_2 was dispersed in an aqueous solution of starch in the same way as other experiments. The UV-visible absorption spectra of this dispersed solution and also that of starch-encapsulated PANI (only) of the same batch of synthesized polymer were recorded. The UV-visible spectra are shown in Figure 4.1.2.

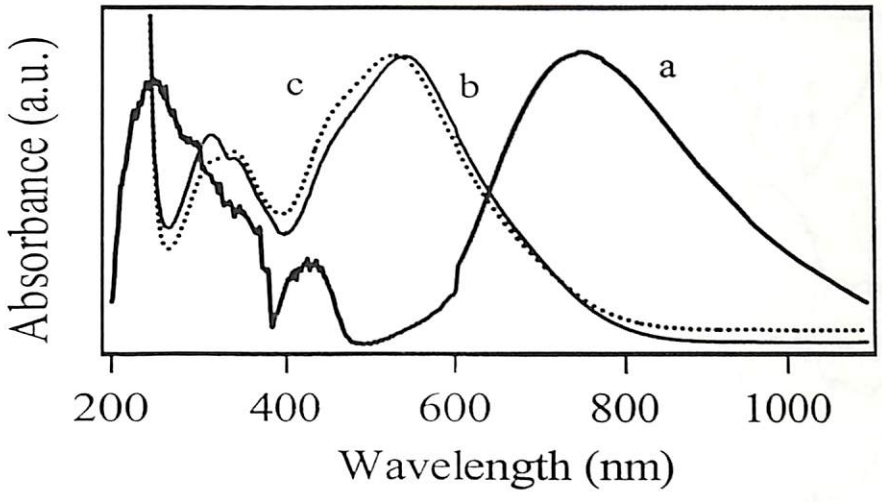

Figure 4.1.2. *UV-visible spectra of (a) PANI and (b) PANI-I_2 complex encapsulated in starch solution. (c) (dotted line) is the PANI-I_2 complex spectrum in starch solution after treatment with chloroform.*

As clear from the figure, iodine treated PANI in starch had a major peak at 538 nm (Figure 4.1.2b), which is quite different from that of PANI in starch occurring at about 800 nm (Figure 4.1.2a) and that of starch-I_2 complex with peak at 600 nm (Figure 4.1.1 B'). Thus in our sequence of experiments, shown in Figure 1, we recovered PANI that did not react with I_2 when being replaced. The small blue shifts of the peaks after treatment with $CHCl_3$, as shown in Figure 4.1.1C'(b) and 4.1.2c are probably due to incorporation of $CHCl_3$ inside the starch cavity. This is plausible as the hydrophobic core of the helical starch moiety may incorporate $CHCl_3$, the presence of which shifts the maximum of absorbance in both the cases. It is also interesting to note here that $CHCl_3$ did not precipitate out PANI from the PANI-starch composite by a process similar to that of I_2 replacing PANI.

We performed the following FTIR studies to further understand the nature of PANI recovered from the complex with starch due to replacement by I_2. When PANI was encapsulated in starch the FTIR absorption spectrum occurred with dominant peaks due to starch (Figure 4.1.3b and 4.1.3c) with no discernible peaks due to PANI. On the other hand when PANI was recovered from starch and FTIR spectrum of the recovered sample was recorded clear peaks due to PANI could be observed at 1575 cm^{-1}, 1491 cm^{-1} and at 1133 cm^{-1} (Figure 4.1.3d). Again only peaks characteristic of starch could be observed upon re-encapsulation (Figure 4.1.3e).

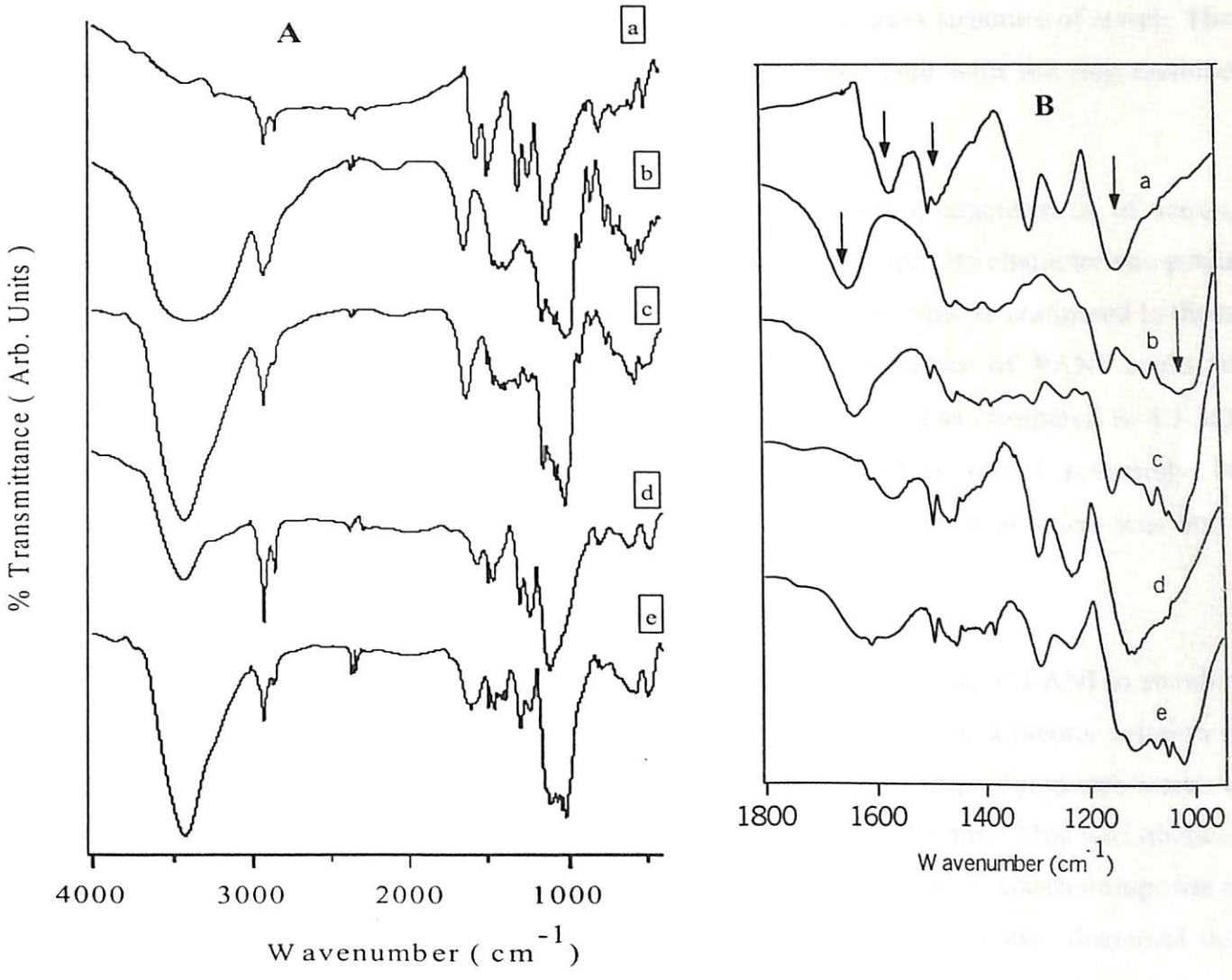

***Figure 4.1.3**: (A) FTIR spectra in KBr pellets of (a) only PANI; (b) only starch (c) PANI encapsulated in starch; (d) PANI recovered from starch (I_2 replacing PANI); (e) PANI re-encapsulated in starch from starch–I_2 complex. (B) Spectra of (a), (b), (c), (d) and (e) respectively, expanded in the range 1000-1800 cm^{-1} for clarity. Solid arrows indicate peaks characteristics of PANI and serrated arrows indicate peaks characteristics of starch.*

The distinctive peaks for starch are described as follows[26]. In the fingerprint region, there are several discernible absorbances at 1156, 1083, 1023 and 937 cm^{-1}, which are associated with native starch and attributed to C–O bond stretching. The peaks at 1083 and 1023 cm^{-1} are characteristic of the anhydroglucose ring O–C stretch. A characteristic peak occurred at 1640 cm^{-1}, which is presumably a feature of tightly bound water present in the starch. A strong absorption band at 1023 cm^{-1}, probably due to the stretching of the C–OH bond, was present in the spectra of the starch. An extremely broad band due to hydrogen bonded hydroxyl groups (O–H) appeared at 3400 cm^{-1} which was attributed to the complex vibrational stretches associated with free, inter and intra-molecular bound hydroxyl groups which make up the gross structure of starch. The band at 2926 cm^{-1} is characteristic of C–H stretches associated with the ring methine hydrogen atoms.

Thus Figures 4.1.3b, 4.1.3c and 4.1.3e show peaks characteristics of starch, which means that even though PANI was encapsulated in starch its characteristic peaks were not dominant over those of starch as shown in Figures 3c and 3e compared to those of starch only (Figure 4.1.3b). However, peaks characteristics of PANI could be observed in the spectrum of the recovered PANI (Figure 4.1.3d as compared to 4.1.3a). Thus the above observations further confirmed that PANI could reversibly be encapsulated into starch and the recovered PANI from the starch solution was not a composite but the polymer only.

Next, we were interested to find out the nature of dispersion of PANI in starch in terms of particle sizes. When solid PANI was dispersed into an aqueous solution of starch in the presence of ultrasonic waves, the polymer was encapsulated into starch in the form of nearly spherical particles of average diameter 10-20 nm. This was obtained from the transmission electron microscopic (TEM) pictures of PANI-starch composite as shown in Figure 4.1.4A. In addition, PANI-Au-NP composite was also dispersed into starch in the form particles of similar sizes (Figure 4.1.4B). In both cases the distributed particle sizes were uniform and they were evenly distributed in the solution as revealed by their TEM micrographs. The presence of Au NPs in starch encapsulated PANI-Au-NP composite was confirmed by characteristic X-Ray diffraction peaks. This is shown in Figure 4.1.4C. As clear from the 2θ values of the occurrence of the peaks, all the three principal Bragg's reflection of Au due to the growth of [111], [200] and [220] planes

occurred. The above observations suggest that polymer PANI particles and the PANI-Au-NP composite were dispersed into the solution of nanometer size dimensions, which were probably encapsulated in the hydrophobic core of starch.

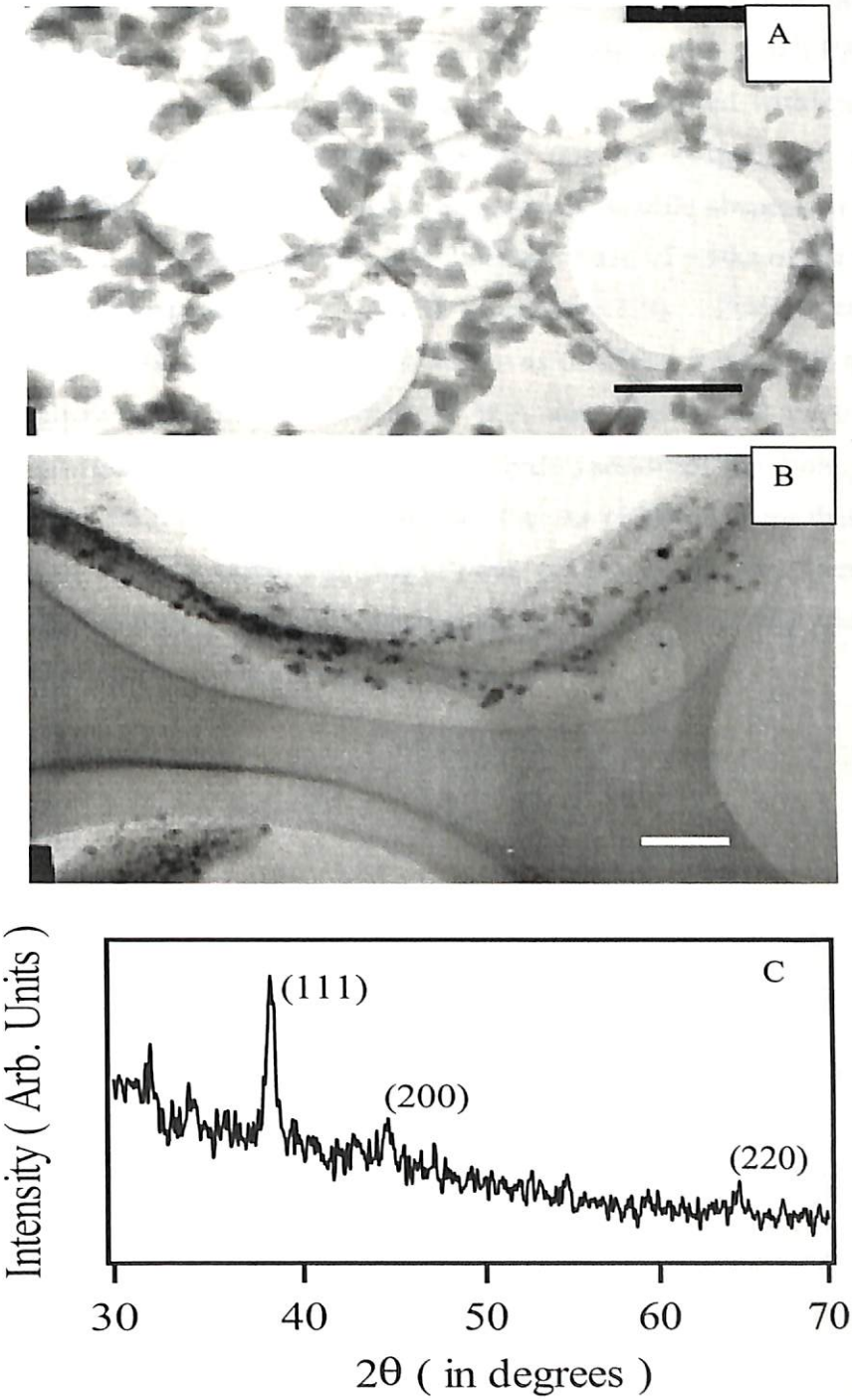

Figure 4.1.4. *TEM of (A) PANI dispersed in aqueous solution of starch (Scale bar = 100 nm) (B) PANI-Au NP composite in starch (Scale bar = 200 nm) (C) Powder XRD pattern recorded from solid PANI-Au-NP-starch composite. The principal Bragg reflections for the Au nanoparticles are identified.*

We carried out our work further to explore the possibility of recovery of the PANI particles from starch solution by digesting the starch with appropriate enzyme. This is feasible as the enzymatic hydrolysis of starch from starch-PANI composite should result precipitation of PANI owing to the loss of the hydrophobic core structure in the composite. Our observation with enzyme hydrolysis of the starch-PANI composite supports this model. When starch dissolved PANI was treated with enzyme diastage (fungal) we observed green precipitate after 30 min of keeping the solution under ambient condition. The color of the solution and UV-visible absorption spectrum with time showed the green color precipitate and disappearance of peaks of the solution at 440 nm and 800 nm corresponding to PANI (Figure 4.1.5). Further confirmation of precipitation of PANI upon enzyme hydrolysis was obtained from FTIR spectrum of the precipitate (not shown here). In addition, this also shows that even though PANI incorporation in starch may result in a helical conformation of the moiety it can still be hydrolyzed using an enzyme. We would also like to point out here that in addition to helical structure of starch encapsulating PANI or the composite there is additional possibility of a large number of starch molecules making an assembly where the PANI is encapsulated by the assembly rather that a single helix.

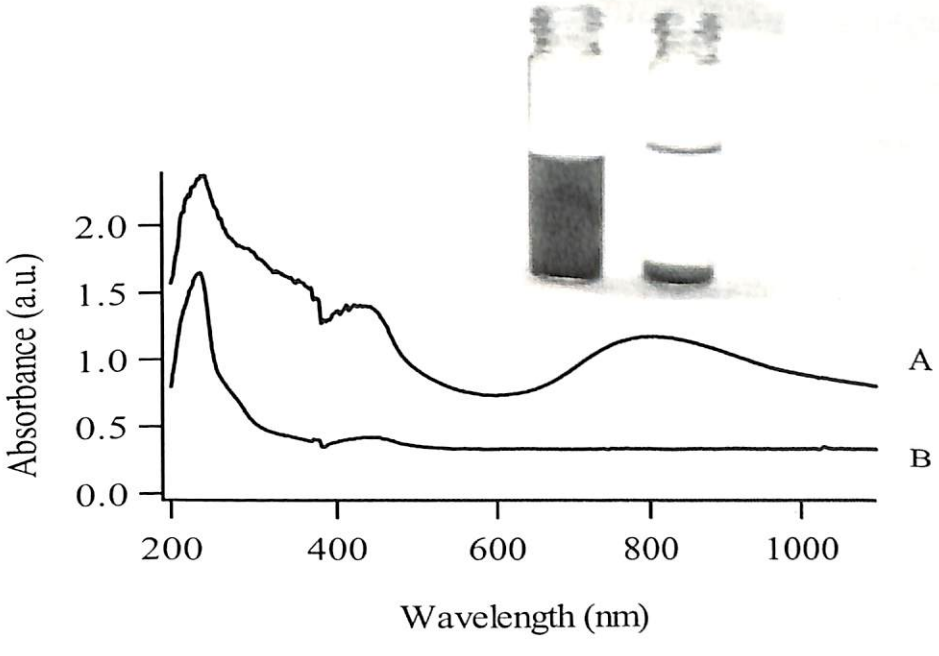

***Figure 4.1.5**: UV-visible spectra representing the hydrolysis of starch by enzyme Diastage (fungal) leading to the precipitation of PANI from starch-PANI composite, recorded (a) immediately after addition of enzyme and (b) after 30 min. On the top are photographs of vials containing the complex at the beginning (left) and 30 min after addition of enzyme (right).* *(see color plate, page 134)*

Finally, it is well known that iodine is incorporated in aqueous starch in the form of a helical structure where alternate I_2 and I_3^- units form a linear chain inside the helix[27]. Also, diameters of I_2 and I_3^- are much smaller than those of PANI particles that we have incorporated in starch. Thus when PANI particles replace iodine from starch there is a net entropy gain, as a large number of such molecules would be liberated compared to the number of particles of PANI incorporated inside starch moiety. On the other hand the reversibility of the process indicate that when iodine molecules replace PANI from starch there must be gain in enthalpy as there would be net loss of entropy. Thus while iodine replacement is entropically favored, PANI replacement must be energetically favored. This makes the process reversible.

4.1.4. Conclusion

In this work we have been able to show that PANI and PANI-Au-NP composite could be dispersed in an aqueous solution of starch using ultrasonic waves as well as using the starch-I_2 template with replacement of I_2 by PANI in the presence of ultrasonic waves. The PANI and the composite were dissolved in the starch solution in the form of uniform particles with 10-20 nanometer diameters. Further, it is also reported that PANI dissolved in starch could be recovered by replacement with molecular iodine both in presence and absence of ultrasonic waves. In addition, the polymer particles could be recovered from the solution by enzyme hydrolysis of starch under ambient condition.

4.1.5 References

1. Kaneko, M.; Nakamura H., *J. Chem. Soc., Chem. Commun.* **1985**, 346

2. (a) Sirringhaus, H.; Tessler, N.; Friend, R. H., *Science* **1998**, 280, 1741 (b) Burroughes, J. H., *Nature* **1990**, 347, 539 (c) Wohlgenannt, M.; Tandon, K.; Mazumdar, S.; Ramsesha, S.; Vardeny, Z. V., *Nature* **2001**, 409, 494 (d) Yu, G.; Gao, J.; Hummelen, J. C.; Wudl, F.; Heeger, A. J.; *Science* **1995**, 270, 1789 (e) Paul, E. W.; Ricco, A. J.; Wrighton, M. S., *J. Phys. Chem.* **1985**, 89, 1441

3. (a) Pages, H.; Topart, P.; Lemordant, D., *Electrochim. Acta* **2001**, 46, 2137 (b) Kitani, A.; Yano, J.; Sasaki, K. J., *Electroanal. Chem.* **1986**, 209, 227

4. Duke, C. B.; Gibson, H. W., *Encyclopedia of Chemical technology*, Kirk-Othmer: John Wiley: New York, **1982**, Vol. 18, p 755

5. (a) Koul, S.; Chandra, R.; Dhawan, S. K., *Polymer*, **2000**, 41, 9305 (b) Joo, J.; Lee, C. Y., *J. Appl. Phys.* **2000**, 88, 513

6. (a) Sukeerthi, S.; Contractor, A. Q., *Anal. Chem.* **1999**, 71, 2231 (b) Xue, H.; Shen, Z.; Li, Y., *Synth. Met.* **2001**, 124, 345 (c) Xie, D.; Jiang, Y.; Pan, W.; Li, D.; Wu, Z.; Li, Y., *Sens. Actuators B,* **2002**, 81, 158

7. Wang, H-L; Gao, J.; Sansinena, J-M.; McCarthy, P., *Chem. Mater.* **2002**, 14, 2546

8. (a) Yue, J.; Wang, Z. H.; Cromack, K. R.; Epstein, A. J.; MacDiarmid, A. G., *J. Am. Chem. Soc.* **1991**, 113, 2665 (b) Wei, X. L.; Wang, Z. H.; Long, S. M.; Bobeczko, C.; Epstein, A. J., *J. Am. Chem. Soc.* **1996**, 118, 2545 (c) Chan, H. S. O.; Neuendorf, A. J.; Ng, S. C.; Wong, P. M. L.; Young, D. J., *Chem. Commun.* **1998**, 1327 (d) Chen, S-A; Hwang, G-W, *J. Am. Chem. Soc.* **1995**, 117, 10055

9. Chan, H. S. O.; Ho, P. K. H.; Ng, S. C.; Tan, B. T. G.; Tan, K. L., *J. Am. Chem. Soc.* **1995**, 117, 8517

10. (a) Liu, W.; Kumar, J.; Tripathy, S.; Senecal, K. J.; Samuelson, L., *J. Am. Chem. Soc.* **1999**, 121, 71 (b) Liu, W.; Cholli, A. L.; Nagarajan, R.; Kumar, J.; Tripathy, S.; Bruno, F. F.; Samuelson, L., *J. Am. Chem. Soc.* **1999**, 121, 11345

11. Huang, J.; Virji, S.; Weiller, B. H.; Kaner, R. B., *J. Am. Chem. Soc.* **2003**, 125, 314

12. Wei, Z.; Zhang, Z.; Wan, M., *Langmuir*, **2002**, 18, 917

13. Lei, Z.; Zhang, H.; Ma, S.; Ke, Y.; Li, J.; Li, F., *Chem. Commun.* **2002**, 676

14. Yoshida, K.; Shimomura, T.; Ito, K.; Hayakawa, R., *Langmuir*, **1999**, 15, 910

15. Liang, L.; Liu, J.; Windisch Jr., C. F.; Exarhos, G. J.; Lin, Y., *Angew. Chem. Int. Ed.* **2002**, 41, 3665

16. Bjorklund, R. B.; Liedberg, B., *J. Chem. Soc., Chem. Commun.* **1986**, 1293

17. For example (a) Li, G.; Fudickar, W.; Skupin, M.; Klyszcz, A.; Draeger, C.; Lauer, M.; Fuhrhop, J. H., *Angew. Chem. Int. Ed.* **2002**, 41, 1828 (b) Meier, W., *Chem. Soc. Rev.* **2000**, 29, 295

18. For example (a) Yang, Z.; Niu, Z.; Lu, Y.; Hu, Z.; Han, C. C., *Angew. Chem. Int. Ed.* **2003**, 42, 1943 (b) Wang, W.; Asher, S. A., *J. Am. Chem. Soc.* **2001**, 123, 12528

19. Fuhrhop, J.-H.; Koning, J., in *Monographs in Supramolecular Chemistry; Molecular Assemblies and Membranes: The Synkinetic Approach* (Ed. J. F. Stoddart), Royal Society of Chemistry, London, **1994**

20. Zhan, B. Z.; White, M. A.; Sham, T. K.; Pincock, J. A.; Doucet, R. J.; Ramana Rao, K. V.; Robertson, K. N.; Caemron, T. S., *J. Am. Chem. Soc.* **2003**, 125, 2195

21. Kramer, M.; Stumbe, J. F.; Turk, H.; Krause, S.; Komp, A.; Delineau, L.; Prokhorova, S.; Kautz, H.; Haag, R., *Angew. Chem. Int. Ed.* **2002**, 41, 4252

22. Sun, Y.; Xia, Y., *Science*, **2002**, 298, 2176

23. Balasubramanian, D.; Raman, B.; Sundari, C. V., *J. Am. Chem. Soc.* **1993**, 115, 74

24. Star, A.; Steuerman, D. W.; Heath, J. R.; Stoddart, J. F., *Angew. Chem. Int. Ed.* **2002**, 41, 2508

25. Sarma, T. K.; Chowdhury, D.; Paul, A.; Chattopadhyay, A., *Chem. Commun.* **2002,** 1048.

26. (a) Goheen, S.; Wool, R. P., *J. Appl. Polym. Sci.,* **1991**, 42, 2691 (b) Kacurakova, M.; Wilson, R. H., *Carbohydr. Poly*m., **2001**, 44, 291 (c) Marcazzan, M.; Vianello, F.; Scarpa, M.; Rigo, A., *J. Biochem. Biophys. Method*s, **1999**, 38, 191 (d) Aburto, J.; Thiebaud, S.; Alric, I.; Borredon, E.; Bikiaris, D.; Prinos, J.; Panayiotou, C., *Carbohydr. Poly*m., **1997**, 34, 101

27. Teitelbaum, R. C.; Ruby, S. L.; Marks, T. J. *J. Am. Chem. Soc.* **1978**, 100, 3215.

4.2 Starch Mediated Shape-Selective Synthesis of Au-Nanoparticles with Tunable Longitudinal Plasmon Resonance

4.2.1 Introduction

Shape selectivity is equally important (if not more) in the generation of metal nanoparticles (NPs) in controlling their optical, electronic, magnetic and catalytic properties[1]. This is especially important for coinage metals like Au and Ag, which have strong surface plasmon resonance oscillations, thus controlling the shape of these NPs is crucial in scheming their surface properties like optical absorption and emission[2], surface enhanced Raman scattering (SERS)[3] and other non-linear optical properties. The requirements have justifiably generated impetus to search and development of physical and chemical methods of generation of shape-selective metal NPs in one, two and three dimensions with geometries such as rods, tubes, wires, triangles, prisms, discs, hexagons and cubes. Among the important technique that have contributed significantly to the growth in this directions are nanosphere lithography[4], photochemical transformations of spherical metal NPs into prisms[5] and nanorods into spherical particles[1c] and various chemical methods of synthesis of metal NPs of different shapes[6]. On the other hand, Xia and coworkers have developed the so-called polyol method of synthesis of Ag nanocubes and Au nanoboxes and also nano rings[7]. Further, Liz-Marzán and coworkers have shown that triangular / hexagonal Au NPs are preferentially absorbed on thin film polyelectrolyte compared to their spherical counterpart[8]. Mirkin and coworkers have developed anisotropic nanoparticles growth protocols of Ag and Au in the form of triangular prisms and nanoframes[9]. Further, for template-mediated synthesis micelles, reverse micelles, vesicles and polymers[10] have been used frequently.

There has also been a parallel recent surge in finding biosynthetic methodology of generating metal and semiconductor NPs using virus, fungi and bacteria as the biosystems[11]. Nanotubular biopolymers like self-assembled peptide templates have also been used to incorporate metal nanowires inside them[12]. The primary aim there has been to find environmentally friendly way of synthesis and use of particular structures of biosystem (especially membranes and polymer self-assembly) for size and shape selective synthesis of NPs. However, there is another possibility of using a naturally

occurring biopolymer like starch as a template for the shape-selective synthesis of NPs, which has not been pursued by any of the methods mentioned. The extra benefit of using starch as the template is that there exists a specific enzyme to digest the polymer, which is useful for targeted delivery and appropriate use of the NPs at a desired site. It is also advantageous that the structures and functions for many biopolymers are well known and hence the physical and chemical process of synthesis and functional properties of nanomaterials in the polymer may be easier to tune. Although there are a large number of methods for shape-selective synthesis of Ag NPs, the same is not true for Au NPs especially with tunable longitudinal plasmon resonance. In this section of chapter 4 we report a method of shape-selective synthesis of Au NPs where the longitudinal plasmon resonance absorption wavelength could be tuned by controlling the concentration of $HAuCl_4$ in the presence of starch acting as the template as well the capping agent. We also report that shape-selective synthesis requires the presence ultrasonic waves during the formation of NPs, otherwise general spherical NPs are produced. H_2O_2 was used for the reduction of $HAuCl_4$[13]. Transmission electron microscopic (TEM) measurements revealed that with increasing initial concentration of $HAuCl_4$ the shape of the NPs formed changed from spherical to triangular to hexagonal. X-ray diffraction (XRD) measurements evidenced the exclusive growth of [111] plane of the fcc lattice of hexagonal Au NPs, while the growth of [111], [200] and [220] lattice planes occurred with the formation of spherical NPs. Finally, addition of a starch-hydrolyzing enzyme to the solution precipitated Au NPs along with the enzyme.

4.2.2.Experimental Section

4.2.2.1 Synthesis. 1.00 g of starch (water soluble, E-Merck) was dissolved in 100 ml of boiling water (MilliQ). The starch solution thus prepared was allowed to cool to room temperature (20-25^{0}C). 20 ml of the starch solution was taken in a separate vial and to it 300 µl of 0.03 M $HAuCl_4$ (Aldrich) solution was added at a time. The mixture was kept for sonication in an ultrasonicator bath (Elma, Transsonic 460/H) for 5 min. 400 µl of 30% H_2O_2 was then added to the solution. The solution was further subjected to sonication for 20 min, upon which reddish violet color appeared which is characteristic of the formation of Au NPs. Further preparations (6 separate samples) were carried out keeping the concentration of starch and H_2O_2 same, however the concentration of $HAuCl_4$ was successively increased by adding 350, 400, 500, 600, 800

and 1000 μl of 0.03 M of the metal salt respectively. The color of the Au NPs changed from reddish purple to violet to brick red respectively for the above preparations with increasing initial concentration of $HAuCl_4$.

We had also prepared Au NPs using starch as the capping agent by reduction of $HAuCl_4$ with H_2O_2, in absence of ultrasonic wave irradiation. In one preparation 300 μl of 0.03 M $HAuCl_4$ was added to 20 ml of 10g/l starch and 400 μl of 30% H_2O_2 was then added to the mixture. The NPs formed within 10 min of H_2O_2 addition. In another sample 800 ml of 0.03 M $HAuCl_4$ was used while concentration of all other reactants were kept constant. The difference in the product formation between the NPs prepared in presence and absence of ultrasonic waves is discussed in the Results and Discussion section.

4.2.2.2 UV-vis studies. UV-visible spectra for the Au NPs were recorded in a Hitachi (Model U-2001) spectrophotometer. Individual NP solution was transferred to a 3 ml cuvette and then the spectrum was recorded in the region of 400 nm to 1100 nm.

4.2.2.3 TEM and XRD measurements. Transmission electron microscopy (TEM) measurements for the Au NPs were performed in a JEOL electron microscope (JEM 100 CX). Each sample was cast on a copper grid, air-dried and the image was recorded at an accelerating voltage of 80 kV. Powder X-ray diffraction studies were carried out in a Seifert powder X-Ray diffractometer (XRD 3003 TT) with Cu-K source (wavelength 1.54 Å) after evaporation of a few drops of the NP solutions on a glass slide.

4.2.2.4 Enzyme hydrolysis. The study of enzyme digestion of starch-Au-NPs was carried out in the pH range of 6.5-6.8. This is essential for effective enzyme activity as the starch digesting enzyme amylase acts in that pH range. The Au-NP-starch solution was subjected to centrifugation followed by washing of the precipitate by water. The process was repeated for several times. The precipitate was then dispersed in water of the same volume as the starting solution. To 10 ml of a diluted (by 4 times) Au NP-starch colloidal solution, 1 ml of 1g/l fungal-diastage (with amylase activity 1:2000) solution in aqueous medium was added. Four of such solutions were kept at different

temperatures (20-25°C, 25-30°C, 35°C and 40°C) in a thermostatted cell holder. Purple colored precipitation took place at different times for samples kept at different temperature. A typical precipitate was recovered by decantation followed by washing in several cycles followed by air-drying. FTIR spectra of the precipitate was recorded in a KBr pellet using a Perkin Elmer (Spectrum one) FTIR spectrophotometer.

4.2.2.5 Enzyme-Au NP precipitation. Au NPs were synthesized in a vial by addition of 400 µl of 30% (v/v) H_2O_2 to 10 ml of $3x10^{-4}$ M $HAuCl_4$ aqueous solution. Purple colored Au NPs were formed within 5 minutes at room temperature with characteristic plasmon resonance band at 535 nm. 5 ml of Au nanoparticles thus synthesized was taken in a separate vial and to it 2 ml 1g/l of the diastage enzyme was added. A purple colored precipitate was obtained from the solution that was left overnight, whereas the parent solution turned colorless, indicating the precipitation of Au nanoparticles coated with the enzyme. The precipitate was decanted and then dried in vacuum to record FTIR spectrum.

4.2.3 Results and Discussions

While pursuing the studies of reduction of $HAuCl_4$ by H_2O_2 in presence of starch, we observed a significant difference in the nature of product formation when the reaction was carried out in presence and absence of ultrasonic waves. The primary control in the reaction condition was the concentration of $HAuCl_4$ for different set of samples. When the concentration of $HAuCl_4$ was increased for different sample runs and the reactions were carried out in absence of ultrasonic waves, we observed a change in position of maximum of absorbance occurring due to transverse plasmon resonance band. There was no observable presence of longitudinal plasmon resonance band. We report the following two cases to provide an example. The results are shown in Figure 4.2.1. As clear from Figure 4.2.1A, in the first reaction, where the concentration of $HAuCl_4$ was 4.2×10^{-4}M, the NPs formed with an absorption maximum at 535 nm while those of the second reaction (1.1×10^{-3} M $HAuCl_4$) occurred with absorbance maximum at 570 nm. In both the cases there was no occurrence of a second absorption, which we had otherwise observed when the reaction was carried out in the presence of ultrasonic waves (discussed at a later part of this section). TEM measurements (Figure 4.2.1B) showed

that nearly spherical particles were formed at the higher $HAuCl_4$ concentration and the average sizes of them were about 100 nm. Thus the shift in the transverse plasmon resonance band in the second case was due to large particle size and not due to the occurrence of special particle shape or size of the NPs formed.

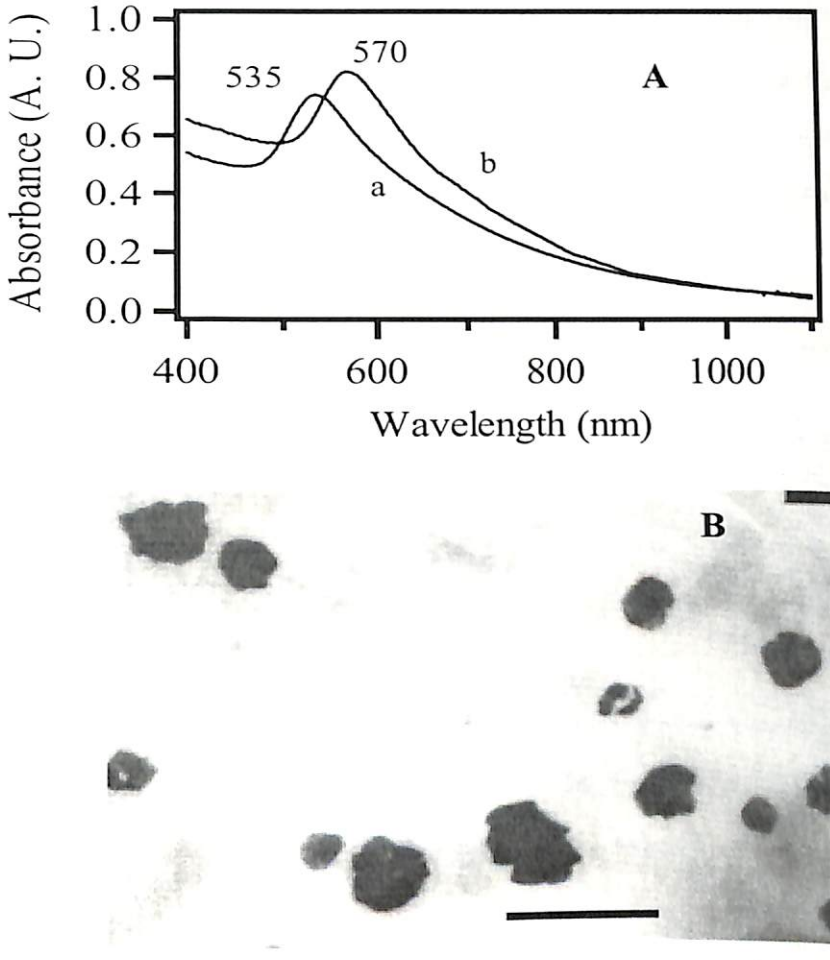

Figure 4.2.1. *(A) UV-visible spectra of Au NPs prepared in starch in absence of ultrasonic wave (a) 300 µl or (b) 800 µl of 0.03 M $HAuCl_4$ was added to 20 ml of 10g/l starch and 400 µl of 30% H_2O_2 was then added to the mixture. The NPs were formed within 10 min of H_2O_2 addition.* ***(B)*** *Transmission electron microscopic picture of the NPs formed corresponding to the UV-visible spectra (b). Scale bar is 200 nm.*

It was quite interesting to observe that when the Au NPs were synthesized in the presence of ultrasonic waves and starch was used in the reaction medium, the results obtained were remarkably different from the ones reported above. As the concentration of $HAuCl_4$ was increased there was an appearance of an additional band, beyond the typical transverse band observed at 535 nm, the wavelength of which red-shifted with

increasing initial concentration of $HAuCl_4$. The UV-visible absorption spectra of Au NPs synthesized with increasing concentration of $HAuCl_4$ are shown in Figure 4.2.2. As evident from the figure, while the transverse plasmon resonance absorption peak (~535 nm) shifted very little, the unidirectional red-shift of the second band, known as the longitudinal plasmon resonance band, occurred with NPs that were generated with increasingly higher $HAuCl_4$ concentration. A comparison with concentration of $HAuCl_4$ versus longitudinal absorption maximum (Table 4.2.A) revealed that an increase in the initial concentration by a factor of about three changed the NP character with having no longitudinal peak to a strong peak at 900 nm, with intermediate concentration generating particles with absorption maxima in between them.

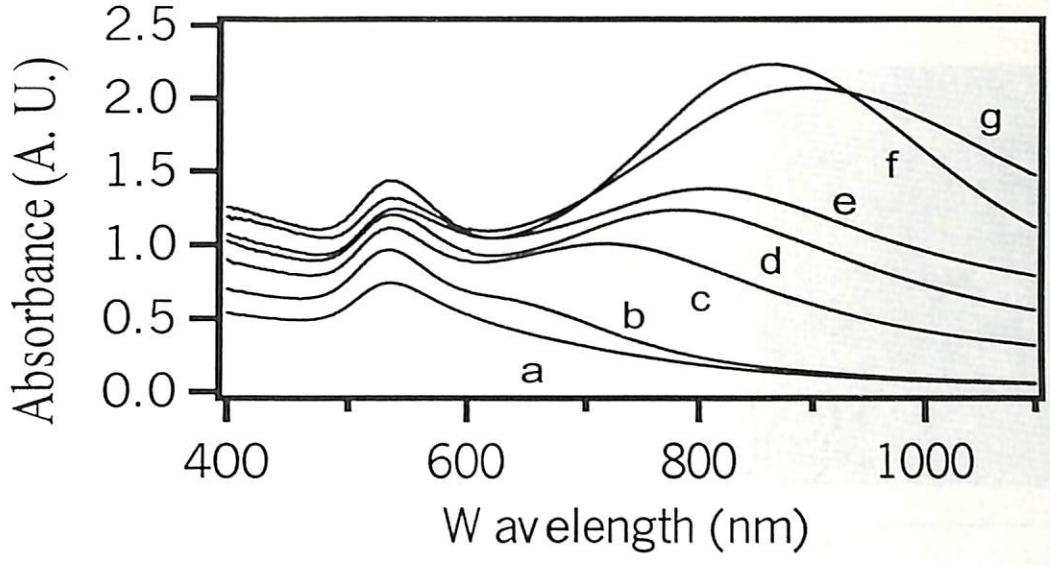

Figure 4.2.2. *UV-visible absorption spectra of Au NPs in aqueous starch solution generated by H_2O_2 reduction of $HAuCl_4$. a, b, c, d, e, f and g are spectra of Au NPs with concentrations of $HAuCl_4$ as in Table 4.2.A.*

Table 4.2.A. Longitudinal plasmon resonance absorption maxima of Au NPs at various $HAuCl_4$ concentrations (as in Figure 4.2.2).

	a	b	c	d	e	f	g
$HAuCl_4$ (10^{-4} M)	4.2	4.9	5.6	7.0	8.4	11.2	14.0
λ_{max} (nm) [Longitudinal]	----	655	715	781	809	865	900

We pursued further investigations to understand the origin of the second band. TEM measurements of the NPs, generated under different $HAuCl_4$ concentrations, revealed that at the lowest initial concentration of $HAuCl_4$ [4.2 x 10^{-4} M] Au NPs formed

were exclusively spherical (Figure 4.2.3A) with average particle size of 15-20 nm. This is consistent with the observed optical absorption spectrum (Figure 4.2.2a) of the NPs that is due to well-known transverse surface plasmon resonance of the Au NPs. As the concentration of $HAuCl_4$ was gradually increased, the formation of particles with shapes changing to dominant triangular forms to dominant hexagonal forms had occurred. For example, at the concentration of 8.4 x 10^{-4}M $HAuCl_4$ about 65 % of the particles formed were triangular in shape (Figure 4.2.3B) with typical particle edge size of 90-110 nm. These particles correspond to the visible absorption spectrum of Figure 4.2.2e. Further increase in the concentration of $HAuCl_4$ to a value of 11.2 x 10^{-4}M lead to the predominant (about 62 %) formation of hexagonal forms of Au NPs with typical particle size of 120 nm (Figure 4.2.3C). The visible absorption spectrum of these particles corresponds to that of figure 4.2.2f.

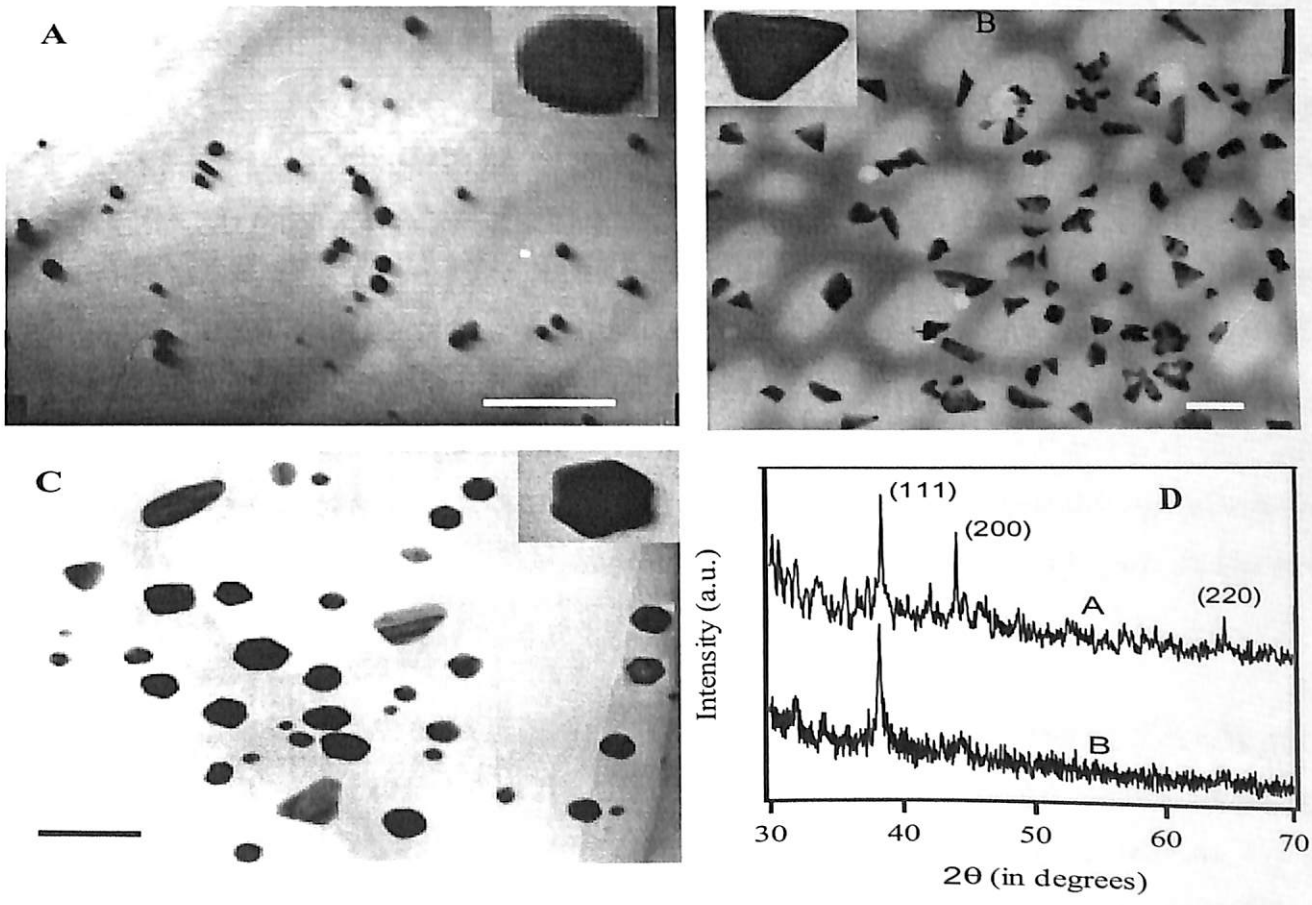

Figure 4.2.3. *(A), (B) and (C) are the TEM micrographs of Au NPs generated with $HAuCl_4$ concentrations equal to a, e and f respectively as mentioned in Table 4.2.A. Scale bar is 200 nm. Insets are expanded micrographs of NPs of different shapes shown for clarity. (D) represents XRD patterns of Au NPs with spherical shape corresponding to (a) and hexagonal particles corresponding to (g) in Figure 4.2.2.*

It is well known that in the case of formation of Au nanorods two characteristic peaks due to transverse and longitudinal plasmon resonance transitions occur[1b]. The peak positions depend on the aspect ratio of the nanorods with higher aspect ratio resulting in longer wavelength occurrence of the longitudinal band. Further, it is known that in the case of Ag NPs, the longitudinal plasmon resonance also occur due to triangular and hexagonal shapes of the NPs generated in the solution with hexagonal particles having higher absorption maximum wavelength (longitudinal) than the triangular ones. In addition, Ag nanodiscs occurring with both the plasmon resonance bands have been synthesized recently[10b].

In the present set of experiments, at higher $HAuCl_4$ concentration, the population of Au nanorods was much less compared to triangular or hexagonal shaped NPs. Thus the occurrence and change in the longitudinal plasmon resonance band were due to formation of NPs of various shapes at different $HAuCl_4$ concentrations. The spherical particles occurred with transverse plasmon resonance band only, while predominant formation of triangular particles gave rise to a second peak at 800 nm, occurring due to longitudinal plasmon resonance, and that due to predominant formation of hexagonal particles occurred at 890 nm. We then pursued XRD measurements to understand the nature of growth of particle with special shapes. The results are shown in Figure 4.2.3D. Powder XRD patterns for spherical NPs revealed growth corresponding to [111], [200] and [220] lattice planes, while that due to hexagonal particles occurred exclusively due to [111] fcc lattice of Au NPs. This is indicative of the formation of discs in the case of growth of hexagonal NPs.

The Au NPs generated in presence of starch were quite stable without any observable change for weeks. On the other hand we were interested to find out the fate of the NPs when the solution had been treated with a starch-digesting enzyme. In other words, what happens to the NPs once released from starch encapsulation? The experiment was performed by addition of 1 ml of 1 g/l of fungal-diastage (amylase activity 1:2000) to 10 ml of diluted Au-NP solution (4 times diluted). Several such samples were prepared, which were then kept at different temperatures for separate runs. Purple colored precipitate occurred at different times, for samples kept at different temperature, with precipitation occurring faster at higher temperature. The time taken for precipitation to occur were as follows: 24-36 hr at 20-25^0 C; 24 hr at 25-30^0 C; 12 hr

at 35^0 C and 8 hr at 40^0 C. The UV-visible absorption spectra of the solution before and after precipitation, shown in Figure 4.2.4 (1 and 2 respectively), confirmed the precipitation. Photographs of a solution before and after precipitation are shown in Figure 4.2.4a and Figure 4.2.4b. We would like to mention here that we also observed precipitation when Au-NPs were prepared in absence of starch and then treated with the enzyme. In addition, precipitation could be observed when H_2O_2 was added to just an enzyme solution of identical concentration.

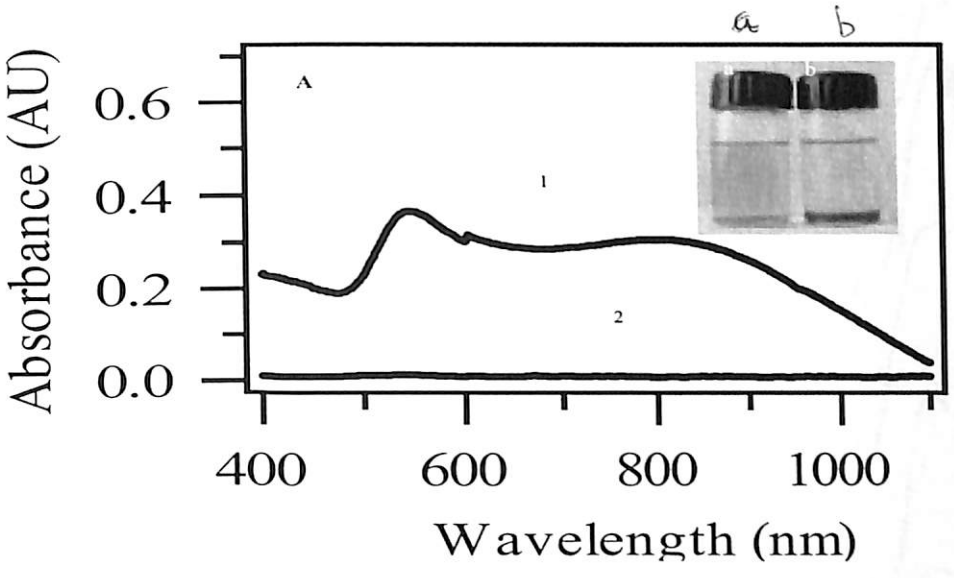

Figure 4.2.4. *UV-vis spectra and photographs of Au-NP containing starch solution (diluted) recorded right after addition of enzyme (1 and a respectively) and 8 hrs after addition (2 and b respectively). The experiment was performed at 40^0C. (see color plate, page 134)*

Interaction of proteins with inorganic metal nanoparticles has constituted a significant aspect of generating self-assembled structures using biological templates. For example, proteins of S-layer of bacterial cell envelope have been used to generate arrays of Au NPs on the cell membrane[14]. Thus interaction of protein α-amylase with Au-NPs may also lead to structure formation responsible for the precipitation of the enzyme along with the NPs. On the other hand there could be excess H_2O_2 and $HAuCl_4$ trapped inside the starch assembly, which could be released by starch digestion, and then possibly react with the enzyme leading to precipitation. As mentioned above addition of H_2O_2 leads to precipitation of the enzyme from an aqueous solution. We then decided to pursue further using FTIR spectroscopic method towards characterization of the results

of interactions between the Au-NPs and starch as well as hydrolysis of the composite by enzyme. FTIR spectrum (2000 – 800 cm^{-1} region) of the starch stabilized Au-NPs is shown in Figure 4.2.5 (a).

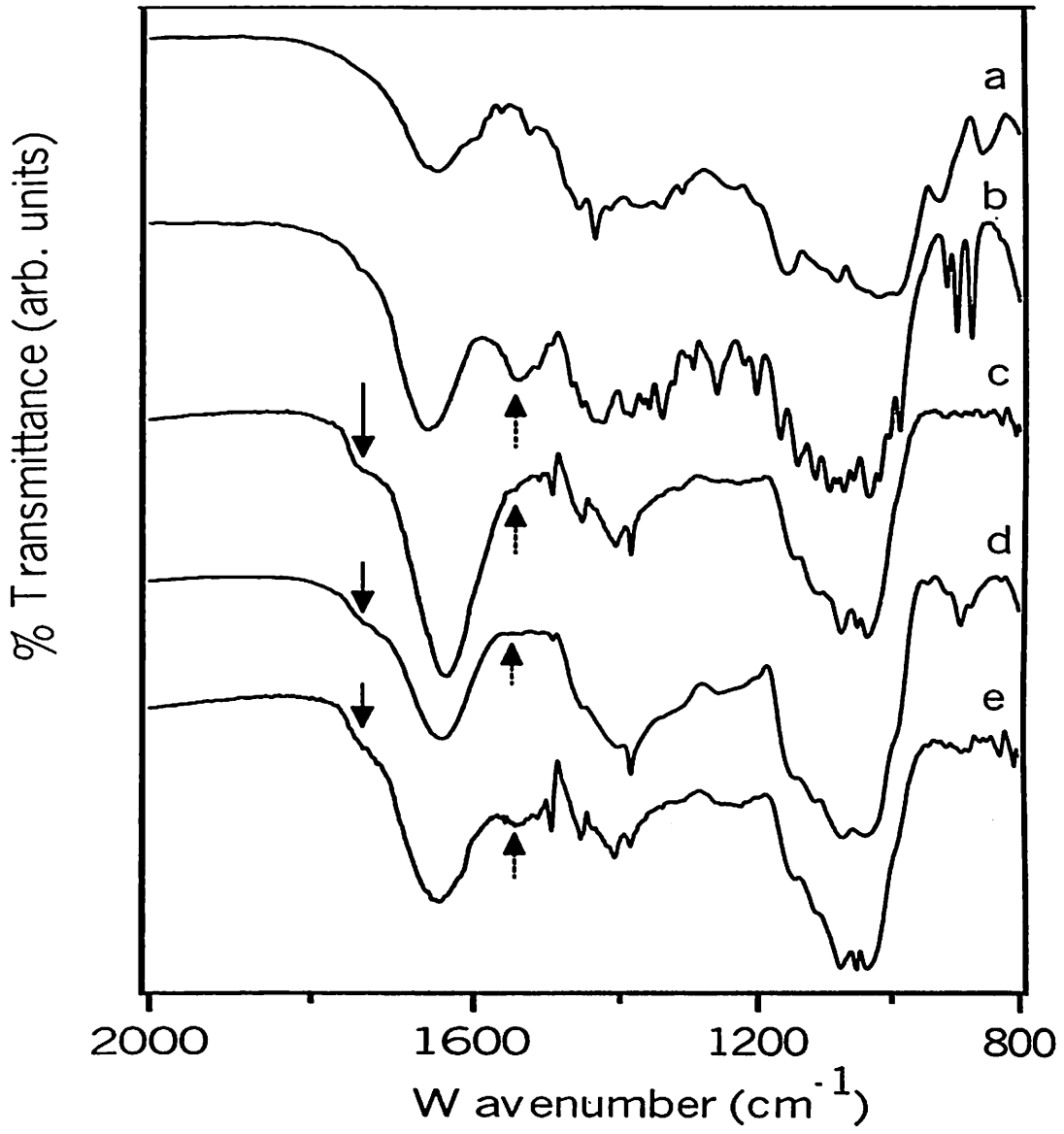

Figure 4.2.5 *FTIR spectra of (a) Au-NP-starch composite, (b) diastage enzyme, (c) the resultant precipitate of the Au-NP containing starch solution after enzyme addition, (d) of the enzyme treated with excess H_2O_2. (e) resultant precipitate of enzyme when added to Au NPs prepared in absence of starch.*

The spectral characteristics are similar to starch suggesting that the Au-NP-starch composite contained starch only and not any oxidized form of it. Also, the peaks characteristic of starch are different from those of enzyme. For example, starch has characteristic peaks at 1640 cm^{-1} and 1020 cm^{-1} (discussed in the previous chapter 4.1). The peaks due to enzyme arise at 1650 cm^{-1} and 1550 cm^{-1} together and the edge of the

peak at 1050 cm^{-1} occurs at a higher wavenumber than that of starch. Thus they can be identified separately in a mixture. We were also interested to find out the composition of the precipitate obtained after addition of α-amylase to the starch-Au-NP composite. The FTIR spectrum of the precipitate is shown in Figure 4.2.5 (c). For better understanding and comparison we also recorded FTIR spectra of various samples, which are enzyme only (Figure 4.2.5 (b)); enzyme treated with excess H_2O_2 (Figure 4.2.5 (d)) and precipitate of the enzyme treated Au-NPs prepared by the presence method in absence of starch (Figure 4.2.5(c)). From the FTIR spectra of the above we conclude that the enzyme also had precipitated along with the Au-NPs. The reason for the above conclusion is as follows. There are two characteristic band of an enzyme like amylase. They are known as amide I band occurring at 1650 cm^{-1} due to ν (C=O) in-plane stretching vibration of the protein backbone and the other one is known as amide II band occurring at 1550 cm^{-1} due to δ (N-H) in-plane bending mode[15]. The peak at 1650 cm^{-1} is a combination of peaks due to different composition such as α helix, β sheet, β-turn and random coil[16]. The peak is known to be sensitive to the environment. The amide I and II peaks can easily be seen in Figure 4.2.5 (b) which is the spectrum of the enzyme only. Our FTIR spectroscopic observations suggest that upon treatment with H_2O_2 the amide II band disappears while the amide I band shifts to a lower wavenumber. On the other hand concurrently there is the appearance of another band at 1740 cm^{-1} generally attributed to C=O stretch in an ester[17]. As can been seen in Figure 4.2.5 (c), (d) and (e) the band at 1740 cm^{-1} occurs as a shoulder peak to that of amide I band. The disappearance of amide II is probably due to loss of N-H in the presence of H_2O_2. The shift of the amide I peak can be explained to occur because of change in the environment due to loss of N-H, while the appearance of a new peak at 1740 cm^{-1} is probably due to generation of a carbonyl group at other location. The precipitation of the enzyme occurs due to change in the primary (and thus secondary) structure of the protein in the presence of H_2O_2. Further, interaction of Au NPs with some of the functional groups generated upon hydrolysis of the enzyme may lead to precipitation of Au NPs along with the enzyme from the solution. In addition, H_2O_2 is known to affect the methionine group of amylase, which may also be possible in our case and leads to precipitation of the enzyme[18].

Finally, aqueous starch (amylose) is known to have helical structure with flexible diameters of the core to accommodate species like molecular iodine and carbon

nanotubes[19]. In the present case, $HAuCl_4$ and H_2O_2 may react inside the core and generate NPs. At lower concentration of $HAuCl_4$ the predominant formation is spherical, while at higher concentration [111] face of the fcc lattice of Au will preferentially grow into symmetrical triangular and hexagonal forms where the inner surface of the helical core would act as the template for the formation of those structures. There is also the possibility of formation of a core due to intermolecular assembly of starch molecules forming a cavity suitable for formation of the above structures.

4.2.4 Conclusion

In a series of experiments performed using starch as template, we have been able to demonstrate the possibility of generation of shape selective Au NPs by using H_2O_2 as the reducing agent with special control of experimental conditions like concentration of $HAuCl_4$ in presence of ultrasonic waves. Our essential observations are that in absence of ultrasonic radiation the NPs formed are spherical in nature. At higher concentration of $HAuCl_4$ formation of spherical NPs with larger particle size accounting for the shift in the transverse plasmon band. In the presence of ultrasonic waves and starch at lower $HAuCl_4$ concentration spherical particles are formed. At a higher concentration predominant formation of triangular particles takes place. At a still higher concentration of $HAuCl_4$ hexagonal discs of Au NPs are formed with the growth of [111] fcc plane of Au. Further the Au NPs could be recovered from the starch moiety using amylase, a starch digestive enzyme.

4.2.5 References

1. (a) Alivastos, A. P. *Science* **1996**, 271, 933 (b) Link, S.; El-Sayed, M. A. *J. Phys. Chem. B* **1999**, 103, 8410 (c) Wang, Z. L. *J. Phys. Chem. B* **2000**, 104, 1153 (d) Hoelderich, W. F. *Catal. Today* **2000**, 62, 115
2. El-Sayed, M. A. *Acc. Chem. Res.* **2001**, 34, 257
3. (a) Nie, S.; Emory, S. R. *Science* **1997**, 275, 1102 (b) Kneipp, K.; Wang, Y.; Kneipp, H.; Perelman, L. T.; Itzkan, I.; Dasari, R. R.; Feld, M. S. *Phys. Rev. Lett.* **1997**, 78, 1667
4. Haynes, C. L.; Van Duyne, R. P. *J. Phys. Chem. B* **2001**, 105, 5599

5. Jin, R.; Cao, Y.; Mirkin, C. A.; Kelly, K. L.; Schatz, G. C.; Zheng, J. G. *Science* **2001**, 294, 1901
6. (a) Jana, N. R.; Gearheart, C. J.; Murphy, C. J. *J. Phys. Chem. B* **2001**, 105, 4065 (b) Foss, C. A.; Hornyak, G. L.; Stockert, J. A.; Martin, C. A. *J. Phys. Chem.* **1994**, 98, 2963 (c) Chang, S. S.; Shih, C. W.; Chen, C. D.; Lai, W. C.; Wang, C. R. *Langmuir* **1999**, 15, 701 (d) Maillard, M.; Giorgio, S.; Pileni, M. P. *Adv. Mater.* **2002**, 14, 1084
7. (a) Sun, Y.; Xia, Y. *Science* **2002**, 298, 2176 (b) Sun, Y.; Xia, Y. *Adv. Mater.* **2003**, 15, 695
8. Malikova, N.; Pastoriza-Santos, I.; Schierhorn, M.; Kotov, N. A.; Liz-Marzan, L. M. *Langmuir* **2002**, 18, 3694
9. Metraux, G. S.; Cao, Y. C.; Jin, R.; Mirkin C. A. *Nano Lett.* **2003**, 3, 519.
10. (a) Chen, S.; Carroll, D. L. *Nano Lett.* **2002**, 2, 1003 (b) Pastoriza-Santos, I.; Liz-Marzan, L. M. *Nano Lett.* **2002**, 2, 903 (c) Yener, D. O.; Sindel, J.; Randall, C. A.; Adair, J. H. *Langmuir* **2002**, 18, 8692
11. (a) Mukherjee, P.; Ahmad, A.; Mandal, D.; Senapati, S.; Sainkar, S. R.; Khan, M. I.; Ramani, R.; Parischa, R.; Ajayakumar, P. V.; Alam, M.; Sastry, M.; Kumar, R. *Angew. Chem. Int. Ed.* **2001**, 40, 3585 (b) Li, Z.; Chung, S. W.; Nam, J. M.; Ginger, D. S.; Mirkin, C. A. *Angew. Chem. Int. Ed.* **2003**, 42, 2306 (c) Lee, S. W.; Lee, S. K.; Belcher, A. M. *Adv. Mater.* **2003**, 15, 689
12. Reches, M.; Gazit, E. *Science*, **2003**, 300, 625
13. Sarma, T. K.; Chowdhury, D.; Paul, A.; Chattopadhyay, A. *Chem. Commun.* **2002**, 1048.
14. Hall, S. R.; Shenton, W.; Engelhardt, H.; Mann, S. *ChemPhysChem* **2001**, 3, 184.
15. Fitter; J.; Heberle J. *Biophys. J.* **2000**, 79, 1629.
16. Claverie, P.; Vigano, C.; Ruysschaert, J. M.; Gerday, C.; Feller G. *Biochimica et Biophysica Acta* **2003**, 119, 1649
17. Larionova, N. V.; Kazanskaya, N. F.; Larionova, N. I.; Ponchel, G.; Duchene, D. *Biokhimiya* **1999**, 64, 1022.
18. Lin, L. -L.; Lo, H. -F.; Chiang, W. -Y., Hu, H. –Y.; Hsu, W. –H.; Chang, C. –T. *Current Microbiology*, **2003**, 46, 211.
19. Star, A.; Steuerman, D. W.; Heath, J. R.; Stoddart, J. F. *Angew. Chem. Int. Ed.*, **2002**, 41, 2508

CHAPTER 5

A POLYANILINE CONTAINING FILTER PAPER AS A SENSOR, ACID-BASE AND END-POINT INDICATOR, ALSO TO FILTER ACIDS AND BASES

5.1 A Polyaniline Containing Filter Paper That Acts as a Sensor, Acid, Base and End Point Indicator and also Filters Acids and Bases

5.1.1. Introduction

Polyaniline (PANI), being an important polymer with tunable electrical conductivity, has been the subject of intense study owing to its application potential in diverse fields such as microelectronics[1], displays[2], electrodes[3], sensors and actuators[4], membranes for gas separations[5], solar cells[6], fuel cells[7] and electro-magnetic interference (EMI) shielding[8]. Also, PANI undergoes non-redox reversible doping / dedoping process[9] based on simple acid base chemistry, enabling control over properties such as optical activity, electrical conductivity and sensor activity, thus making it unique in the class of conjugated polymers. As a natural consequence of its importance, a large number of synthetic protocols have been developed with application specific functionalization of PANI backbone[10], enhancement of biocompatibility of the polymer using enzymes as catalysts for synthesis[11], synthesis of PANI nanofibers and nanotubes[12], metal nanoparticle-PANI composite[13] and cabon nanotube doped PANI[14]. Further, an inclusion complex of PANI in cyclodextrin has been synthesized to generate "insulated molecular wire"[15]. Prominent applications of PANI as sensor include its use as ammonia vapor sensor[16], glucose biosensor[17] and ascorbic acid sensor[18]. One of the ways of constructing a sensor involves fabrication of a thin film of PANI on a substrate. In general thin films are made by methods like spin coating, spraying, fiber spinning, electrospinning, electrochemical polymerization on the surface, dip-coating and Langmuir-Blodgett technique. Further, PANI thin films and microtubules have been grown in porous membranes for sensor application[4a,19]. PANI has also been synthesized electrochemically inside ordered macroporous carbon[20]. However, it would be even more advantageous if these thin films were to act not only as sensors but also would be able to filter acids and bases and other species based on the acid-base properties of the polymer and perform chiral separation based on the chiral property of a dopant[21] in the polymer or the polymer itself. In other words, can we make a filter paper that would filter acids and bases from a solution and would be able to filter selective chiral molecules?

This chapter consists of the report of a new idea that constitutes synthesis of PANI in an ordinary commercially available filter paper and then use the filter paper (a) as a sensor for ammonia vapor and solution, (b) as an acid-base and end-point indicator and (c) to filter an acid and a base from solution. The primary aim is to use PANI embedded in a filter paper for any of the above functions. The emeraldine salt form of PANI is known as organic metal because of its high electrical conductivity. The salt appears green in color and has characteristic absorbance with peaks at around 800 nm and 430 nm. Upon treatment with a base the color changes to blue with characteristic absorbance at around 600 nm and 300 nm. This form of PANI is called emeraldine base, which has lower electrical conductivity. Interestingly, the same base could again be converted back to salt upon treatment with acid. The structures of two forms and their reversible convertibility are schematically shown in Figure 5.1.1.

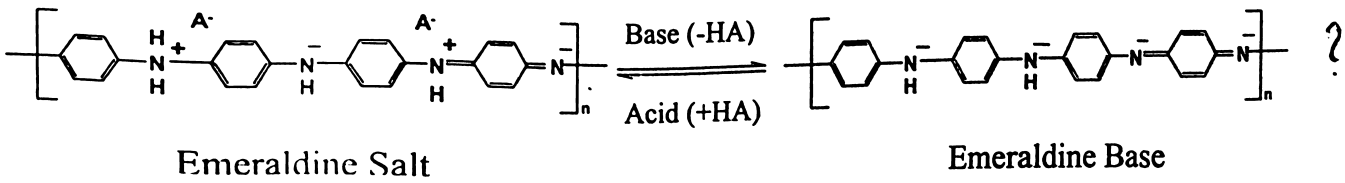

Figure 5.1.1. The basic chemical skeletons of Emeraldine Salt (green form) and Emeraldine base (blue form) PANI and their reversible conversion by treatment with base and acid.

It is natural that the change of color as well as electrical conductivity could be a good premise for developing acid base sensors using PANI as the sensing material. The additional advantage of the fast response time of color and electrical conductivity change makes all the more sense to use PANI as a sensing material. However, the primary challenge is in fabricating suitable device containing thin film of PANI for sensor application. The conventional methods of film deposition mentioned above may not be suitable for specific application such as fabricating filtration devices. What we have introduced is a very different, easy and versatile approach of growing the polymer in an ordinary filter paper with the potential for having virtually any polymer with room wide open for stereochemical, electrical charge, acid, base and other form of specificity. In addition, once an active

material is embedded in the filter paper the paper itself can act as a filter to specific separation of materials present in a solution.

Fibrous cellulose containing filter papers are useful in single use and efficient filtration device for separation of solid precipitates from a solution. They are inexpensive, easy to produce in different shapes and sizes and they come with different pore sizes required for different filtration application. Also, they could be folded into virtually any form of geometrical shape that many applications would demand. Therefore an ordinary filter paper could potentially be used as the base substrate for fabrication of indicators, sensors and membranes for filtration of acids and bases and separation of chiral molecules with appropriate active materials embedded in it. Efforts have to be made in meeting these demands through finding newer ways of incorporating active materials into the filter paper. As a first step in this direction we find the idea of growing polymers in the filter paper appealing and appropriate. In comparison to commercially available membranes, the fibrous nature of the paper could be an additional advantage in terms of growing polymer in them. One could possibly grow polymers in these filter papers in such a way that the fibers of filter paper get intertwined with the growing polymer and at the same time not clogging the bulk pores needed for filtration. In addition, if the polymer itself acts as sensors, indicators and filters of specific species, the basic criterion of stability of the material in the paper would easily be met. Further, if stable polymers could be incorporated in the paper, the possibilities of applications would be immense as the properties of the polymer could easily be modified with the incorporation of appropriate changes in the monomer. Based on this premise we have ventured to start by synthesizing PANI in ordinary commercially available filter papers. A well-known technique of synthesis of PANI involves simple mixing of water-soluble anilinium ions and H_2O_2 without the need of rigorous experimental conditions. Thus, if synthesized and remain stable, PANI containing filter paper as such would act as acid base sensor, indicator and would filter acid and base with the PANI as the sensing element.

In our method, aqueous acidic aniline solution in several drops was poured on to a filter paper placed on a glass plate. H_2O_2 solution was then added in several drops to the filter paper before it had become dry. Green coloration of the paper, that is characteristic of PANI formation, could be observed in a few minutes after the addition of the second solution. PANI formation in the filter paper was also possible if the sequence of addition of

the above solutions was just the opposite. Once PANI was formed in the filter paper it did not come out in acid and base solution or in acetone and toluene solvents. However, there was no significant PANI formation if the filter paper was first soaked with acidic aniline solution and then placed in a solution containing H_2O_2. On the other hand coloration in the solution could be observed indicating the transfer of anilinium ions from the filter paper to the solution followed by formation of PANI in the solution. The same was also true for the procedure worked in the reverse order of addition of solutions. We also show that the PANI containing filter paper could be used for ammonia vapor and liquid sensing as well as acid and base filtration.

5.1.2 Experimental Section

Preparation of conducting polyaniline embedded filter paper: Commercially available Whatman 40 filter papers were cut into about 5 cm diameter circular pieces. A stock solution of anilinium chloride was prepared by mixing 300 µl of distilled aniline in 5 ml 2M HCl solution in Milli Q water. 300 µl of the stock anilinium chloride solution was poured in several drops over the a filter paper using a pipette and the paper was allowed to remain soaked for 2-3 min. To the filter paper 200 µl of 30% H_2O_2 was then added drop by drop and the paper was allowed to dry. The filter paper turned light green in about 15 min and then to dark green in about 30 min. The filter paper was dried followed by washed thoroughly with water and ethanol for several times before it was kept for drying again.

The green form of polyaniline (emeraldine salt) in the filter paper could be converted to the blue form (emeraldine base) upon treatment with 2 ml of 0.1M NaOH solution needed for each of the filter papers. Treatment of either of emeraldine salt and base with 0.01 M $NaBH_4$ solution converted the paper into a colorless (a little brownish) form (Leucoemeraldine), which could again be converted back to emeraldine form upon treatment with the addition of 200 µl of 30% H_2O_2. Pieces of the green filter paper individually were kept immersed in vials containing dimethyl formamide (DMF), dimethyl sulfoxide (DMSO), acetone and toluene to test whether PANI came out in any solvent. It was found that PANI from the filter paper did not come out in acetone and toluene whereas the color of solutions of DMSO and DMF turned blue in presence of the paper, while the color of the paper did

not change. On the other hand when these papers were again treated with DMSO and DMF for the second time there was no coloration in the solvents and the filter papers did not exhibit any observable change in color or texture. In addition, treatment of the paper with $3x10^{-2}$ M aqueous sodium dodecyl sulfate had no observable effect on the paper.

Conducting polyaniline embedded filter paper as acid-base indicator: To demonstrate the use of the polyaniline embedded filter paper as an acid-base indicator we kept the green paper (2 cm x 1 cm) in 0.1 M HCl solution and the solution was titrated against 0.1 M NaOH solution. In another identical set 0.1 M HCl was titrated by 0.1 M NaOH solution where phenolphthalein indicator was added instead of the filter paper. We found that the paper turned blue exactly at the same point in titration when the other solution containing phenolphthalein turned pink. In other words both the titration gave equal end-point value. The same filter paper could be used several times as an acid-base indicator, as treatment of the blue form of PANI with acid regenerated the green form of PANI.

Conducting polyaniline embedded filter paper as vapor and solution sensor: The green filter paper was cut into a rectangular piece (1 cm x 0.5 cm) and was kept hanging in a stoppered vial that contained ammonia solution in aqueous medium. The filter paper turned blue immediately after keeping in the vial with minimum ammonia concentration in the solution at a value of 45 ppm. On the other hand when the same paper was dipped into a solution containing a minimum of 14 ppm of ammonia the paper turned blue that could be detected by naked eye.

Change in pH of an aqueous solution upon filtration through the PANI embedded filter paper: The aim of the present experiment was to find out the changes in pH of a solution after passing through the paper. First a basic solution of NaOH was passed through a green paper (emeraldine salt). For each run, a circular piece (3 cm diameter) of green filter paper was folded and placed inside a funnel that was kept above a 5 ml sample vial. 3ml of NaOH solution was passed through a single filter paper with drop-by-drop addition. Thus for a sequence of three filtration steps we started with a 12 ml of NaOH solution of which 3 ml was kept for measuring pH (measured value of 10.56) and the rest 9 ml was passed through

3 filter papers (separately in 3ml portions for each paper and then remixed). For the next filtration 3ml was saved for pH measurement and the rest 6 ml was passed through 2 papers. From the recovered 6 ml solution 3 ml was saved for pH measurement and the last 3ml portion was passed through a filter paper resulting in a pH of 7.41.

Successive filtrations changed the pH as below.

pH= 10.56 $\xrightarrow{1^{st}\text{ Filtration}}$ pH= 9.46 $\xrightarrow{2^{nd}\text{ Filtration}}$ pH= 8.53 $\xrightarrow{3^{rd}\text{ Filtration}}$ pH= 7.41

In the same way, when acid solutions (3 ml HCl portions) were passed successively through blue filter papers (previously converted from green to blue form by treatment with NaOH solution and then washed thoroughly and dried) the following values of pH were obtained.

pH= 2.36 $\xrightarrow{1^{st}\text{ Filtration}}$ pH= 2.55 $\xrightarrow{2^{nd}\text{ Filtration}}$ pH= 3.18

Instrumentation: UV-visible spectra of pieces of filter paper (1cm diameter) were recorded using a Perkin-Elmer spectrophotometer (Model Lambda 25) in diffuse reflectance mode. Diffuse reflectance FTIR spectra of the papers were recorded using Perkin-Elmer FTIR spectrophotometer (Model Spectrum One A). The scanning electron micrographs were performed after sputtering the filter papers with gold. Micrographs were recorded in a JEOL SEM (Model No. JSM 6700F) machine operating at 20 KV.

5.1.3 Results and Discussion

The UV-visible absorption spectrum of the green filter paper resulted due to the formation of PANI (emeraldine salt) in the filter paper is shown in Figure 5.1.2A (a). The absorption spectrum was recorded in diffuse reflectance mode. As clear from the figure, the UV-visible absorption indicated formation of emeraldine salt (green) with characteristic absorption maxima at around 800 nm and 400 nm. This is similar to the emeraldine salt spectrum of bulk PANI prepared under identical experimental condition in the solution

phase. The longitudinal peak at 800 nm is characteristic for the formation of conductive polyaniline inside the filter paper.

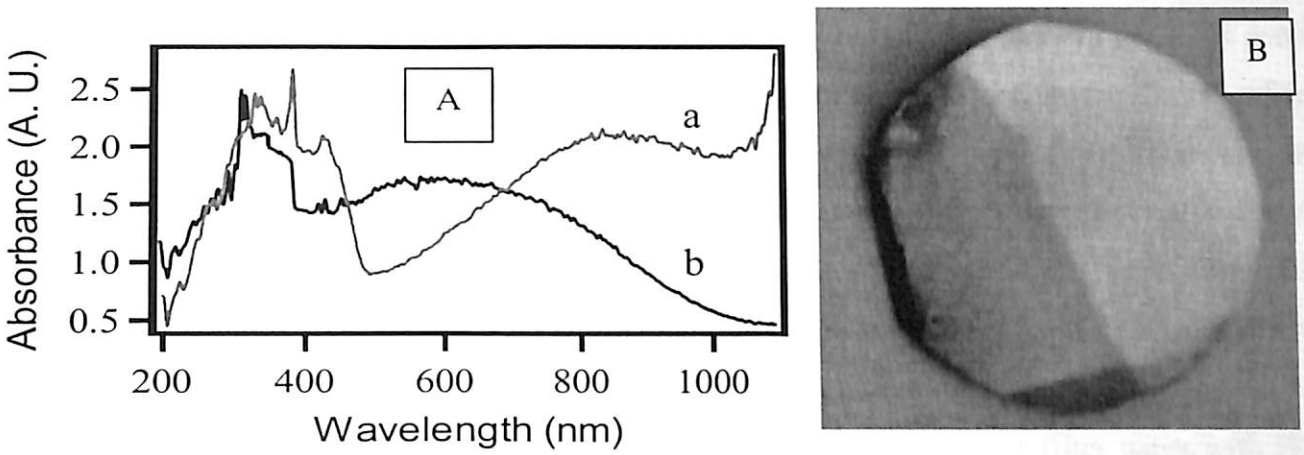

*Figure **5.1.2**. **A**. Diffuse reflectance UV-visible spectra of emeraldine base (blue line) and emeraldine salt (green line) of PANI synthesized in a filter paper. **B**. A filter paper containing PANI (green) with a part of the paper turning blue when treated with NaOH solution. (See color plates, Page 135)*

The green filter paper upon treatment with NaOH solution became blue with absorption maxima at 600 nm and 300 nm (Figure 5.1.2A (b)), which is same as the emeraldine base (blue) form of PANI. The shift in the peak position in the UV-visible spectra indicates the formation of the base, which is reported to have lower conductivity than the corresponding emeraldine salt form. The blue form (base) could again be converted into the green form (salt) with the UV-visible spectrum identical to the original green form. This means that even though the PANI was formed in a filter paper, the optical absorption characteristic and the chemical convertibility between the salt and the base forms remain intact which is important for further application. Shown in Figure 5.1.2B is the photograph of a filter paper with green emeraldine salt and associated blue base obtained by treating a part of the paper with NaOH. It is interesting to note that the same filter paper could possibly be used as a sensor for either of acid and base as a part of it would respond to acid while the other part would respond to base.

To ascertain the formation of polyaniline on the filter paper we performed the FTIR spectra of the polyaniline incorporated filter paper in the diffuse reflectance mode. FTIR spectroscopic evidences showed that PANI synthesized in the filter paper had same characteristic vibrational transitions as those of emeraldine salt and base prepared in the bulk under identical experimental condition. In other words, the peaks corresponding to emeraldine salt and base forms of PANI in bulk were also present in the FTIR spectra of them in the filter paper. FTIR spectra of four samples recorded in the diffuse reflectance mode are shown in Figure 5.1.3. The four samples are of (A) an ordinary filter paper that we have used as the substrate for growing polymer in it; (B) the filter paper after addition of HCl and H_2O_2 on it followed by drying; (C) the filter paper containing green form of PANI; and (D) the filter paper with blue form of PANI. As can be seen from the spectra, there is no apparent difference between the spectrum of filter paper alone and that of the filter paper treated with HCl and H_2O_2. This suggests that treatment of the filter paper with HCl and H_2O_2 did not change the chemical composition of the paper.

A comparison between the spectra in Figure 5.1.3C and 5.1.3D reveals that characteristic peaks at 1490 and 1580 cm^{-1} due to emeraldine form of PANI are present in samples containing salt and base forms of the polymer and the same peaks are absent in Figure 5.1.3A and 5.1.3B which are those of the filter paper alone and the filter paper treated with H_2O_2 and HCl. In both the spectra 5.1.3C and 5.1.3D a weak and broad band around 3400 cm^{-1} appeared, which is assigned to the N-H stretching mode of polyaniline. One notable difference in the spectra of emeraldine salt and base form was the presence of a strong band at 1150 cm^{-1} in 5.1.3C that was absent in 5.1.3D. The peak termed as "electronic like band" is characteristic of extensive electron delocalization in case of emeraldine salt form of polyaniline, which was absent in case of the base form. The presence of the peak characterizes the conductivity of the polyaniline formed inside the cellulose matrix in filter paper. In case of the emeraldine salt formed in the filter paper the intensity of the benzoid (1490 cm^{-1}) band was equal to the band at 1580 cm^{-1} due to quinoid ring deformation, however in case of emeraldine base form the intensity of the benzoid band was much less than the quinoid band, this observation agrees well with the previous reports[22] for

emeraldine salt and base in solution. Thus diffuse reflectance FTIR spectroscopy confirms the formation of the emeraldine salt and base form of polyaniline in the filter paper.

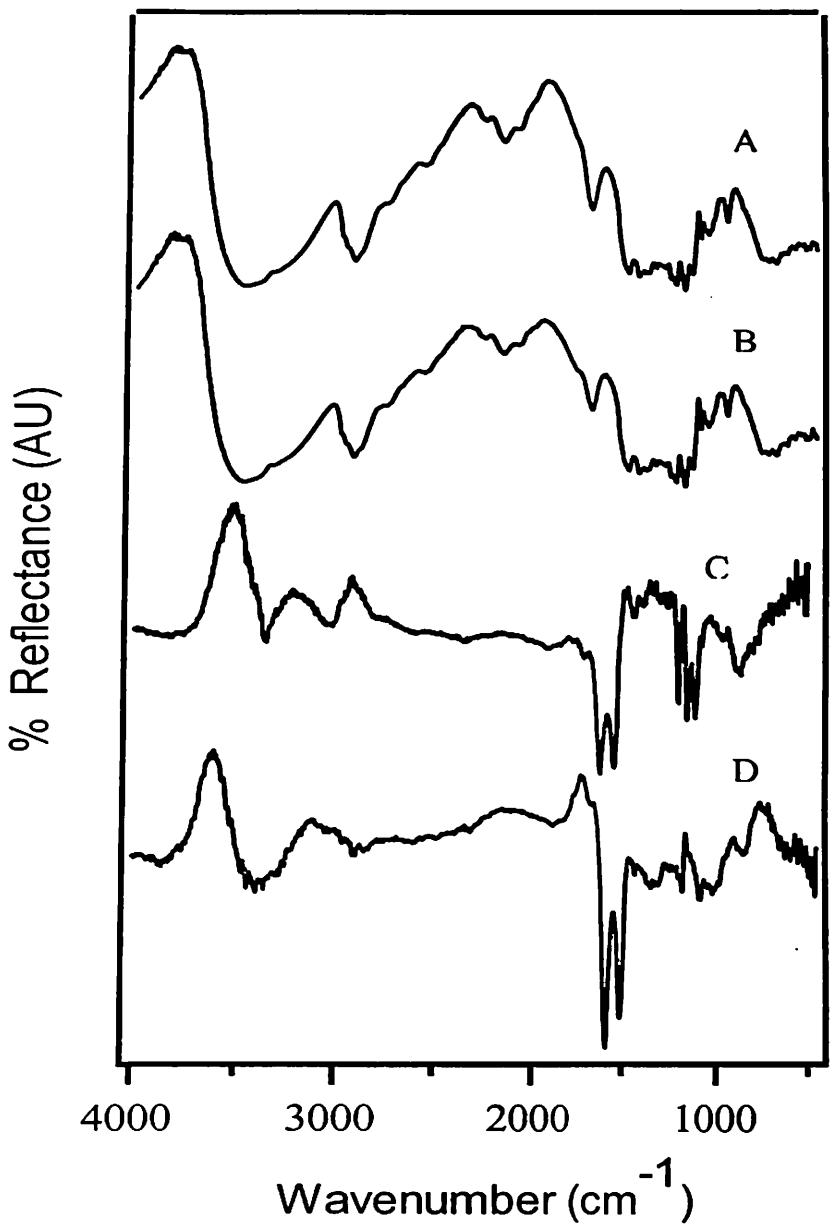

*Figure **5.1.3**. FTIR spectra of (A) an ordinary filter paper that we have used as the substrate for growing polymer in it; (**B**) the filter paper after addition of HCl and H_2O_2 on it and then dried; (**C**) the filter paper containing green form of PANI; and (**D**) the filter paper with blue form of PANI.*

Scanning electron microscopic measurements revealed that PANI grew in the filter paper into long fibrous network. A micrograph of the filter paper (Figure 5.1.4A) that we have used shows the presence of pores in the paper that are of dimensions on the order of

200 nm. When the same paper was coated with PANI, the pores were not observed whereas long-range fibrous network of PANI could be observed (Figure 5.1.4B). This observation does not necessary mean that the pores were filled by PANI. On the contrary they were probably intact as we had found that the filtration rate of the same solution by the coated and uncoated filter papers were the same. Thus PANI was retained in the filter paper possibly by interconnected network of polymer fibers, which were intertwined with those of the filter paper and that is the reason for stability of PANI in the filter paper when treated with acid, base and organic solvents. The growth of polymer in the paper does not follow the microscopic template of the paper. On the other hand, there is the possibility of the nature of growth of the polymer decided by the flow of reactants through the channels of the paper.

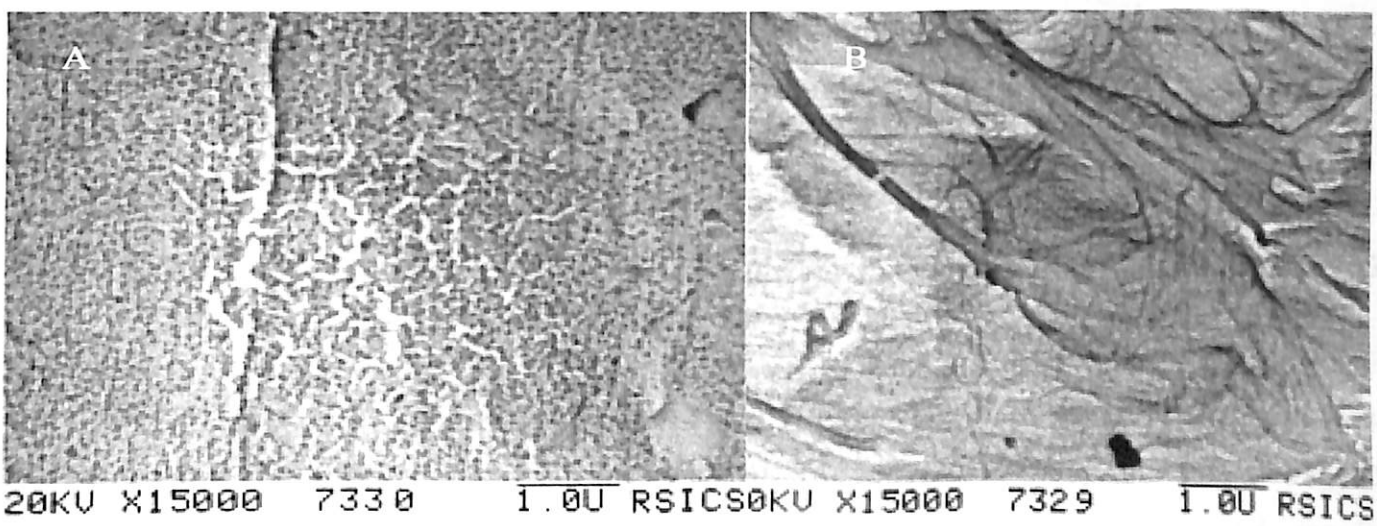

*Figure **5.1.4**. Scanning electron micrographs of a filter paper (A) and the paper coated with PANI (B). Bar is 1μm.*

We have further used these PANI coated filter papers as a sensor for acid and base. When green PANI-paper was treated with ammonia solution, the paper turned blue at the lowest concentration of 14 ppm. On the other hand the same paper could detect ammonia vapor from an aqueous solution of the same having concentration of 45 ppm. Similar results were obtained with NaOH solution. In Figure 5.1.5A and 5.1.5B we show the photographs of two filter papers one in in 0.1 M NaOH solution and the other one is water. As evident from the photographs, while the paper in water remained green, the paper in NaOH solution had turned blue. Thus it clearly demonstrates the ability of the PANI coated filter paper to

act as a sensor for NaOH solution. We also mention here that one such filter paper (green) was used for finding the end-point of titration of HCl solution with NaOH and the end-point was found to be exactly the same as that was found using phenolphthalein indicator.

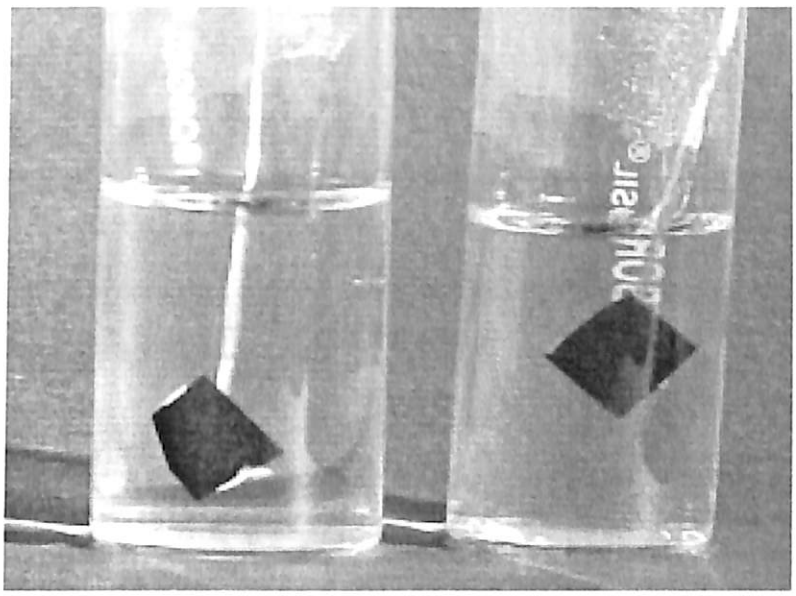

*Figure **5.1.5**. Photographs of filter paper (green form) when kept in (A) 0.1 M NaOH solution and (B) in H_2O. (See color plates, Page 135)*

Finally, we also have used these papers for acid and base filtration. We have passed HCl solution successively through two blue filter papers put in conical funnels such that the filtrate of the first filtration was collected and passed through the second one (see experimental section). The pH of each solution was measured. We found significant change in the pH after passing through the papers. Our results are as follows: starting solution before filtration had a pH 2.36. After first filtration the pH was 2.55 and the same was at 3.18 after second filtration. Thus the ability of the PANI containing filter paper to act as acid filter was clearly demonstrated. In the same way we found that using the green filter paper and filtration of a starting solution with pH 10.56 resulted into pH 9.46 after first filtration, 8.53 after second filtration and 7.41 after the third filtration. We also show some of these results photographically in Figure 5.1.6 where the first solution (A) had a pH of 10.1, the second one (B) was the result of two consecutive filtrations and had a pH 8.3 and third one

(C) was the result of a third filtration and had a pH of 7.2. Phenolphthalein indicator was added to all three solutions after filtration was complete and only for taking photographs.

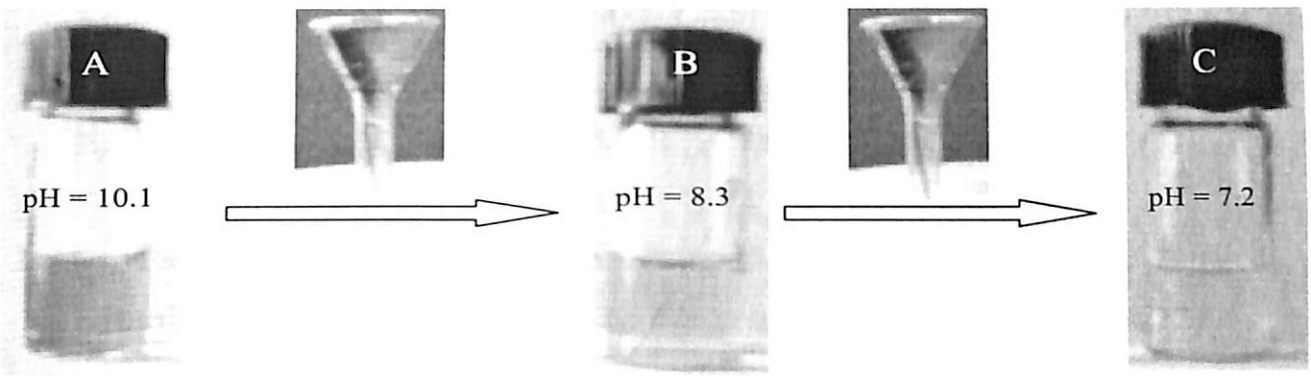

*Figure **5.1.6**. Photographs of solutions (A) NaOH solution treated with phenolphthalein; (B) A part of (A) passed through green filter paper and then treated with phenolphthalein; (C) a part of (B) passed through another green filter paper and then treated with phenolphthalein.* *(See color plates, page 136)*

5.1.4 Conclusion

In this chapter we have reported a new method for the synthesis of conducting PANI in a filter paper. The optical characteristics of PANI in the paper were the same as those in the bulk prepared under identical condition. The PANI in the paper could be reversibly converted between different forms. We have also demonstrated the ability PANI containing filter paper as an acid / base sensor and also to filter acid and base. The use of the filter paper as an ammonia sensor has been possible with a sensing ability as low as 45 ppm solution concentration for vapor sensing and at 14 ppm minimum concentration for sensing of ammonia in solution.

5.1.5 References

1. (a) Sirringhaus, H.; Tessler, N.; Friend, R. H. *Science* **1998**, 280, 1741 (b) Burroughes, J. H.; *Nature* **1990**, 347, 539 (c) Wohlgenannt, M.; Tandon, K.; Mazumdar, S.; Ramsesha, S.; Vardeny, Z. V.; *Nature* **2001**, 409, 494 (d) Yu, G.; Gao, J.; Hummelen, J. C.; Wudl, F.; Heeger, A. J.; *Science* **1995**, 270, 1789 (e) Paul, E. W.; Ricco, A. J.; Wrighton, M. S.; *J. Phys. Chem.* **1985**, 89, 1441

2. (a) Pages, H.; Topart, P.; Lemordant, D.; *Electrochimica Acta* **2001**, 46, 2137 (b) Kitani, A.; Yano, J.; Sasaki, K. J.; *Electroanal. Chem.* **1986**, 209, 227

3. For example (a) Lefenfeld, M.; Blanchet, G.; Rogers, J. A. *Adv. Mater.*, **2003**, 15, 1188 (b) Bartlett, P. N.; Simon, E.; *J. Am. Chem. Soc.*, **2003**, 125, 4014 (c) Kang, X.; Jin, Y.; Cheng, G.; Dong, S.; *Langmuir*, **2002**, 18, 10305

4. (a) Sukeerthi, S.; Contractor, A. Q.; *Anal. Chem.* **1999**, 71, 2231 (b) Xue, H.; Shen, Z.; Li, Y.; *Synth. Met.* **2001**, 124, 345 (c) Xie, D.; Jiang, Y.; Pan, W.; Li, D.; Wu, Z.; Li, Y.; *Sensors and Actuators B* **2002**, 81, 158 (d) Wang, H-L.; Gao, J.; Sansinena, J-M.; McCarthy, P.; *Chem. Mater.* **2002**, 14, 2546

5. (a) Kaner, R. B.; *Synth. Met.*, **2002**, 125, 65 (b) Stolarczyk, A.; Lapkowski, M.; *Synth. Met.*, **2001**, 121, 1385 (c) Xie, D.; Jiang, Y.; Pan, W.; Li, D.; Wu, Z.; Li, Y.; *Sensors and Actuators B* **2002**, 81, 158

6. (a) Tan, S. X.; Zhai, J.; Wan, M. X.; Jiang, L.; Zhu, D. B.; *Synth. Met.*, **2003**, 137, 1511 (b) Chen, S. A.; Fang, Y.; *Synth. Met.*, **1993**, 60, 215

7. (a) Kitani, A.; Akashi, T.; Sugimoto, K.; Ito, S.; *Synth. Met.*, **2001**, 121, 1301 (b) Doubova, L.; Mengoli, G.; Musiani, M. M.; Valcher, S.; *Electrochim. acta*, **1989**, 34, 337

8. (a) Hong, Y. K.; Lee, C. Y.; Jeong, C. K.; Lee D. E.; Kim, K.; Joo, J.; *Review in Scientific Instrument*s, **2003**, 74, 1098 (b) Koul, S.; Chandra, R.; Dhawan, S. K.; *Polyme*r, **2000**, 41, 9305 (c) Joo, J.; Lee, C. Y.; *J. Appl. Phy*s. **2000**, 88, 513

9. Heeger, A. J.; *Angew. Chem. Int. E*d. **2001**, 40, 2591

10. (a) Yue, J.; Wang, Z. H.; Cromack, K. R.; Epstein, A. J.; MacDiarmid, A. G.; *J. Am. Chem. Soc.* **1991**, 113, 2665 (b) Wei, X. L.; Wang, Z. H.; Long, S. M.; Bobeczko, C.; Epstein, A. J.; *J. Am. Chem. Soc.* **1996**, 118, 2545 (c) Chan, H. S. O.; Neuendorf, A. J.; Ng, S. C.; Wong, P. M. L.; Young, D. J.; *Chem. Commun.* **1998**, 1327 (d) Chen, S-A; Hwang, G-W.; *J. Am. Chem. Soc.* **1995**, 117, 10055 (e) Chan, H. S. O.; Ho, P. K. H.; Ng, S. C.; Tan, B. T. G.; Tan, K. L.; *J. Am. Chem. Soc.* **1995**, 117, 8517

11. (a) Liu, W.; Kumar, J.; Tripathy, S.; Senecal, K. J.; Samuelson, L.; *J. Am. Chem. Soc.* **1999**, 121, 71 (b) Liu, W.; Cholli, A. L.; Nagarajan, R.; Kumar, J.; Tripathy, S.; Bruno, F. F.; Samuelson, L.; *J. Am. Chem. Soc.* **1999**, 121, 11345

12. (a) Huang, J.; Virji, S.; Weiller, B. H.; Kaner, R. B.; *J. Am. Chem. Soc.* **2003**, 125, 314 (b) Wei, Z.; Zhang, Z.; Wan, M.; *Langmuir*, **2002**, 18, 917 (c) Zhang, L.; Wan, M.; *Nanotechnology*, **2002**, 13, 750

13. Sarma, T. K.; Chowdhury, D.; Paul, A.; Chattopadhyay, A.; *Chem. Commun.* **2002**, 1048

14. Zengin, H.; Zhou, W.; Jin, J.; Czerw, R.; Smith Jr., D. W.; Echegoyen, L.; Carroll, D. L.; Foulger, S. H.; Ballato, J.; *Adv. Mater.* **2002**, 14, 1480

15. Yoshida, K.; Shimomura, T.; Ito, K.; Hayakawa, R.; *Langmuir*, **1999**, 15, 910

16. (a) Lee, Y-S; Joo, B-S; Choi, N-J; Lim, J-O; Huh, J-H; Lee, D-D; *Sensors and Actuators* B, **2003**, 93, 148 (b) Matsuguchi, I. J.; Sugiyama, G.; Sakai, Y.; *Synth. Metals*, **2002**, 128, 15 (c) Domansky, K.; Baldwin, D. L.; Grate, J. W.; Hall, T. B.; Li, J.; Josowicz, M.; Janata, J.; *Anal. Chem.* **1998**, 70, 473

17. (a) Sirkar, K.; Revzin, A.; Pishko, M. V.; *Anal. Chem.* **2000**, 72, 2930 (b) Xue, H. Shen, Z.; Li, Y.; *Synth. Metals*, **2001**, 124, 345

18. Bossi, A. I.; Piletsky, S. A.; Piletska, E. V.; Righetti, P. G.; Turner, A. P. F.; *Anal. Chem.* **2000**, 72, 4296

19. (a) Martin, C. R.; *Acc. Chem. Res.* **1995**, 28, 61 (b) Parthasarathy, R.; Martin, C. R.; *Chem. Mater*, **1994**, 6, 1027 (c) Parthasarathy, R.; Martin, C. R.; *Nature*, **1994**, 369, 298

20. Lei, Z.; Zhang, H.; Ma, S.; Ke, Y.; Li, J.; Li, F.; *Chem. Commun.* **2002**, 676

21. Huang, J.; Egan, V. M.; Guo, H.; Yoon, J-Y; Briseno, A. L.; Rauda, I. E.; Garrell, R. L.; Knobler, C. M.; Zhou, F.; Kaner, R. B.; *Adv. Mater.*, **2003**, 15, 1158

22. (a) Lu, F. L.; Wudl, F.; Nowak, M.; Heeger, A. J.; *J. Am. Chem. Soc.* **1986**, 108, 8311 (b) Sun, Y.; MacDiarmid, A. G.; Epstein; A. J.; *J. Chem. Soc. Chem. Commun.* **1990**, 529

COLORED FIGURES

Chapter 3.1

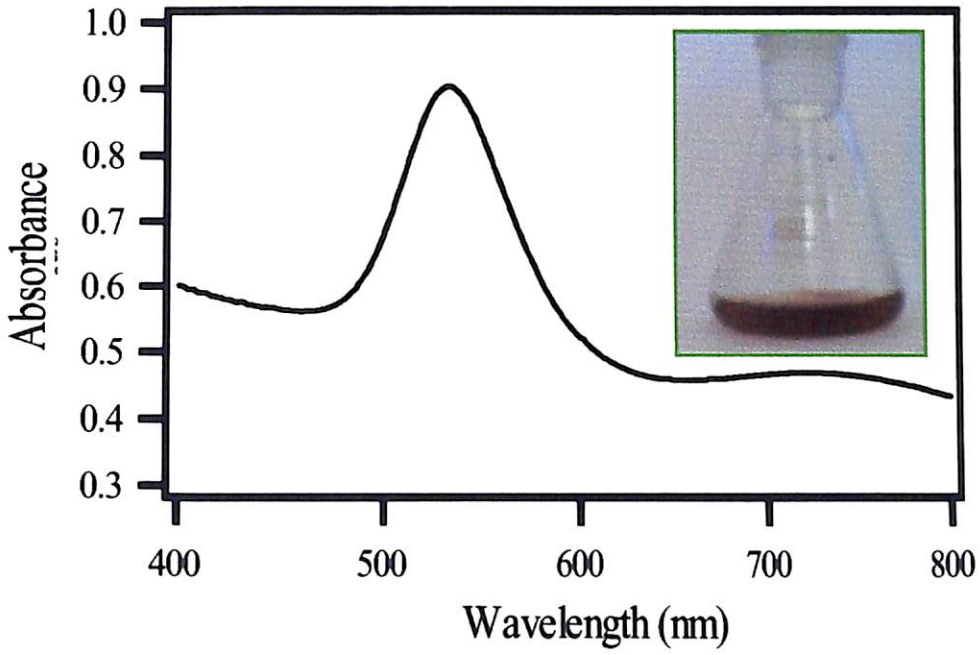

*Figure **3.1.2**. UV-visible absorption spectrum of the Au nanoparticles synthesized by our method in aqueous medium. The photograph is of purple colored Au nanoparticles in a conical flask.* ***(page 54)***

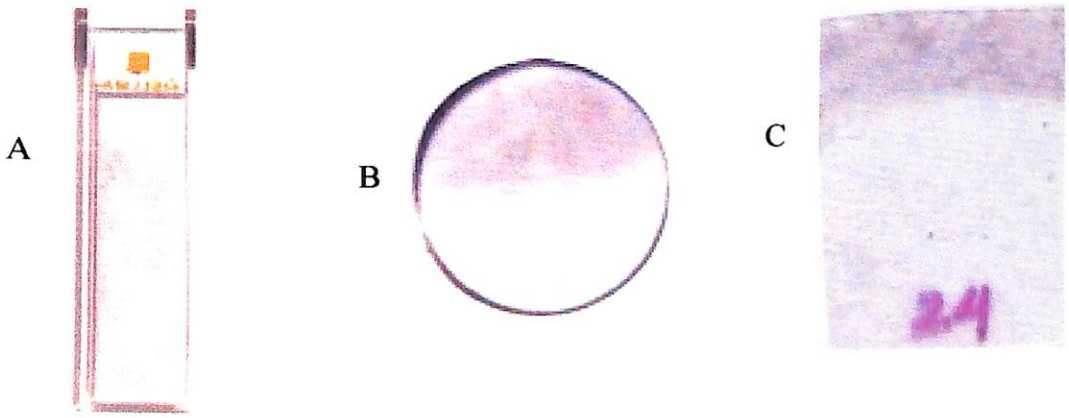

*Figure **3.1.4**. Photographs of Au NP– coated (A) quartz cuvette, (B) quartz disk and (C) OHP paper.* ***(page 56)***

Chapter 3.1

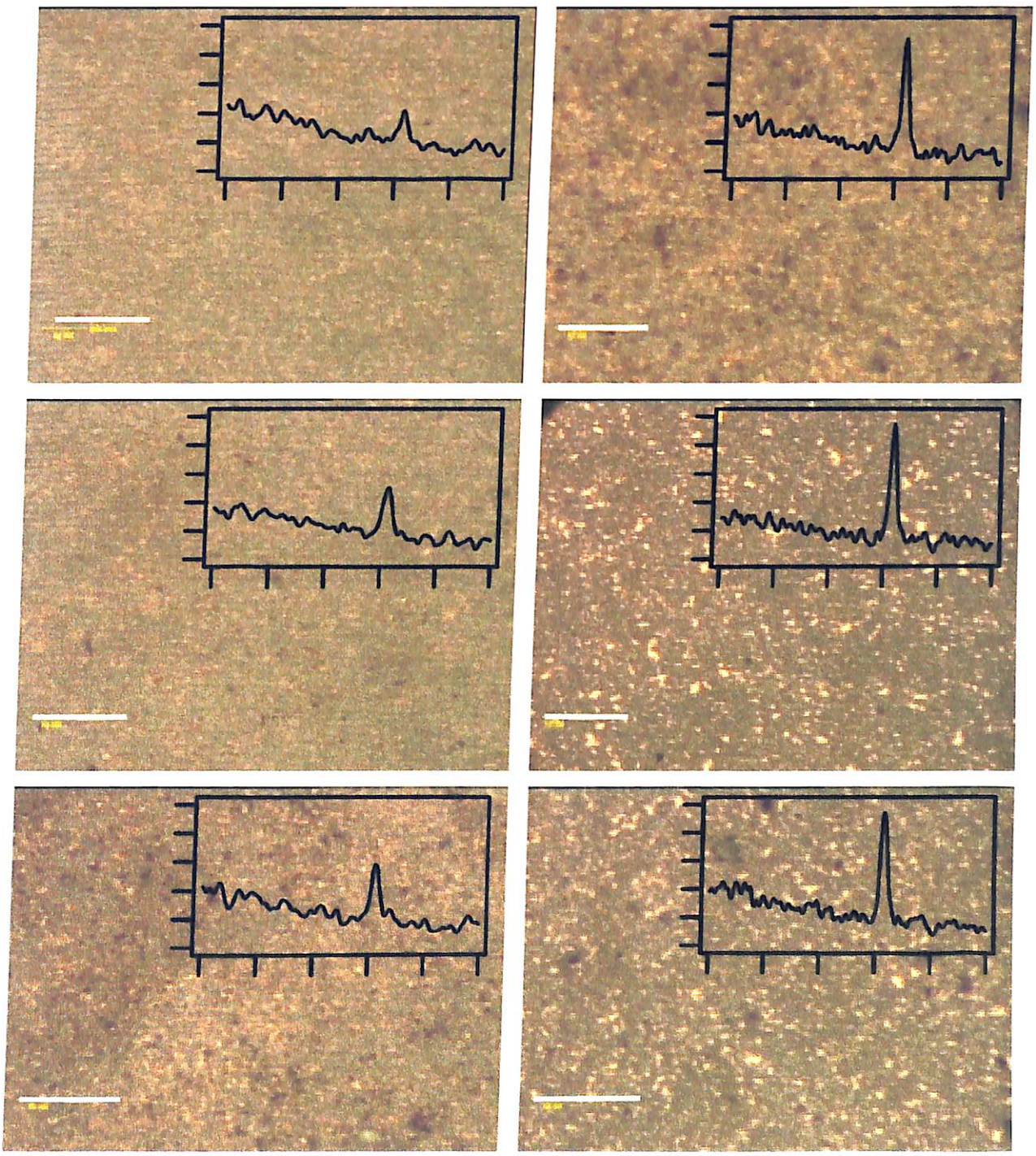

Figure 3.1.7. Time dependence of deposition of Au NPs on glass slides as observed by optical microscopic and XRD measurements. Scale bar in optical micrographs is 10 μm. **(page 59)**

Chapter 4.1

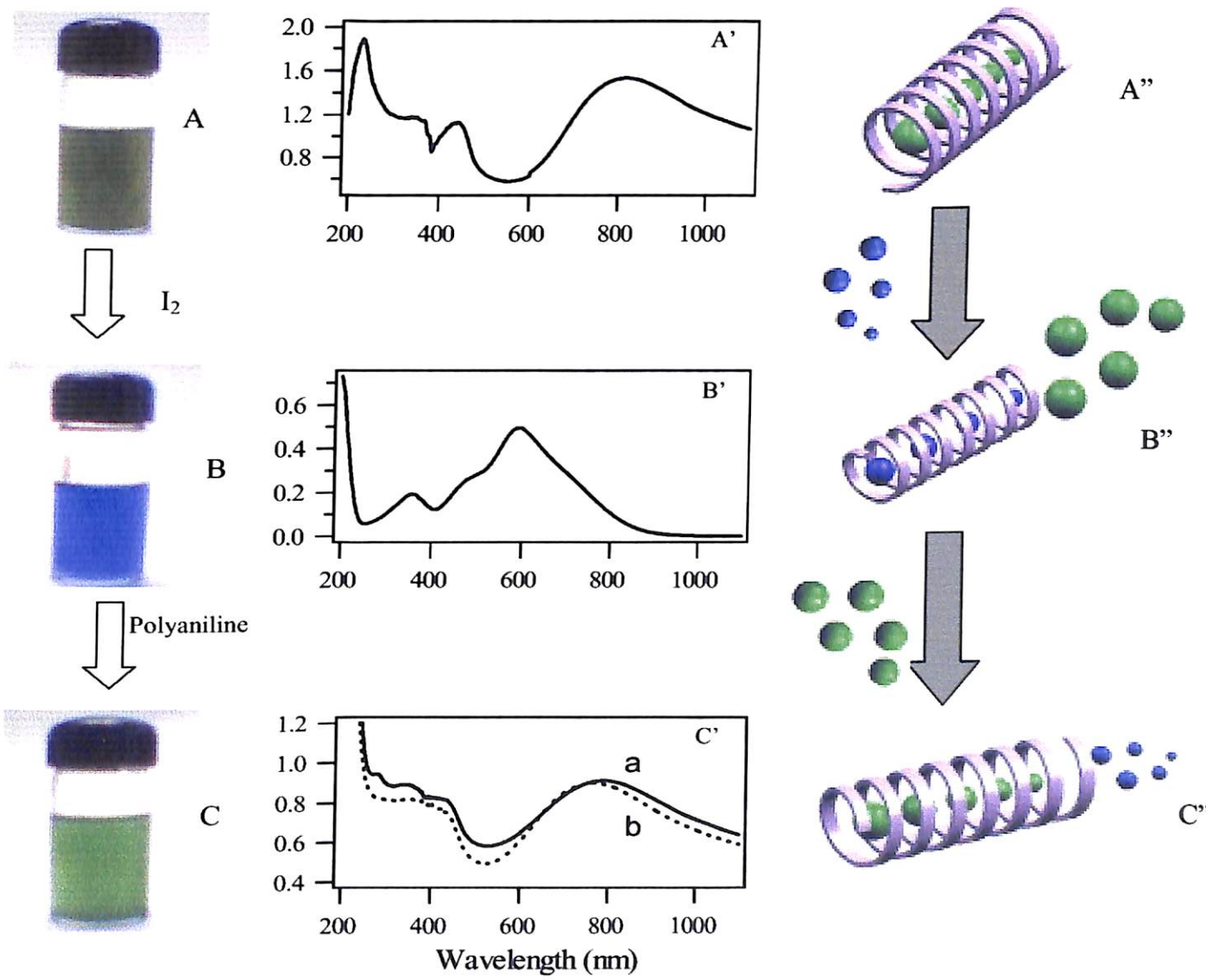

Figure 4.1.1**. Photographs of (A) starch solubilized PANI, (B) I_2 in starch replacing PANI and (C) PANI again in starch replacing I_2. (A') and (B') are UV-vis absorption spectra of sample in (A) and (B) respectively. (C') (a) UV-vis absorption spectra of sample in C and (b) after treatment of the solution by $CHCl_3$. (A''), (B") and (C") are schematic representation of a model of the processes in (A), (B) and (C) respectively.* ***(page 92)

Chapter 4.1

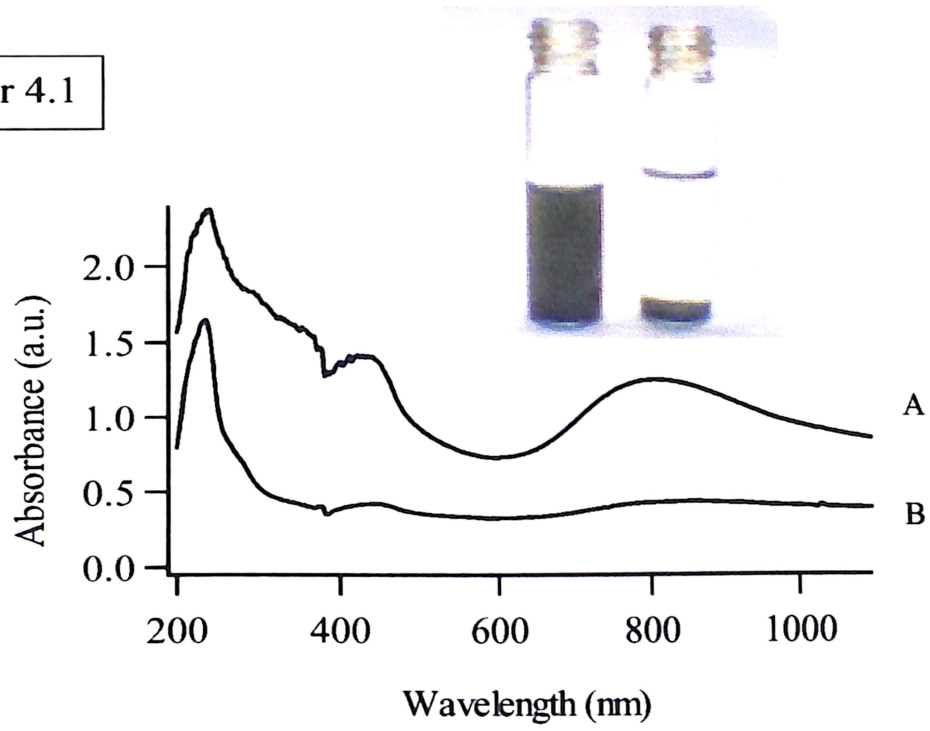

***Figure 4.1.5**: UV-visible spectra representing the hydrolysis of starch by enzyme Diastage (fungal) leading to the precipitation of PANI from starch-PANI composite, recorded (a) immediately after addition of enzyme and (b) after 30 min. On the top are photographs of vials containing the complex at the beginning (left) and 30 min after addition of enzyme (right).* (**Page 98**)

Chapter 4.2

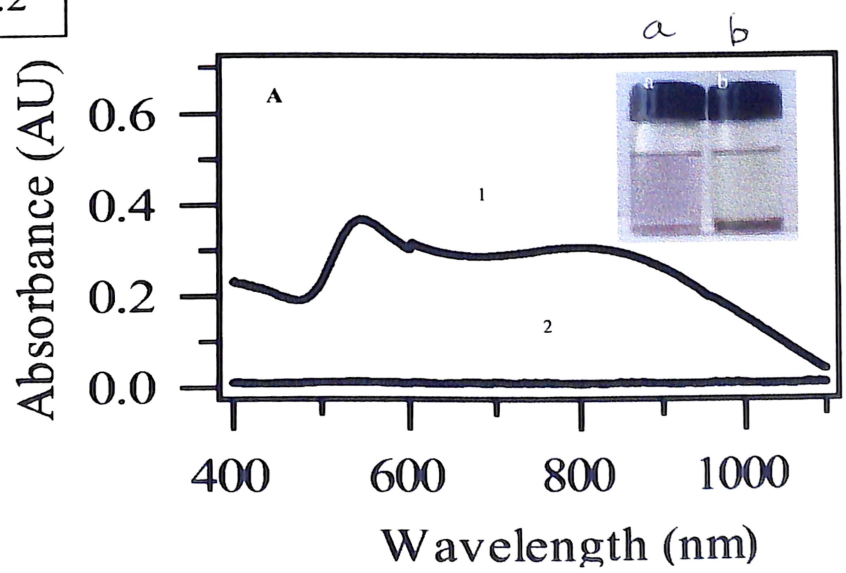

***Figure 4.2.4.** UV-vis spectra and photographs of Au-NP containing starch solution (diluted) recorded right after addition of enzyme (1 and a respectively) and 8 hrs after addition (2 and b respectively). The experiment was performed at 40^{0}C.* (**page 111**)

Chapter 5.1

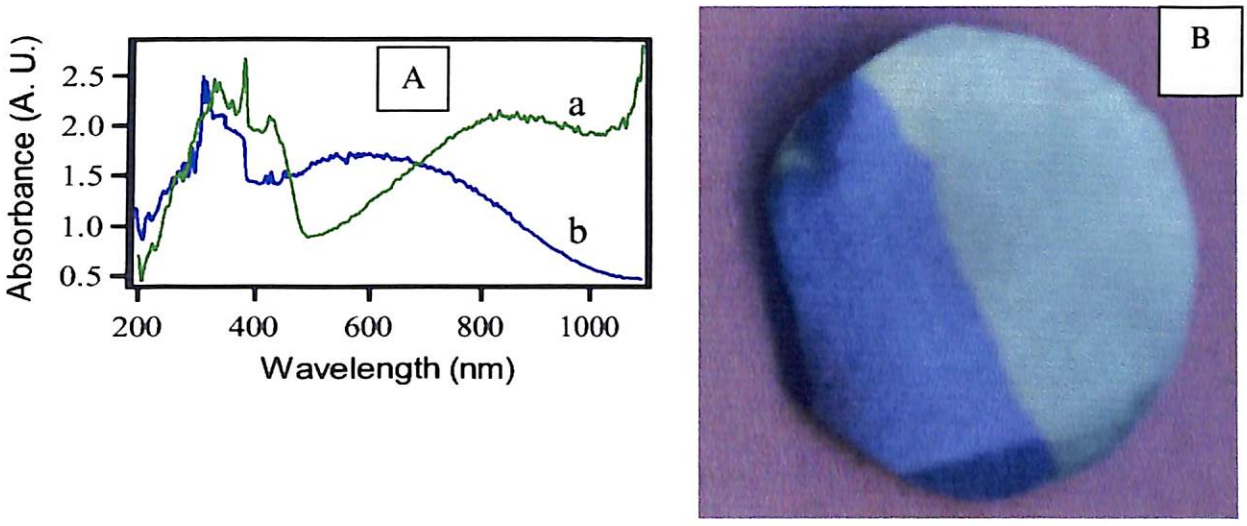

Figure ***5.1.2****. **A**. Diffuse reflectance UV-visible spectra of emeraldine base (blue line) and emeraldine salt (green line) of PANI synthesized in a filter paper. **B**. A filter paper containing PANI (green) with a part of the paper turning blue when treated with NaOH solution.* ***(page 122)***

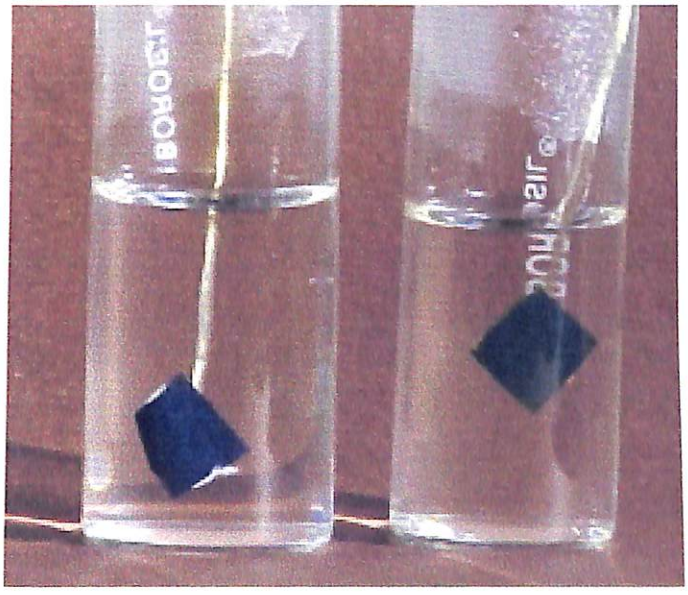

Figure ***5.1.5****. Photographs of filter paper (green form) when kept in (A) 0.1 M NaOH solution and (B) in H_2O.* ***(page 126)***

Chapter 5.1

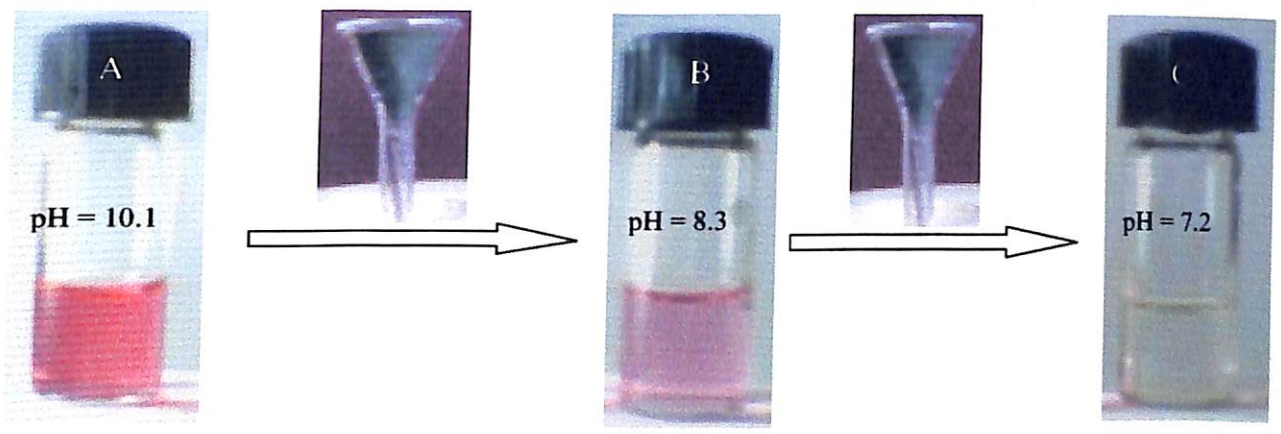

*Figure **5.1.6**. Photographs of solutions (A) NaOH solution treated with phenolphthalein; (B) A part of (A) passed through green filter paper and then treated with phenolphthalein; (C) a part of (B) passed through another green filter paper and then treated with phenolphthalein.* ***(page 127)***

List of Publications

1. **"Simultaneous Measurement of Flowing Fluid Layer and Film Thickness of a Soap Bubble Using a UV-Visible Spectrophotometer"**

   Tridib Kumar Sarma and Arun Chattopadhyay, *Langmuir*, **2001**, 17, 6399-6403

2. **"Visible Spectroscopic Observation of Controlled Fluid Flow up along a Soap Bubble Film from a Pool of Solution"**

   Tridib Kumar Sarma and Arun Chattopadhyay, *J. Phys. Chem. B*, **2001**, 105, 12503-12507

3. **"Synthesis of Au nanoparticle–conductive polyaniline composite using H_2O_2 as oxidising as well as reducing agent"**

   Tridib Kumar Sarma, Devasish Chowdhury, Anumita Paul and Arun Chattopadhyay, *Chem. Commun*. **2002**, 1048-1049

4. **"Reversible Encapsulation of Nanometer Size Polyaniline and Polyaniline-Au-nanoparticle Composite in Starch"**

   Tridib Kumar Sarma and Arun Chattopadhyay (revised version submitted).

5. **"Starch Mediated Shape-Selective Synthesis of Au-NPs with Tunable Longitudinal Plasmon Resonance"**

   Tridib Kumar Sarma and Arun Chattopadhyay (in communication).

6. **"A Polyaniline Containing Filter Paper that Acts as a Sensor, Acid, Base and End-point Indicator and also Filters Acid and Base"**

   Dipak Dutta, Tridib Kumar Sarma, Devasish Chowdhury and Arun Chattopadhyay (manuscript to be resubmitted).

7. **"A Simple Method of Electroless Deposition of Au Nanoparticles on Two and Three - Dimensional Surfaces of Various Materials"**

   Tridib Kumar Sarma, Manabendra Ray and Arun Chattopadhyay (manuscript under preparation)

8. **"Spreading and Recoil of a Surfactant Containing Water Drop on Glass Supported Alcohol Films"**

   Devasish Chowdhury, Surya Protim Sarkar, Dipankar Kalita, Tridib Kumar Sarma, Anumita Paul and Arun Chattopadhyay, *Langmuir*, **2004**, (accepted for publication).